NOAA ATLAS No. 9

Atlas of Southern Hemisphere 500 mb Teleconnection Patterns Derived from National Meteorological Center Analyses

Camp Springs, Md.
March 1992

U.S. DEPARTMENT OF COMMERCE
National Oceanic and Atmospheric Administration
National Weather Service

NOAA ATLAS No. 9

Atlas of Southern Hemisphere 500 mb Teleconnection Patterns Derived from National Meteorological Center Analyses

Vernon E. Kousky, Gerald D. Bell
Climate Analysis Center
National Meteorological Center
National Weather Service

Camp Springs, MD.
March 1992

U.S. DEPARTMENT OF COMMERCE
Rockwell A. Schnabel, Acting Secretary
National Oceanic and Atmospheric Administration
Dr. John A. Knauss, Under Secretary
National Weather Service
Dr. Elbert W. Friday, Jr., Assistant Administrator

Table of Contents

Atlas of Southern Hemisphere 500 mb Teleconnection Patterns Derived from National Meteorological Center Analyses

ABSTRACT

An atlas of teleconnection patterns, based on monthly mean 500 mb geopotential height anomalies, is presented for the Southern Hemisphere. Height anomalies are computed with respect to the 1979-1988 base period monthly means for a 10 degree latitude by 10 degree longitude grid. These anomalies then serve as the basis for a point correlation analysis for the Southern Hemisphere winter (May - September) and summer (November - March) seasons.

1. INTRODUCTION

With the establishment of the South American Desk within the Meteorological Operations Division of the National Meteorological Center (NMC) increased attention has been given to model forecasts in the Southern Hemisphere. As forecasting experience has increased so has the demand for climatological information on Southern Hemisphere teleconnection patterns. Having found the teleconnection atlas of Namias (1981) extremely useful in interpreting Northern Hemisphere anomaly patterns, forecasters sought a similar atlas for the Southern Hemisphere. This work is an attempt to meet their needs.

The discussion is organized such that data and analysis techniques are described in section 2. A synoptic description of the climatological mean 500 mb circulation features is then presented in section 3. Features which exhibit little seasonal variability, as well as features which exhibit pronounced seasonal variability, are described in this section. It should be noted that this synoptic discussion is designed exclusively to provide the forecaster with a "quick-look" at the key climatological mean mid-tropospheric circulation features, upon which the subsequent teleconnection patterns are superimposed. The primary one-point teleconnection patterns are then described in section 4.

The maps are organized such that monthly climatological mean (1979-1988) 500 mb height fields are presented first. These analyses highlight mean jet positions, mean trough and ridge positions, and regions of strong flow diffluence/confluence. Regions of large height field variability are also identified on the analyses. The winter (May - September) one-point correlation patterns are then presented, followed by the summer (November - March) one-point correlation patterns. Correlation

patterns were also computed using three-month seasons. Those patterns (not shown) are, in most cases, quite similar to the ones shown here for five-month seasons.

Both a summarization table and a teleconnectivity map (Wallace and Gutzler 1981) immediately precede the correlation patterns for each season. The tables summarize the primary structural characteristics of the teleconnection patterns for the given season. The teleconnectivity maps identify the base points which are associated with the strongest teleconnection patterns. Both the tables and the teleconnectivity maps provide the basis for a descriptive summary of the major Southern Hemisphere teleconnection patterns in section 4.

2. DATA AND ANALYSIS

The one point correlation patterns are based on the monthly final analyses of 500 mb geopotential height obtained from the NMC global data assimilation system (GDAS) for the period 1979-1990. During this period changes were made in the GDAS which greatly affected geopotential height analyses in the vicinity of mountainous terrain. Consequently, the derived patterns should not be considered true teleconnection patterns for points in the vicinity of elevated topography (e.g., over subtropical South America and the adjacent South Atlantic, over eastern Africa and over Indonesia).

Correlations are computed using the height anomaly time series at each point for a 10 degree latitude by 10 degree longitude grid. Anomalies are computed with respect to the 1979-1988 base period monthly means. Following Wallace and Gutzler (1981), the teleconnectivity maps are computed by plotting at each base point the strongest negative correlation value associated with that point, as determined from the one-point correlation maps. Arrows are then drawn connecting the various centers of strong teleconnectivity to the grid points with which they show the strongest negative correlation on their respective one-point correlation maps. As with the teleconnection patterns, the teleconnectivity patterns should not be considered true patterns in the vicinity of elevated topography.

3. CLIMATOLOGICAL FIELDS

The Southern Hemisphere climatological mean (1979-1988) 500 mb circulation is summarized for each calendar month in Figs. 1-6. The left panels in each figure show the climatological mean 500 mb height field (solid contours, interval is 120 m) and the corresponding standard deviation field (dashed contours, interval is 30 m). Regions in which standard deviation values exceed 125 m are shaded. The right panels in each figure show departures

from the climatological zonal mean: termed standing waves (contour interval is 30 m).

3a. Quasi-permanent features

Zonal flow clearly dominates the hemispheric circulation throughout the year. The zonally averaged zonal mean climatological wind speeds peak sharply near 50°S in January, and exhibit a broad maximum extending between 30°S and 50°S in July (Trenberth 1979, Trenberth 1981). Well-defined departures from zonal flow (termed standing waves), which are most prominent in zonal wave-1, can also be identified in all months. For the purposes of this Atlas, specific standing wave features which exhibit relatively little geographic variability from season to season are summarized in this sub-section. Standing wave features which exhibit pronounced geographic variability from season to season are summarized in Section 3b.

Certain features of the zonal wave 1 pattern exhibit relatively little geographic variability from season to season (van Loon and Jenne 1972; and Randel 1987). Important synoptic aspects of these wave features are summarized as follows. Over the central and western Indian Ocean, a standing trough at high latitudes, coupled with a standing ridge at middle latitudes, is associated with a mean annual jet position near 50°S. This pattern reflects strong zonal flow and an absence of blocking throughout the middle and high latitudes of the Indian Ocean sector (Trenberth and Mo 1985). Over the South Pacific, a quasi-permanent standing wave pattern having opposite polarity to that noted over the Indian Ocean sector is observed; a standing wave ridge axis is observed at high latitudes and a standing wave trough axis is observed in middle latitudes. This pattern reflects broad diffluent flow throughout the western and central South Pacific in all months. The pattern also reflects a double jet structure over the South Pacific, with separate speed maxima centered at the date line near 65°S and equatorward of New Zealand near 25-30°S (Arkin et. al. 1986; Trenberth 1987).

Finally, height field variability in all months is maximized between 45°S and 65-70°S, within the main belt of westerlies (Trenberth 1981). Contours of standard deviation are closely aligned with the height field contours, and exhibit very strong zonal symmetry. Individual standard deviation maxima are also strongly zonally elongated throughout the year. Seasonal variations in the distributions of height field variance are described in section 3b.

3b. Seasonal variations

Seasonal variations in the standing wave pattern are strongly controlled by zonal wavenumber 1, and are most pronounced over the Indian and South Pacific Ocean basins. Over

the Indian Ocean sector, standing wave trough axes are observed to the southwest of Australia and to the south of Africa between January and July. During this same period, a weaker amplitude standing wave ridge axis, displaced equatorward and westward from the standing wave trough, strengthens slowly during April - July after reaching minimum amplitude in January.

Between August and October a single standing trough is observed over the south-central Indian Ocean. This trough is larger in amplitude than is observed over the region during January - July, and is associated with an intensification and eastward shift of the mean jet to its late-winter/early fall position over the central Indian Ocean. During October, this standing wave trough weakens and redevelops further west. The mean trough axis then becomes located over the western Indian Ocean during November and December. Also, as the warm season progresses, the standing ridge axis over the western Indian Ocean weakens.

Over the southern South Pacific Ocean, a well-defined standing wave ridge is observed during all months of the year. The ridge axis retrogresses slowly from the central to the western South Pacific between November and July, and intensifies markedly from the warm to the cold season. The ridge reaches maximum amplitude in June. Farther north, a standing wave trough begins to amplify during May. The trough subsequently expands westward and occupies the entire mid-latitude belt from western Australia to the central South Pacific (the mean trough axis is located near 150-160^{o}W) during June-August. Thus, the cool season standing wave pattern over the western South Pacific is dominated by a ridge at high latitudes and by a trough at middle latitudes. This pattern is consistent with diffluent flow throughout the central South Pacific, and with a maximum occurrence of blocking events at high latitudes of the western and central South Pacific (van Loon 1956; Mo 1983; Trenberth and Swanson 1983; Lejenäs 1984; Kayano and Kousky 1990). During September and October, the standing wave pattern weakens, and the central South Pacific ridge shifts to the high latitudes of the eastern South Pacific.

Over the hemisphere as a whole, height field variability is maximized within the main belt of westerlies, with maximum values of standard deviation ranging from 110 m to 150 m throughout the year. The areal extent of large height field variability (standard deviation values greater than 125 m) is smallest during the warm season (November - February) and largest during the cool season, particularly in April and May. In all seasons, height field variability is maximized to the south of New Zealand and over the central Indian Ocean (see Trenberth 1981 and Trenberth 1982 for a more detailed description of the variance characteristics of the Southern Hemisphere 500 mb height field).

4. **DISCUSSION**

The one-point correlation patterns in both seasons tend to assume one of the four configurations described below. These configurations are used as a basis for summarizing in tabular form the primary structural characteristics of the teleconnection patterns. The summary table for each season is located just prior to the correlation charts for that season.

The four basic teleconnection patterns are defined as follows:

Meridional dipole, zonally elongated: Zonally elongated anomalies with at least one primary negative correlation center displaced meridionally from the primary positive correlation center.

Wave 3 (or 4) pattern: Well-defined zonal wave 3 (or 4) pattern at the base-point latitude.

Wave 3 (or 4) pattern with zonal symmetry: Regions of positive and negative correlation extend zonally around the hemisphere, but with well-defined zonal wave 3 (or 4) pattern at the base-point latitude.

Isolated Anomaly: Primary positive correlation center is surrounded by regions of strong negative correlation. No well-defined regions of positive correlation are found away from the primary center.

4a. Winter (May - September)

Zonally elongated features are particularly strong when reference points are taken at subtropical latitudes and near the pole. The patterns at 20^{o}S and 30^{o}S tend to be zonally elongated, with one primary negative correlation center displaced poleward from the base point by approximately 30^{o} latitude. The correlation patterns then assume a wave 3 structure between 40^{o}S and 50^{o}S over the South Atlantic and over the Indian Ocean, but remain zonally elongated throughout the South Pacific until 50^{o}S. The pattern over the South Pacific then maintains a wave 3 structure throughout much of the 50^{o}S and 60^{o}S latitude bands. This wavenumber 3 pattern has been discussed thoroughly by Mo and White (1985). The eastward shift of the wave 3 pattern toward higher latitudes of the South Pacific, and toward lower latitudes of the Atlantic and Indian Oceans, appears to reflect the climatological poleward displacement of the mean jet position over the South Pacific relative to the other ocean basins (see section 3).

Poleward of the climatological mean westerlies, the correlation patterns assume a more zonally elongated structure. A significant exception is noted over the high latitudes of the

eastern South Pacific, where the pattern exhibits a strong isolated anomaly structure. This structure partly reflects the occurrence of persistent blocking episodes. During these blocking episodes, positive anomalies are observed over the block region, surrounded by negative anomalies to the east, west and north (Bell 1991). Finally, negative correlations with the South Pole tend to be most pronounced near 45°S over the Indian and Atlantic Oceans.

The winter teleconnectivity patterns show strong regional variations, with certain regions experiencing standing wave oscillations having distinct nodes and antinodes. Similar patterns have been previously determined for the Northern Hemisphere (Wallace and Gutzler 1981). Teleconnectivity values are highest from south of Australia eastward through the central Pacific, and are generally lowest over the Atlantic and Indian Ocean sectors. High teleconnectivity over the western South Pacific is related to blocking activity (enhanced westerlies) when positive (negative) height anomalies are observed at high latitudes. In contrast, low teleconnectivity values over the Indian and Atlantic Oceans are associated with minimum blocking activity. The teleconnectivity pattern over the eastern South Pacific resembles the Pacific/South American (PSA) pattern identified by Mo and Ghil (1987). This pattern tends to be well pronounced during blocking episodes and during equatorial Pacific warm episodes (Karoly 1989).

4b. Summer (November - March)

The summer patterns resemble their winter counterparts in featuring zonally elongated structures in the subtropics and poleward of 60°S. In mid-latitudes, the summer pattern is more zonally elongated than its winter counterpart, but tends to maintain a wave number 3 or 4 structure. These features have been documented by Mo and White (1985) using 500 mb heights and by Trenberth and Christy (1985) using sea level pressures. The summer correlation patterns at 60°S differ from their winter counterparts in that they exhibit the following features: a more isolated anomaly pattern over the South Atlantic and Indian Oceans, and a more zonally elongated pattern over the western and central South Pacific.

The summer teleconnectivity pattern is similar to the corresponding winter pattern, in that maximum teleconnectivity is confined primarily to the middle and high latitudes of the western and central South Pacific. The primary differences between the two charts are found over the eastern Indian and eastern South Pacific Oceans. The wintertime north-south dipoles over both regions are absent during summer. Over the eastern Pacific this reflects a reduction in the frequency of blocking activity and an absence of the PSA pattern during the warm season. The large negative correlation centered near 10°S,140°W

is part of the zonally symmetric pattern of height anomalies which shows a reversal between low and mid-latitudes (see, for example, the one-point correlation maps for 20°S,140°W and for 50°S,30°E).

5. ACKNOWLEDGMENTS

We are grateful to Kingtse Mo and Ed O'Lenic for reviewing the atlas. Special thanks go to John Kopman for his suggestions and help in preparing the figures.

6. REFERENCES

Arkin, P. A., V. E. Kousky, and E. A. O'Lenic, 1986: Atlas of the tropical and subtropical circulation derived from National Meteorological Center operational analyses. Dept. of Commerce, NOAA Atlas No. 7. Copies can be obtained from the Climate Analysis Center, W/NMC52, 5200 Auth Rd, Washington D.C., 20233.

Bell, G. D., 1991: Diagnosis of a blocking episode over the south-central South Pacific. Proceedings of the Sixteenth Climate Diagnostics Workshop. Los Angeles, CA, October 1991, (in press).

Karoly, D. J., 1989: Southern Hemisphere circulation features associated with El Nino-Southern Oscillation events. J. Climate, **2**, 1239-1252.

Kayano, M. T., and V. E. Kousky, 1990: Southern Hemisphere blocking: A comparison between two indices. Meteorol. Atmos. Phys., **42**, 165-170.

Lejenäs, H., 1984: Characteristics of southern hemisphere blocking as determined from a long time series of observational data. Quart. J. Roy. Meteor. Soc., **100**, 967-979.

Mo, K. C., 1983: Persistent anomalies of the Southern Hemisphere circulation. Proceedings of the First International Conference on Southern Hemisphere Meteorology, Sao José dos Campos, SP, Brazil, August 1983, Amer. Meteor. Soc., 70-72.

Mo, K. C., and G. H. White, 1985: Teleconnections in the Southern Hemisphere. Mon. Wea. Rev., **113**, 22-37.

Mo, K. C., and M. Ghil, 1987: Statistics and dynamics of persistent anomalies. J. Atmos. Sci., **44**, 877-901.

Namias, J., 1981: Teleconnections of 700 mb height anomalies for the Northern Hemisphere. CALCOFI Atlas No. 29, Scripps Institution of Oceanography, La Jolla, CA, 92093, 265 pp.

Randel, W. J., 1987: A study of planetary scale waves in the southern winter troposphere, Part 1: wave structure and vertical propagation. J. Atmos. Sci., **44**, 917-935.

Trenberth, K. E., and G. S. Swanson, 1983: Blocking and persistent anomalies in the Southern Hemisphere. Proceedings of the First International Conference on Southern Hemisphere Meteorology, Sao José dos Campos, SP, Brazil, August 1983, Amer. Meteor. Soc., 73-76.

Trenberth, K. E., 1979: Interannual variability of the 500 mb zonal mean flow in the Southern Hemisphere. Mon. Wea. Rev., **107**, 1515-1524.

Trenberth, K. E., 1981: Observed Southern Hemisphere eddy statistics at 500 mb: frequency and spatial dependence. J. Atmos. Sci., **38**, 2585-2605.

Trenberth, 1982: Seasonality in Southern Hemisphere eddy statistics at 500 mb. J. Atmos. Sci., **39**, 2507-2520.

Trenberth, K. E., 1987: The zonal mean westerlies over the Southern Hemisphere. Mon. Wea. Rev., **115**, 1528-1533.

Trenberth, K. E., and J. R. Christy, 1985: Global fluctuations in the distribution of atmospheric mass. J. Geophys. Res., **90**, 8042-8052.

Trenberth, K. E., and K. C. Mo, 1985: Blocking in the Southern Hemisphere. Mon. Wea. Rev., **113**, 3-21.

van Loon, H., 1956: Blocking action in the southern hemisphere, Part I. Notos, **5**, 171-177.

van Loon, H., and R. L. Jenne, 1972: The zonal harmonic standing waves in the Southern Hemisphere. J. Geophys. Res., **77**, 3846-3855.

Wallace, J. M., and D. S. Gutzler, 1981: Teleconnections in the geopotential height field during the Northern Hemisphere winter. Mon. Wea. Rev., **109**, 784-812.

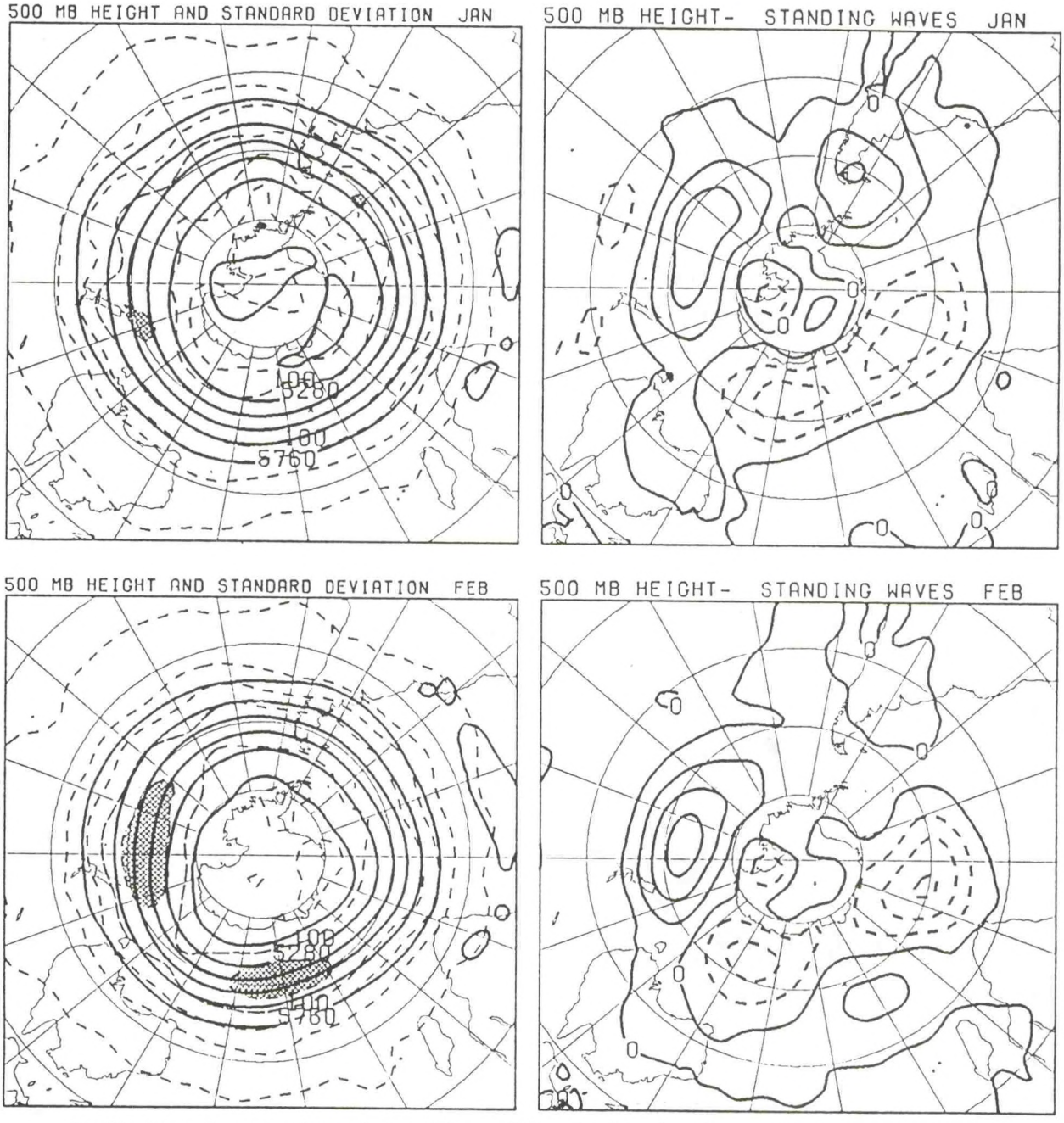

Left-hand panels show the climatological mean 500 mb heights (solid) and standard deviation (dashed) for January (top) and February (bottom). Right-hand panels show the corresponding climatological mean 500 mb height field with zonal means removed (termed standing waves). Contour interval for heights is 120 m, and for both standard deviation and standing waves is 30 m. Regions in which standard deviation values exceed 125 m are shaded. Analyses are based on monthly mean 500 mb maps for the period 1978-1988.

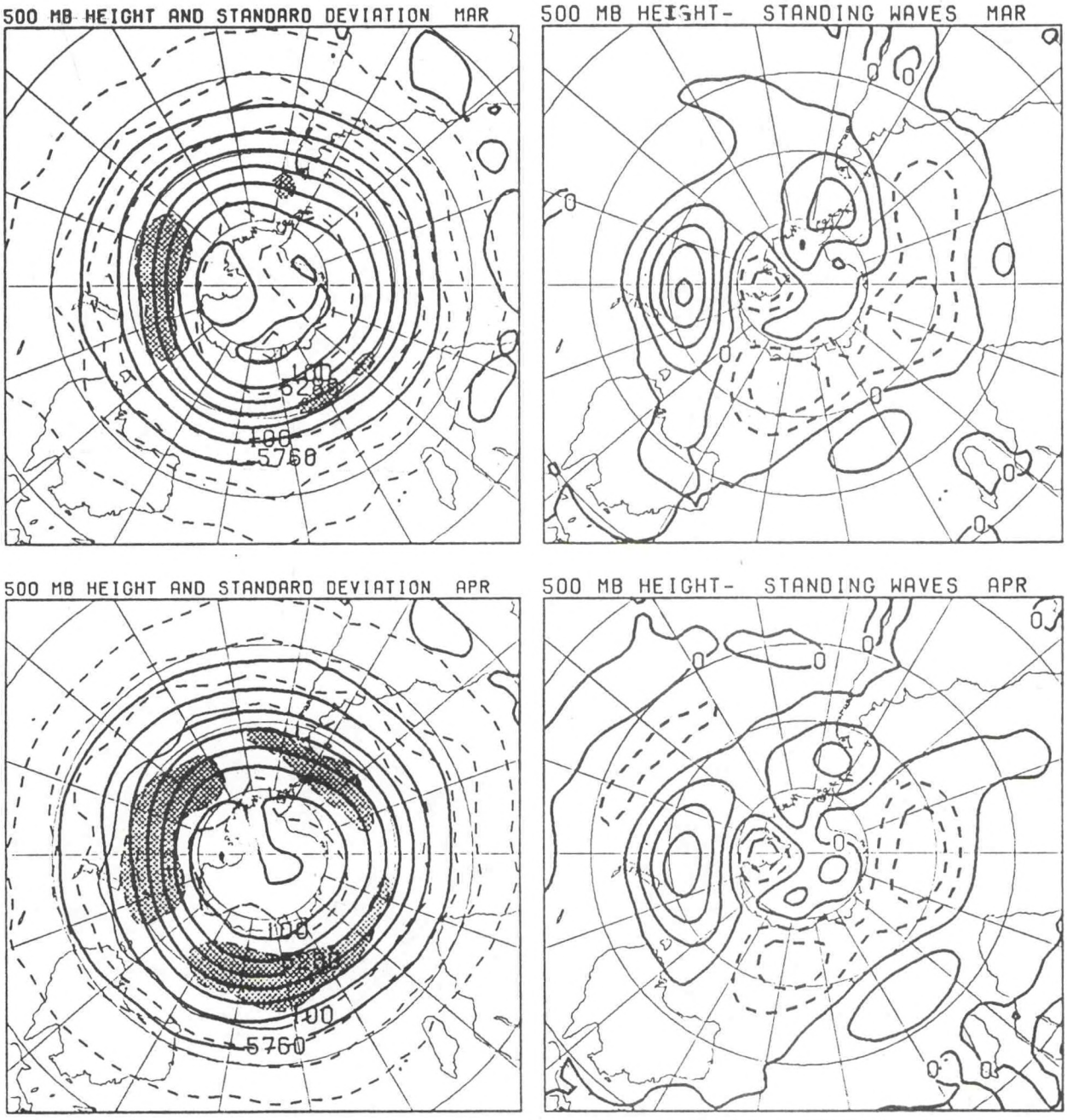

Left-hand panels show the climatological mean 500 mb heights (solid) and standard deviation (dashed) for March (top) and April (bottom). Right-hand panels show the corresponding climatological mean 500 mb height field with zonal means removed (termed standing waves). Contour interval for heights is 120 m, and for both standard deviation and standing waves is 30 m. Regions in which standard deviation values exceed 125 m are shaded. Analyses are based on monthly mean 500 mb maps for the period 1978-1988.

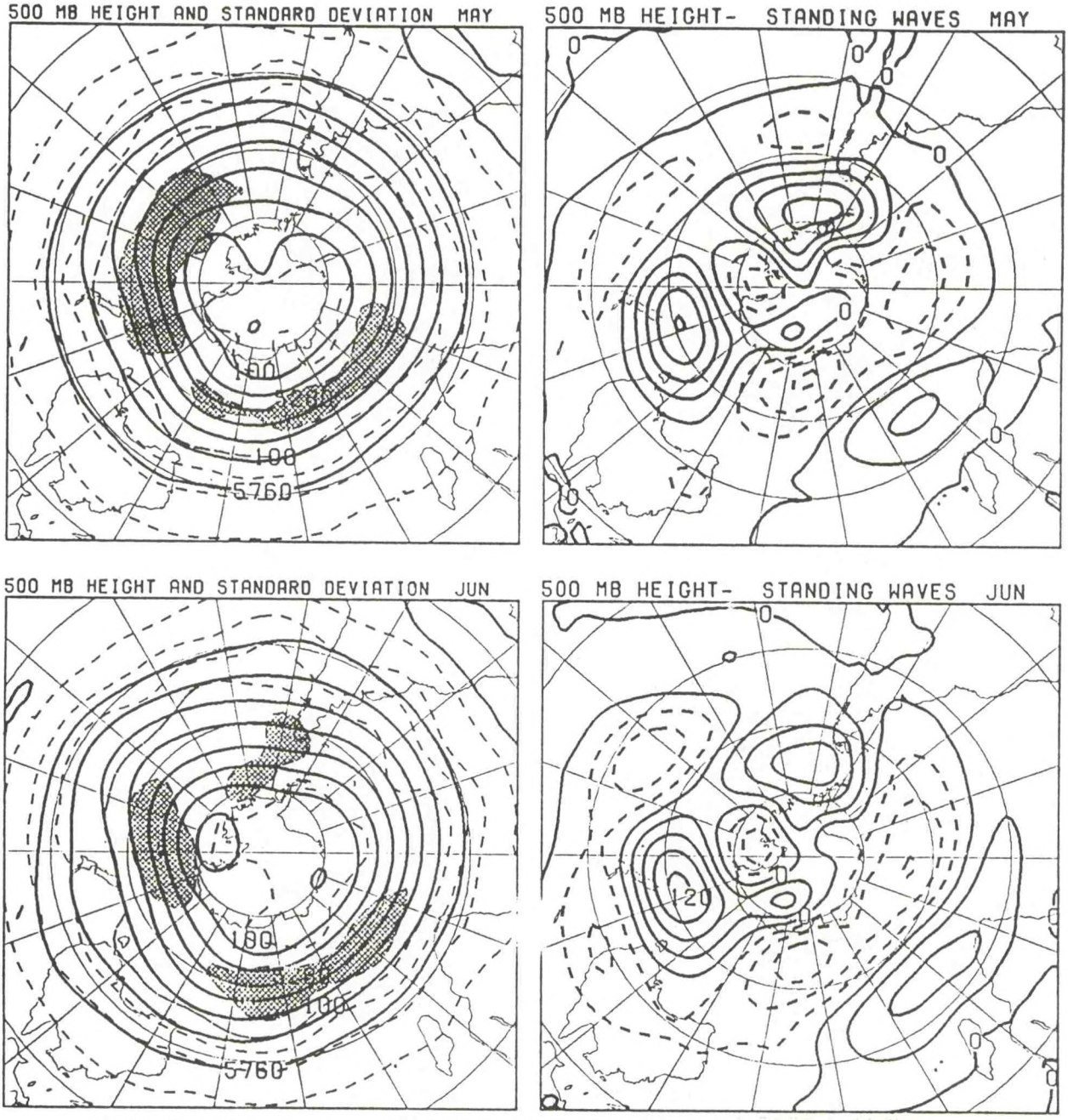

Left-hand panels show the climatological mean 500 mb heights (solid) and standard deviation (dashed) for May (top) and June (bottom). Right-hand panels show the corresponding climatological mean 500 mb height field with zonal means removed (termed standing waves). Contour interval for heights is 120 m, and for both standard deviation and standing waves is 30 m. Regions in which standard deviation values exceed 125 m are shaded. Analyses are based on monthly mean 500 mb maps for the period 1978-1988.

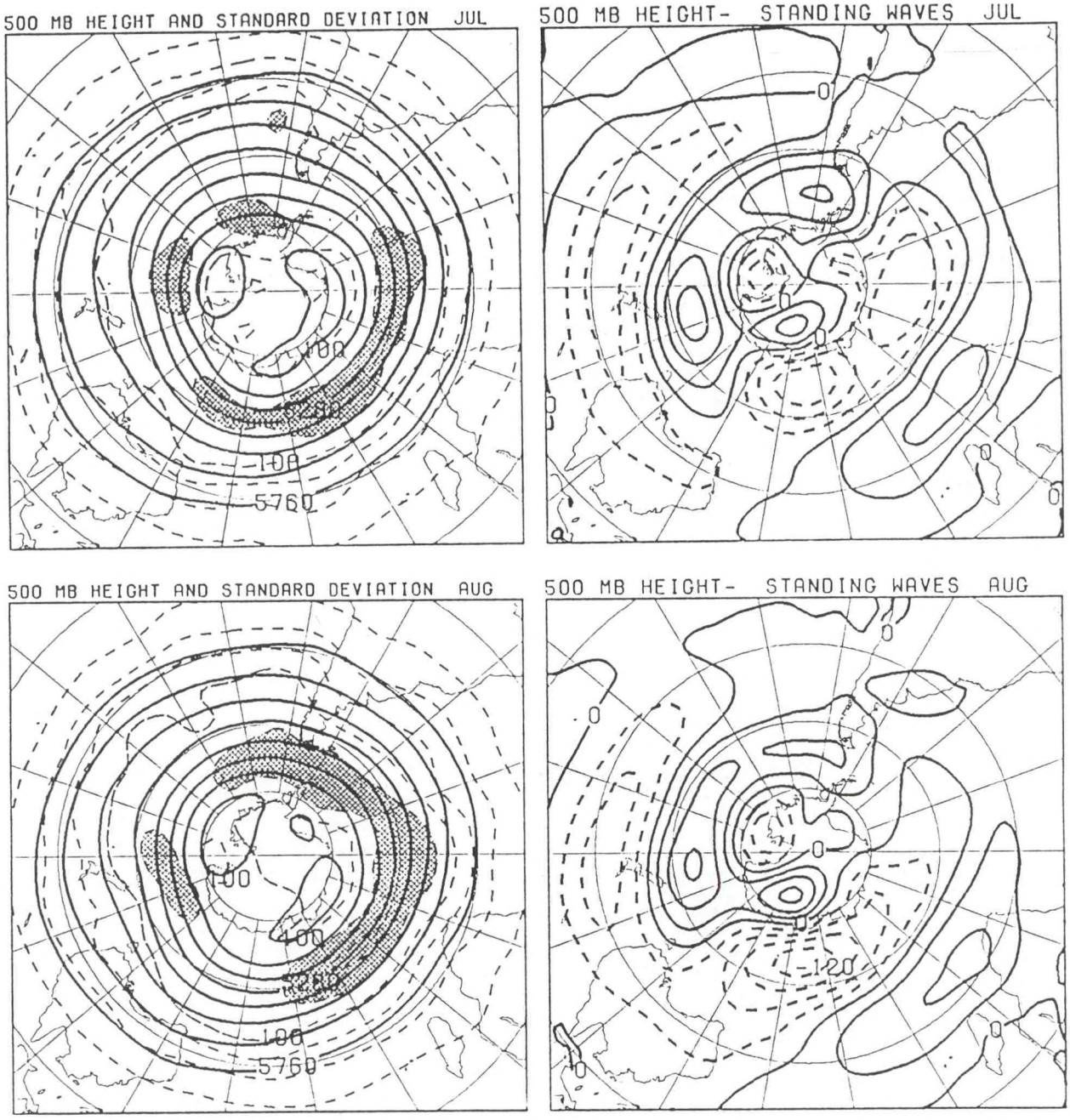

Left-hand panels show the climatological mean 500 mb heights (solid) and standard deviation (dashed) for July (top) and August (bottom). Right-hand panels show the corresponding climatological mean 500 mb height field with zonal means removed (termed standing waves). Contour interval for heights is 120 m, and for both standard deviation and standing waves is 30 m. Regions in which standard deviation values exceed 125 m are shaded. Analyses are based on monthly mean 500 mb maps for the period 1978-1988.

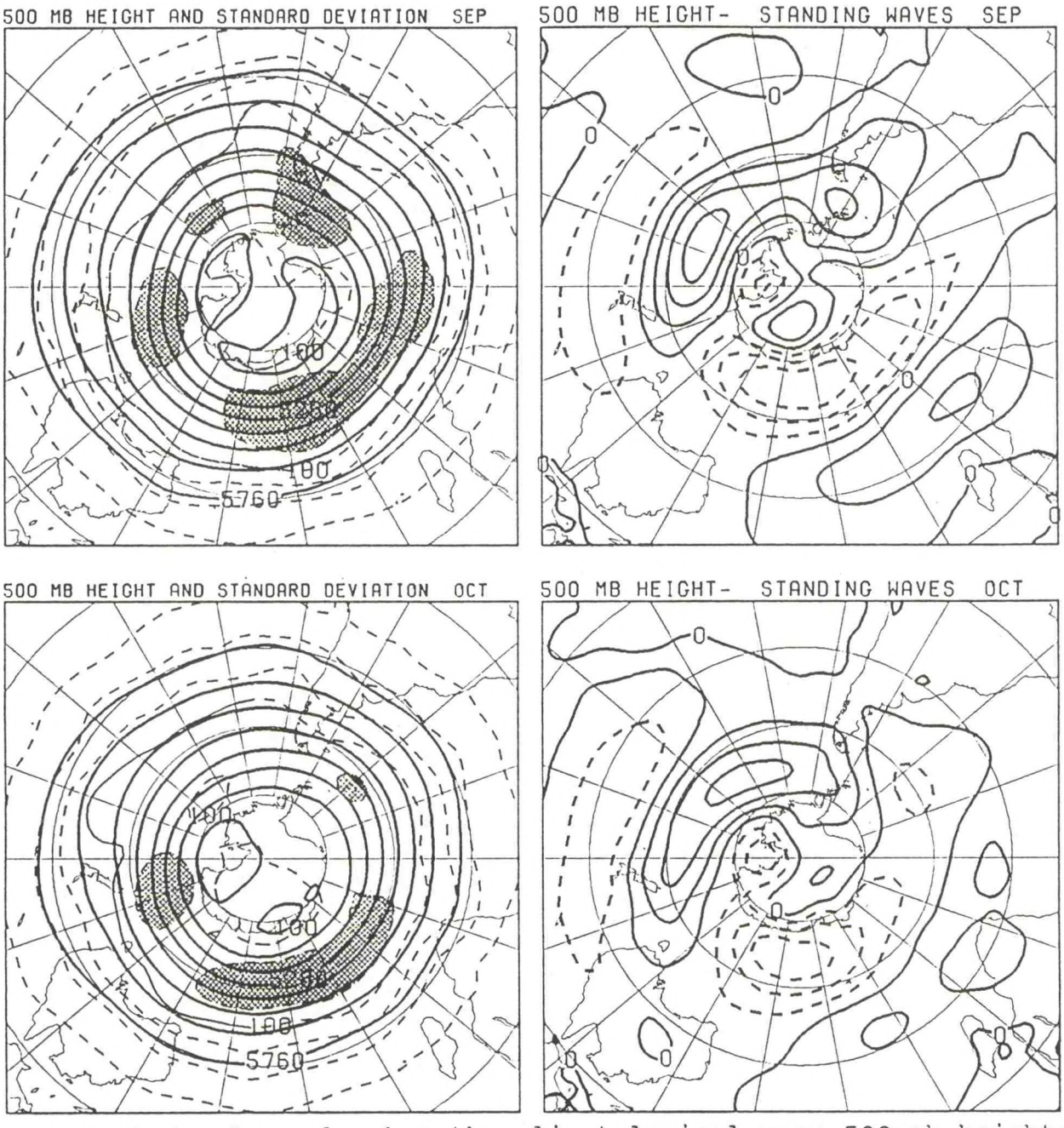

Left-hand panels show the climatological mean 500 mb heights (solid) and standard deviation (dashed) for September (top) and October (bottom). Right-hand panels show the corresponding climatological mean 500 mb height field with zonal means removed (termed standing waves). Contour interval for heights is 120 m, and for both standard deviation and standing waves is 30 m. Regions in which standard deviation values exceed 125 m are shaded. Analyses are based on monthly mean 500 mb maps for the period 1978-1988.

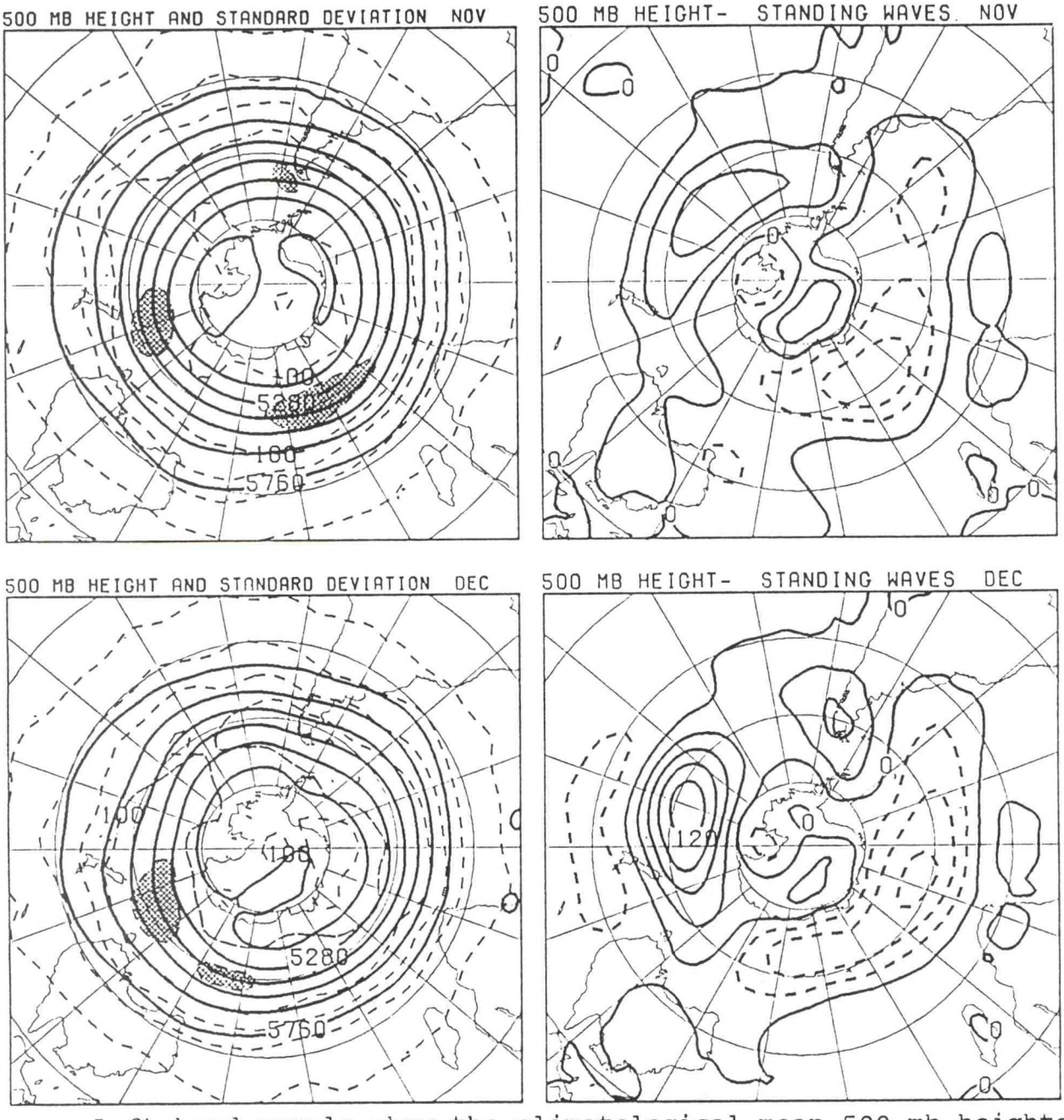

Left-hand panels show the climatological mean 500 mb heights (solid) and standard deviation (dashed) for November (top) and December (bottom). Right-hand panels show the corresponding climatological mean 500 mb height field with zonal means removed (termed standing waves). Contour interval for heights is 120 m, and for both standard deviation and standing waves is 30 m. Regions in which standard deviation values exceed 125 m are shaded. Analyses are based on monthly mean 500 mb maps for the period 1978-1988.

WINTER (MAY–SEPT)

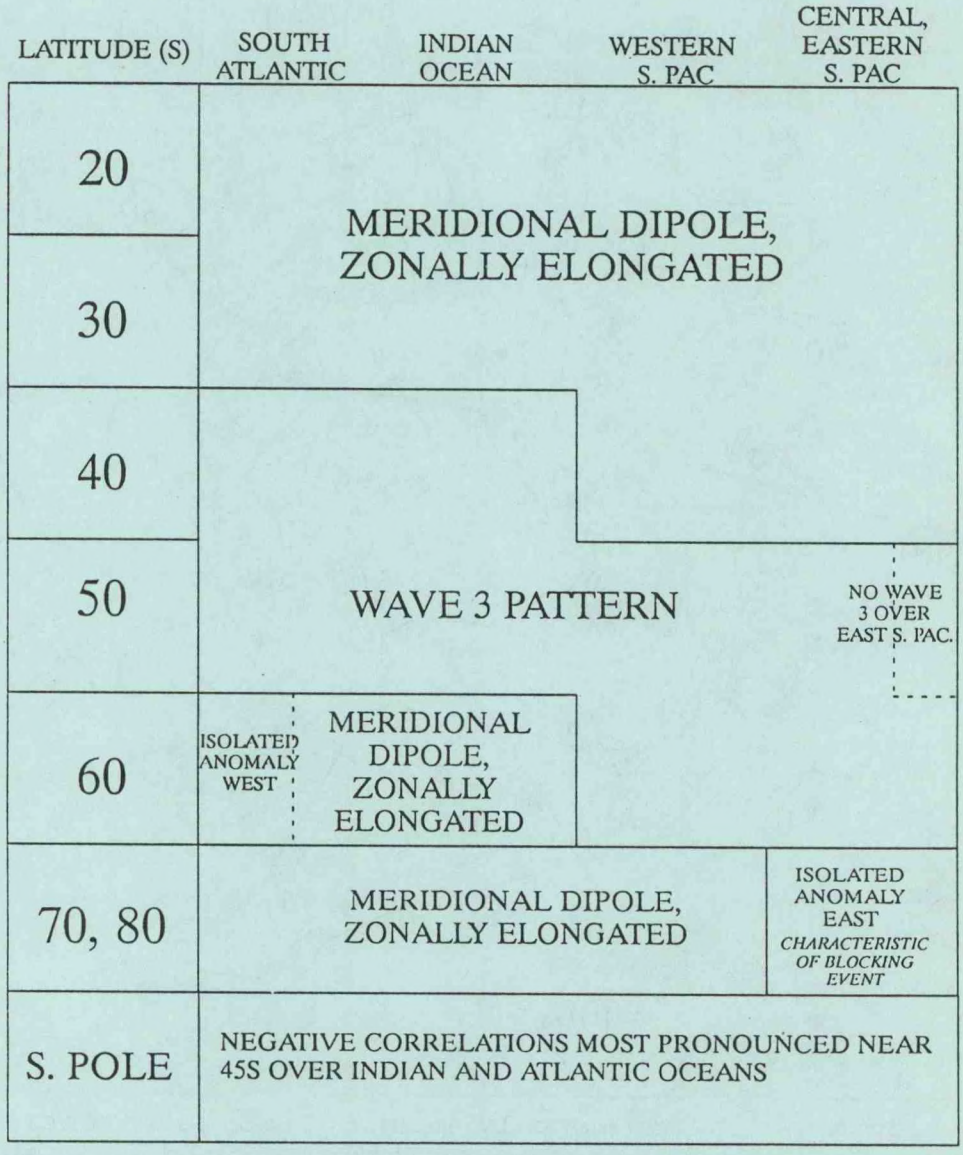

TABLE 1: Summary of wintertime (May - September) teleconnection patterns determined subjectively from one-point teleconnection maps computed from monthly mean 500 mb height anomalies for the period 1979-1990. Patterns are identified at 10^{o} latitude increments for five primary regions: The South Atlantic, the Indian Ocean, the western South Pacific, the central and eastern South Pacific, and the polar region. See Introduction for a description of terms.

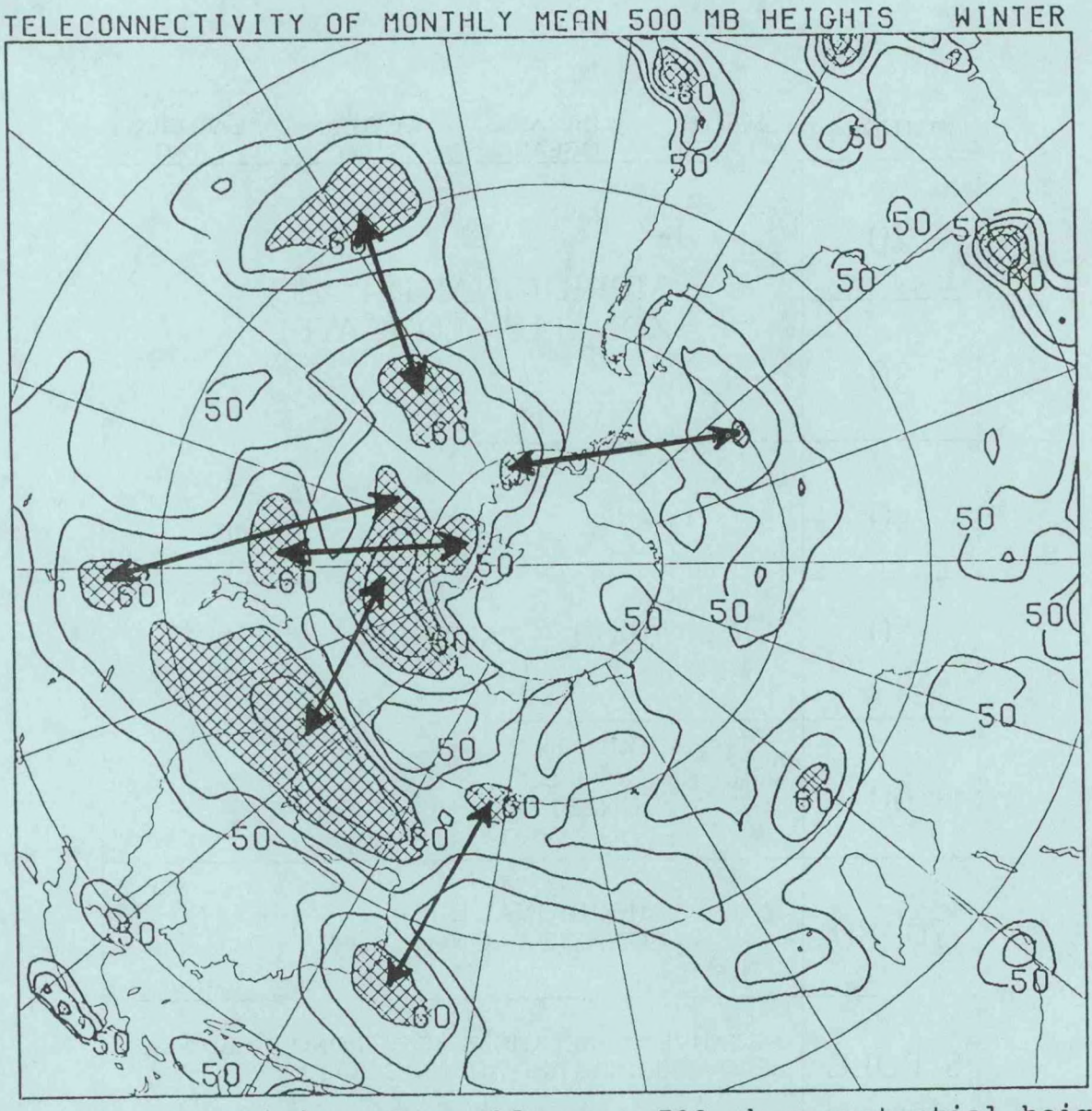

Teleconnectivity of monthly mean 500 mb geopotential height anomalies for the Southern Hemisphere cold season (May - September), showing the strongest negative correlations (negative signs omitted) for each one-point correlation map plotted at the base grid point. Correlations are multiplied by 100 and are only contoured for values less than -0.5. Values less than -0.6 are shaded. Arrows connect centers of strongest teleconnectivity with grid points which show strongest negative correlation on their respective one-point correlation maps. High teleconnectivity values in the vicinity of elevated terrain are due to changes in model resolution and/or changes in analysis procedures. For those regions the values should be ignored (see text).

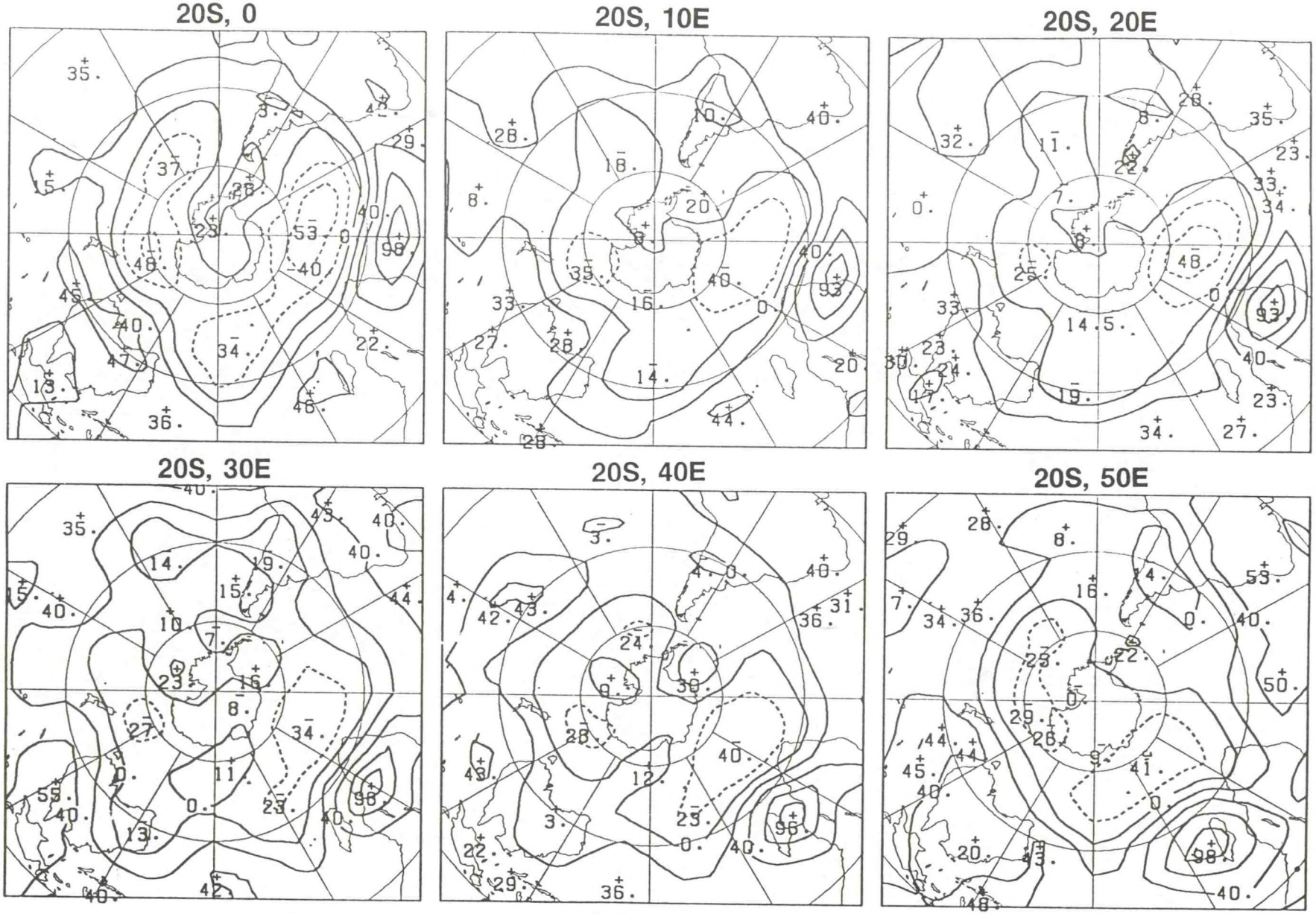
20S, 0
20S, 10E
20S, 20E
20S, 30E
20S, 40E
20S, 50E

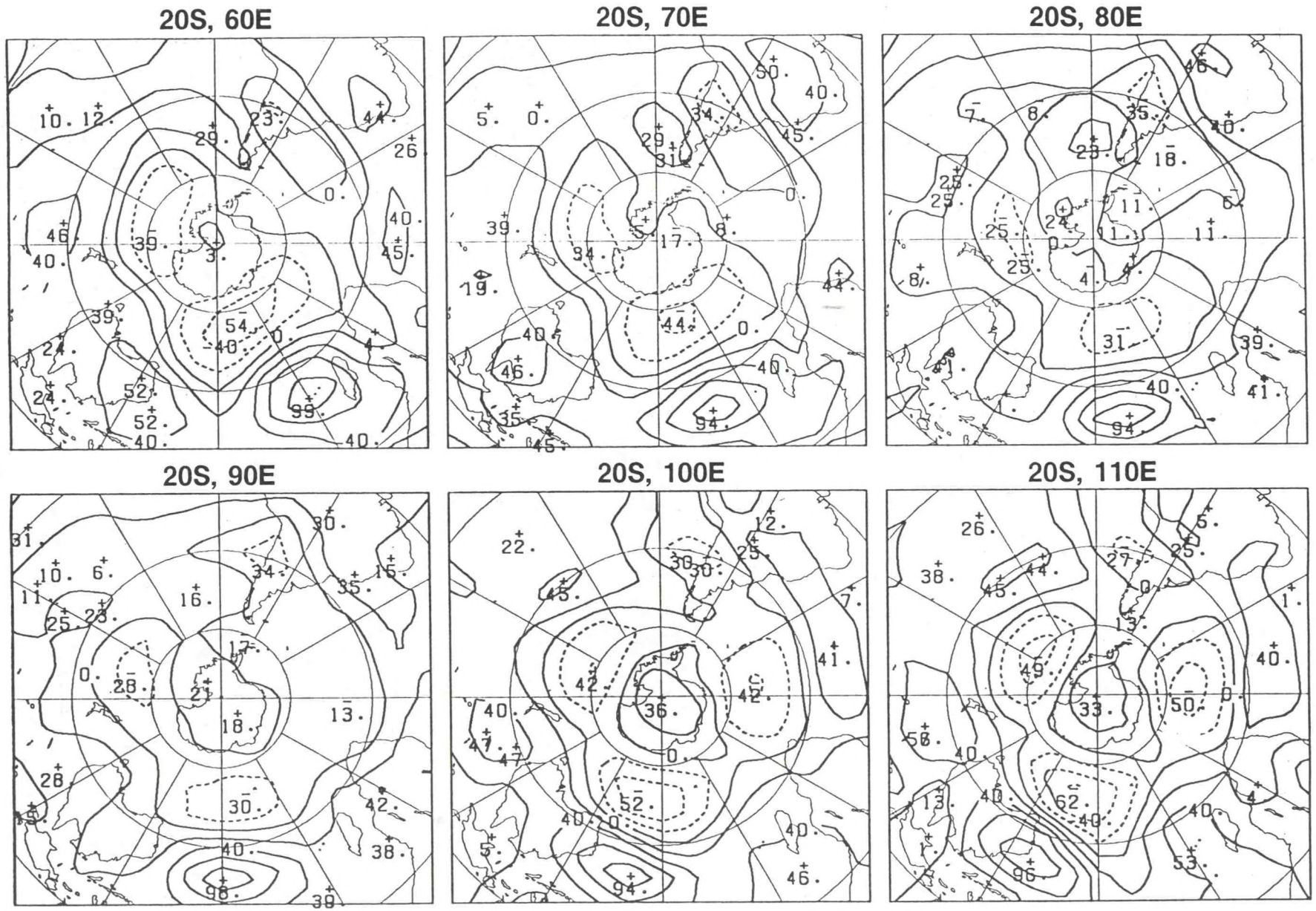
20S, 60E
20S, 70E
20S, 80E
20S, 90E
20S, 100E
20S, 110E

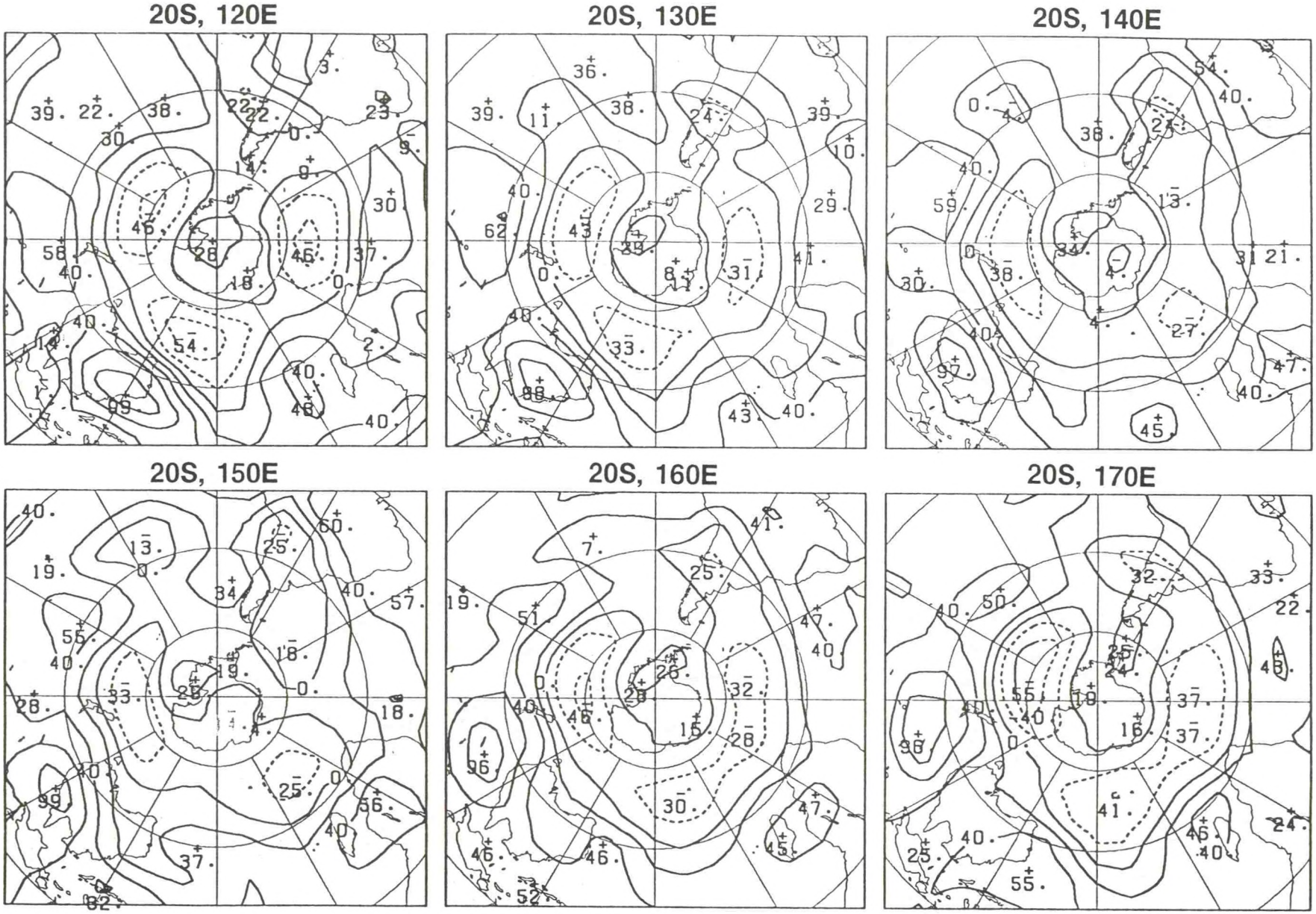
20S, 120E
20S, 130E
20S, 140E
20S, 150E
20S, 160E
20S, 170E

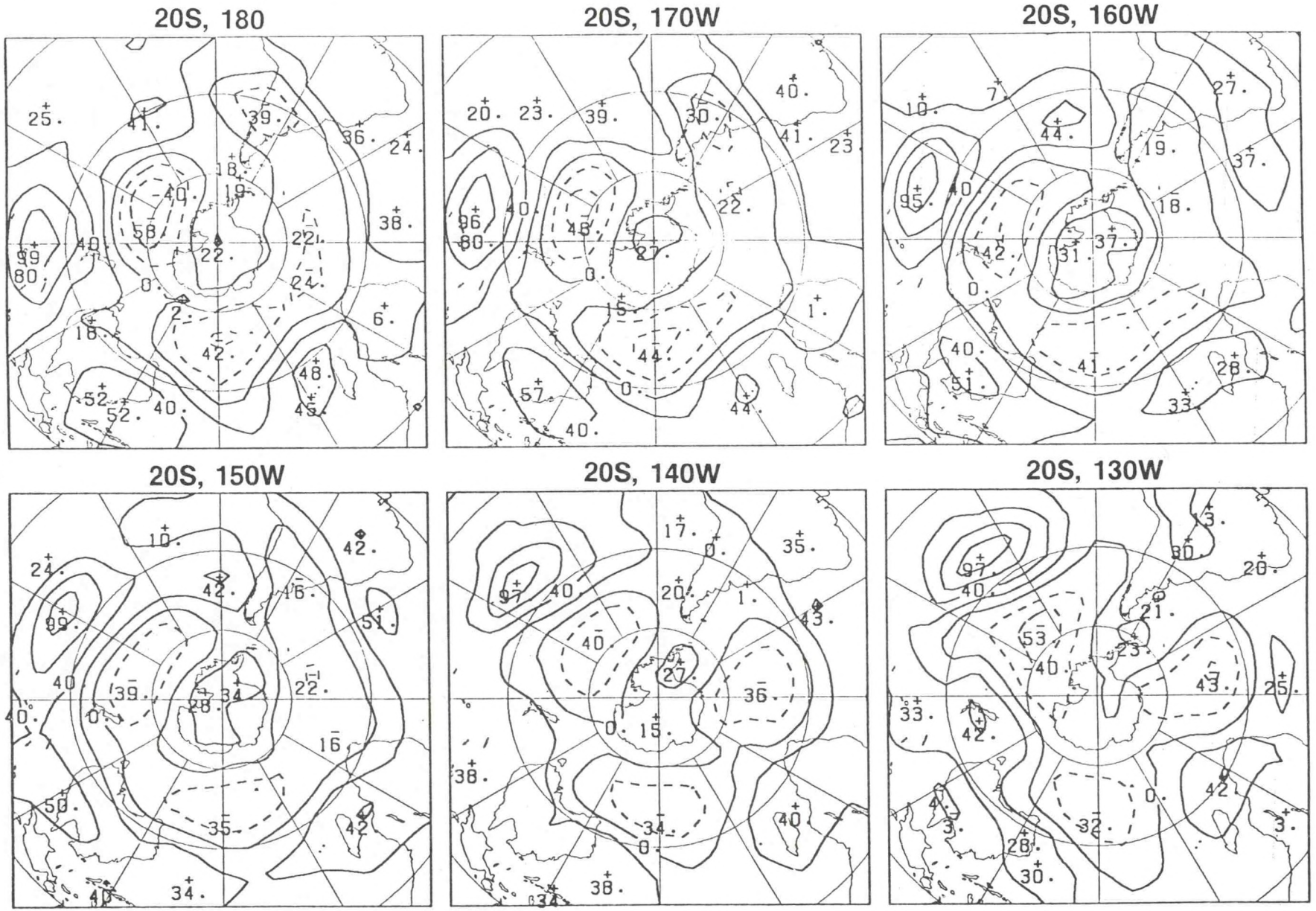
20S, 180
20S, 170W
20S, 160W
20S, 150W
20S, 140W
20S, 130W

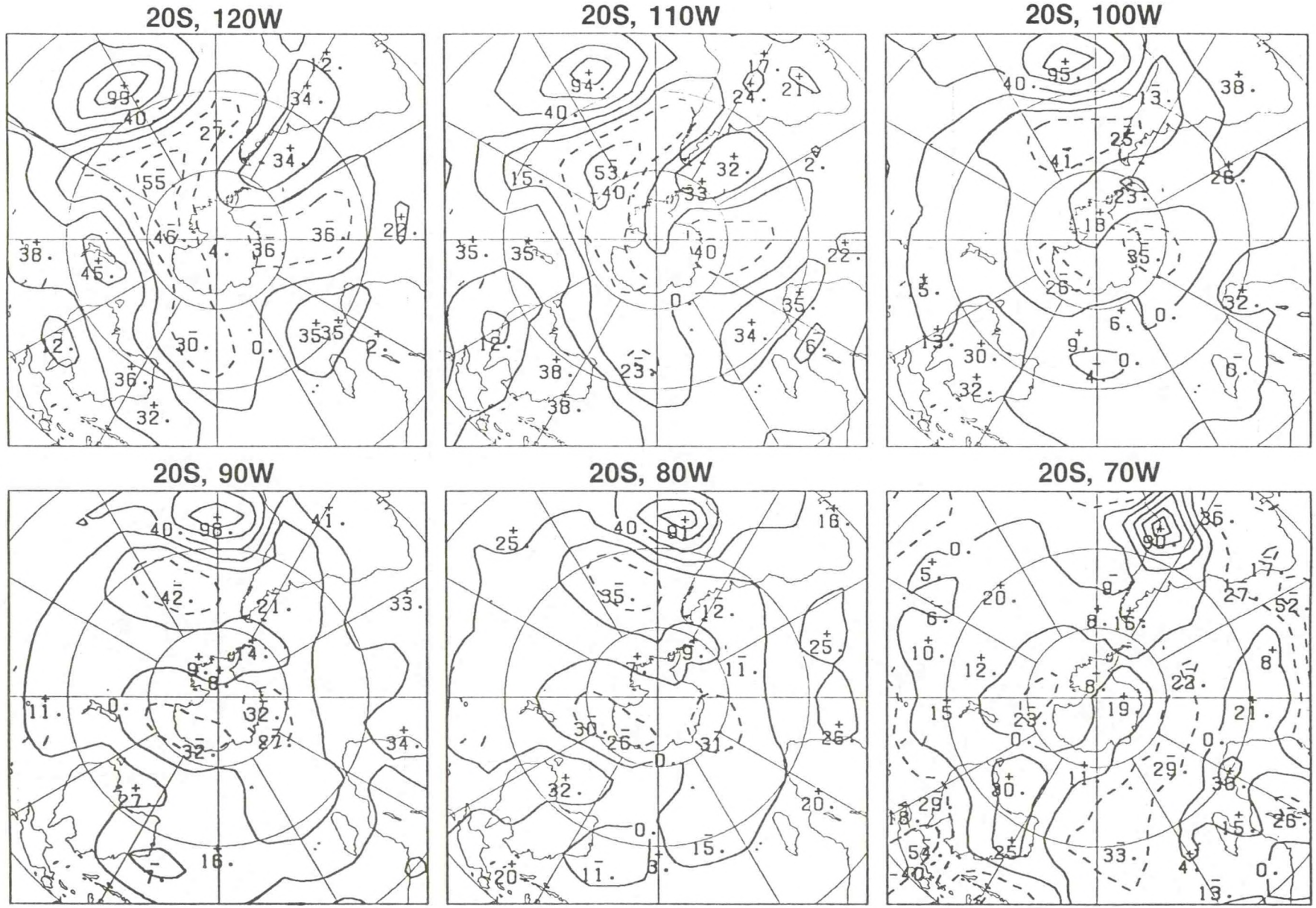
20S, 120W
20S, 110W
20S, 100W
20S, 90W
20S, 80W
20S, 70W

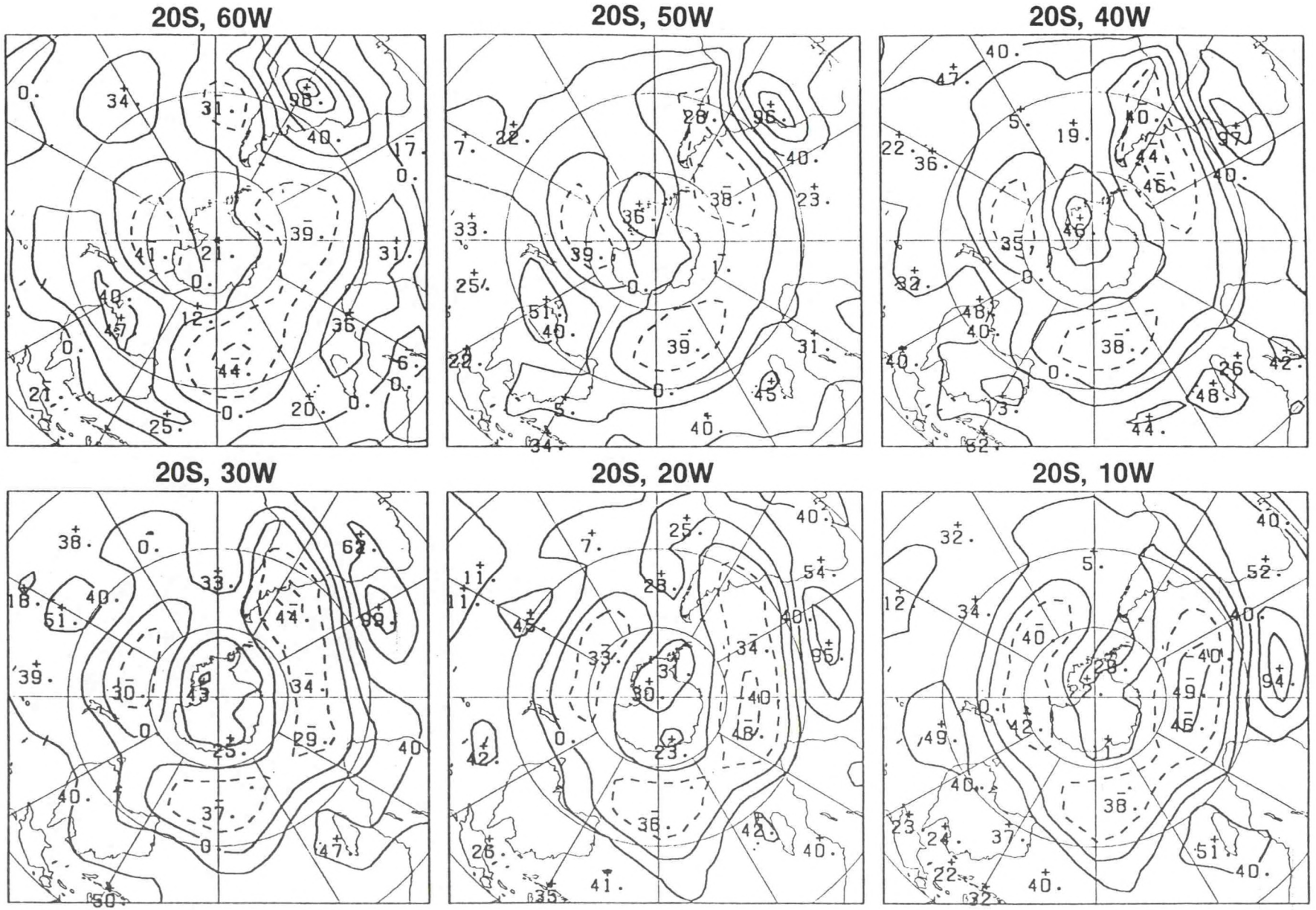
20S, 60W
20S, 50W
20S, 40W
20S, 30W
20S, 20W
20S, 10W

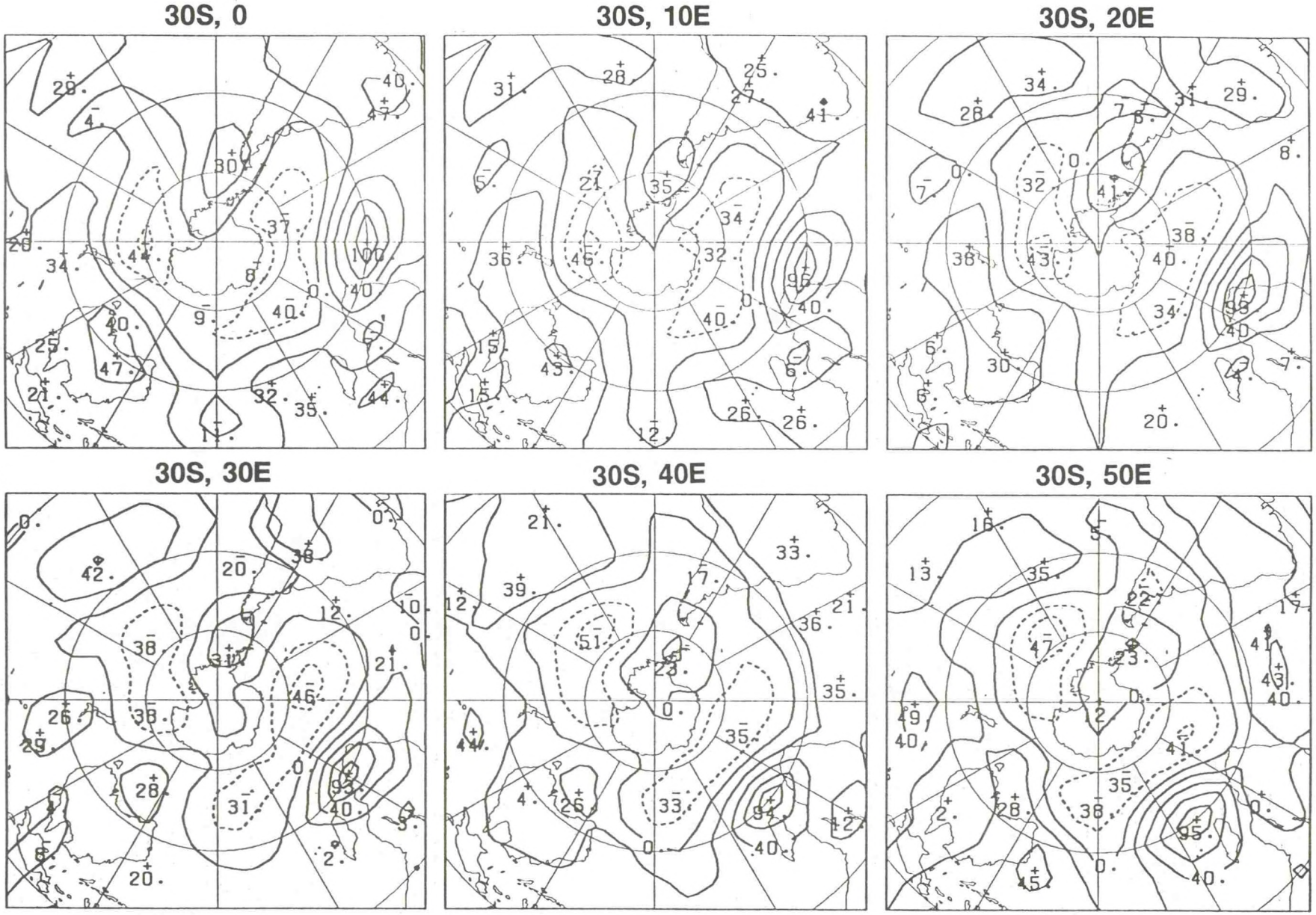
30S, 0
30S, 10E
30S, 20E
30S, 30E
30S, 40E
30S, 50E

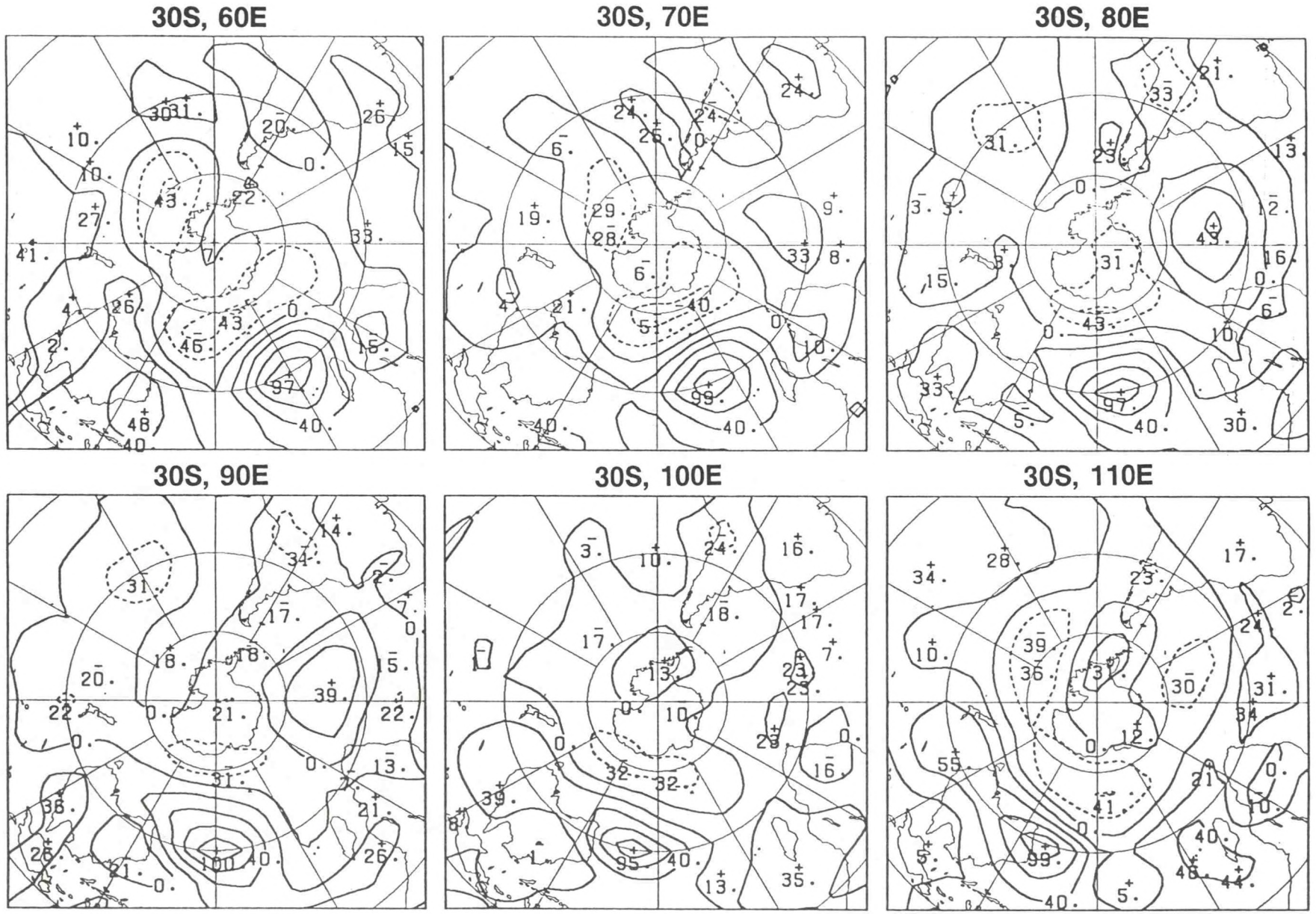
30S, 60E
30S, 70E
30S, 80E
30S, 90E
30S, 100E
30S, 110E

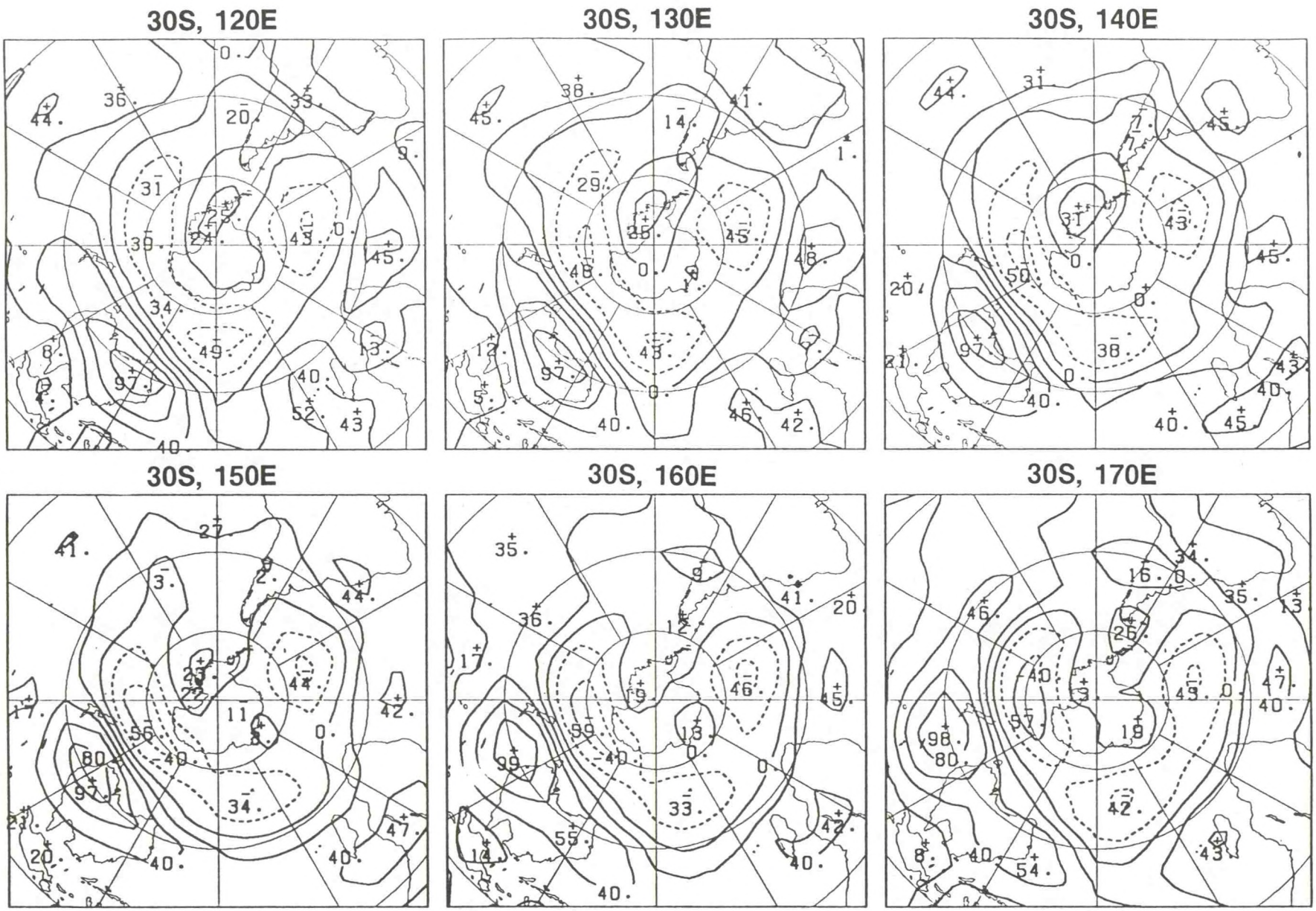
30S, 120E
30S, 130E
30S, 140E
30S, 150E
30S, 160E
30S, 170E

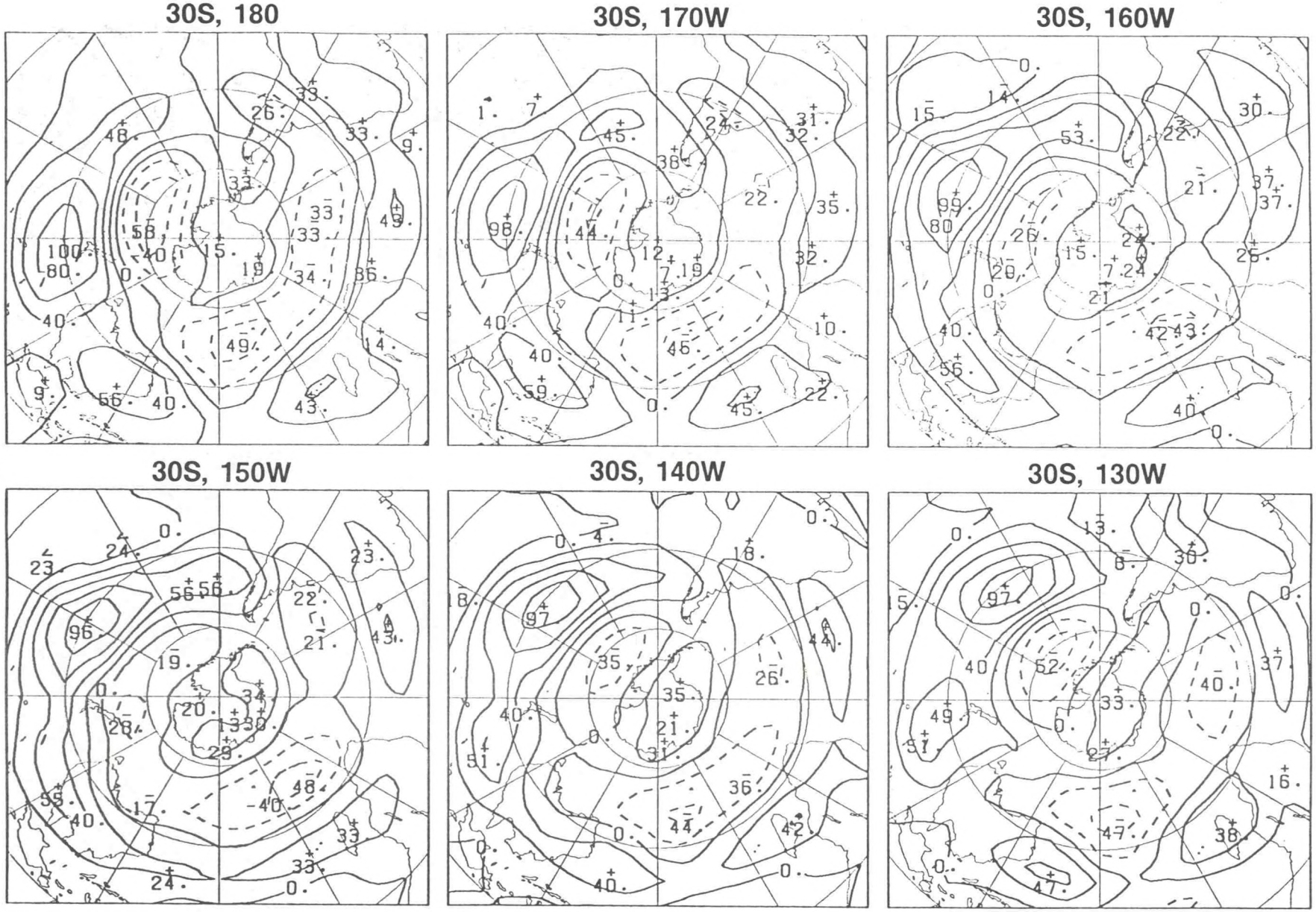
30S, 180
30S, 170W
30S, 160W
30S, 150W
30S, 140W
30S, 130W

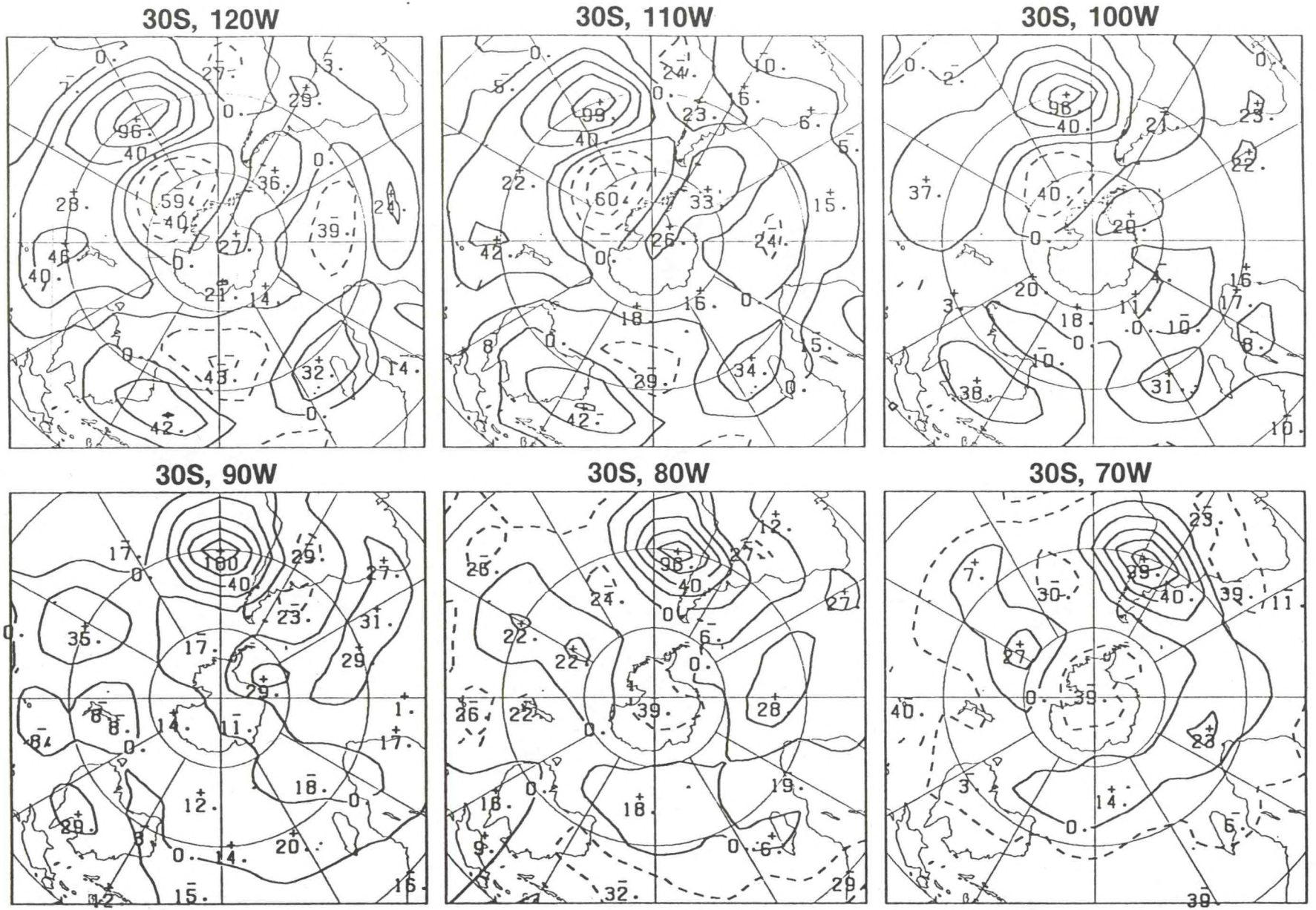
30S, 120W
30S, 110W
30S, 100W
30S, 90W
30S, 80W
30S, 70W

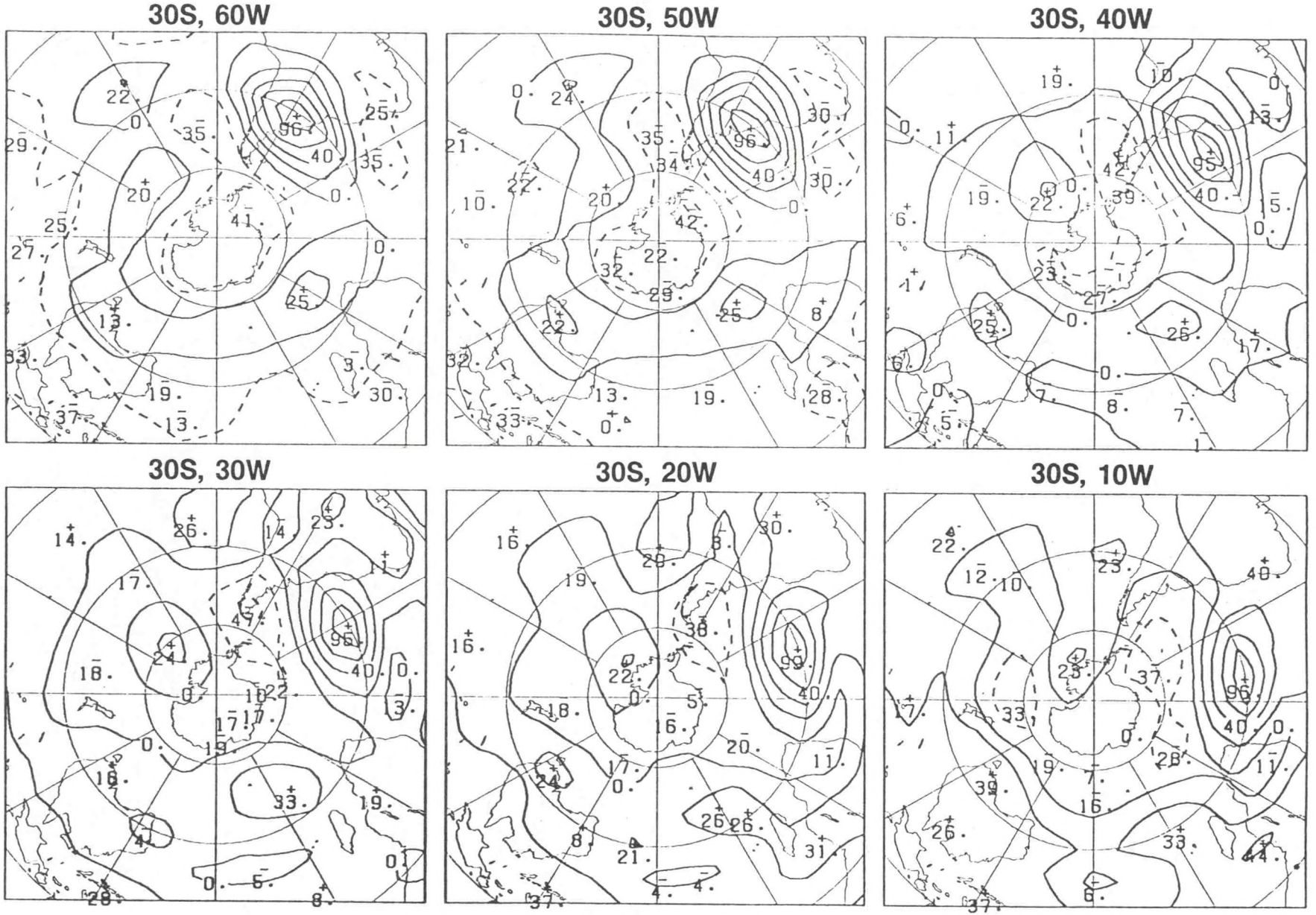
30S, 60W
30S, 50W
30S, 40W
30S, 30W
30S, 20W
30S, 10W

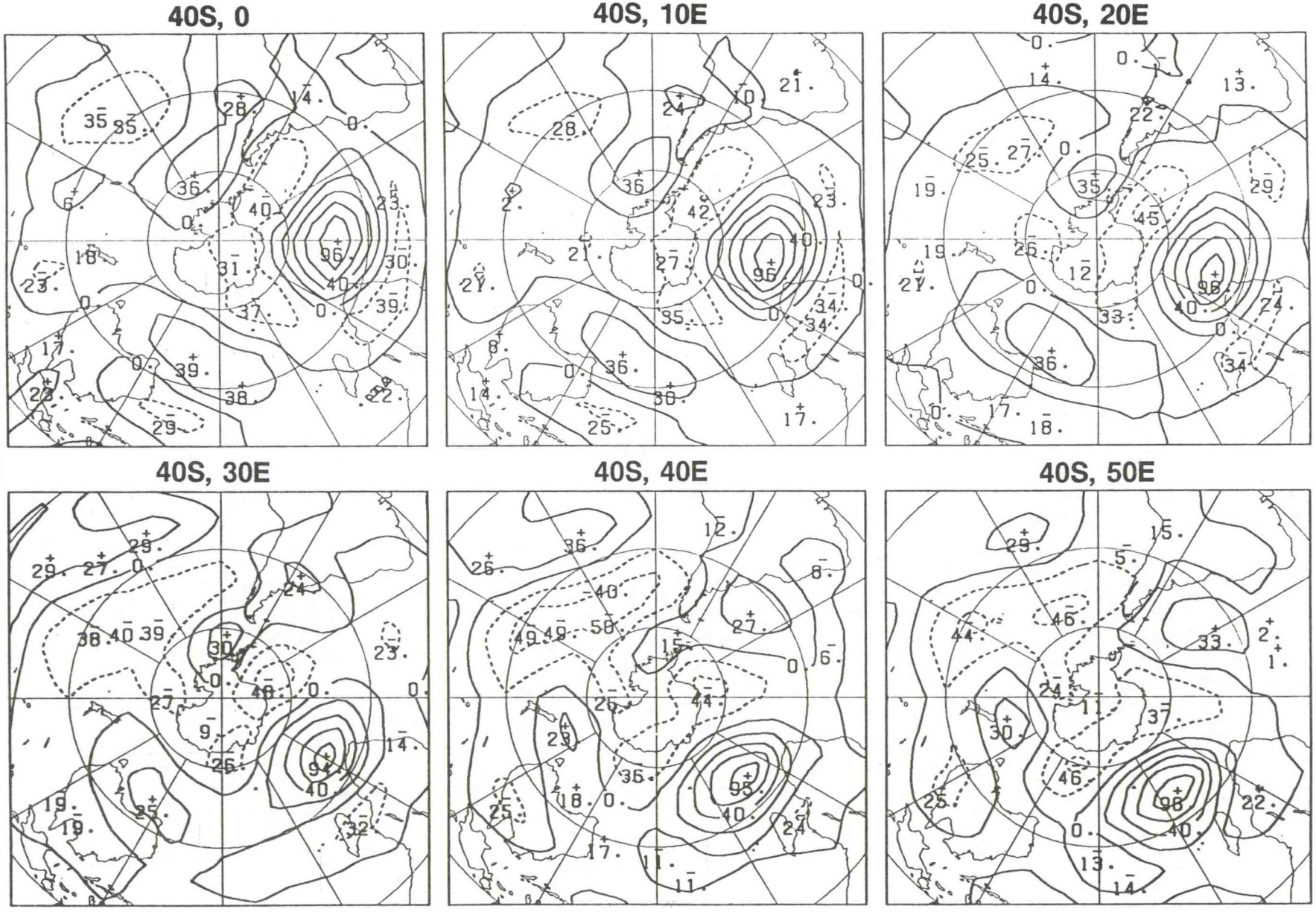
40S, 0
40S, 10E
40S, 20E
40S, 30E
40S, 40E
40S, 50E

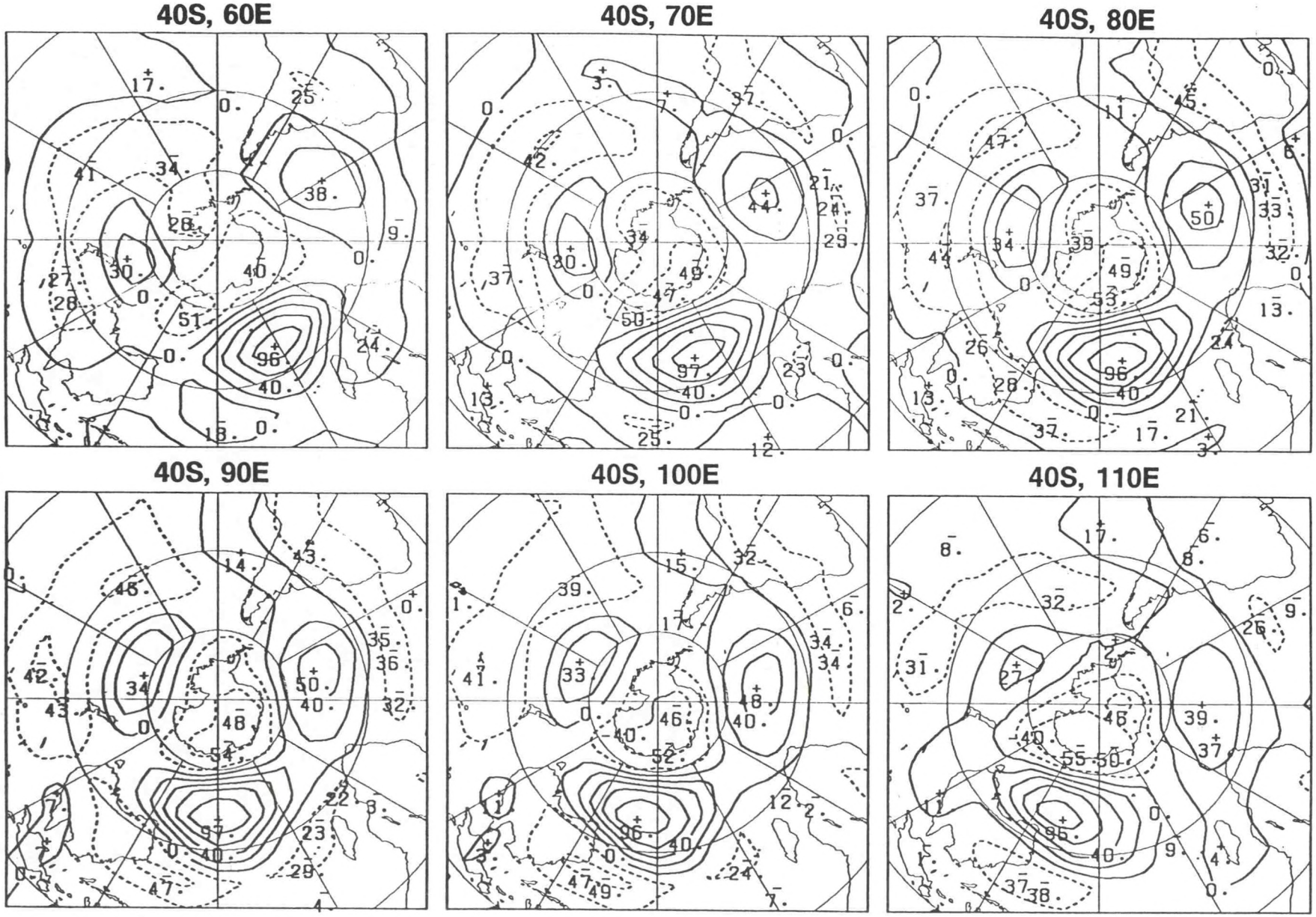
40S, 60E
40S, 70E
40S, 80E
40S, 90E
40S, 100E
40S, 110E

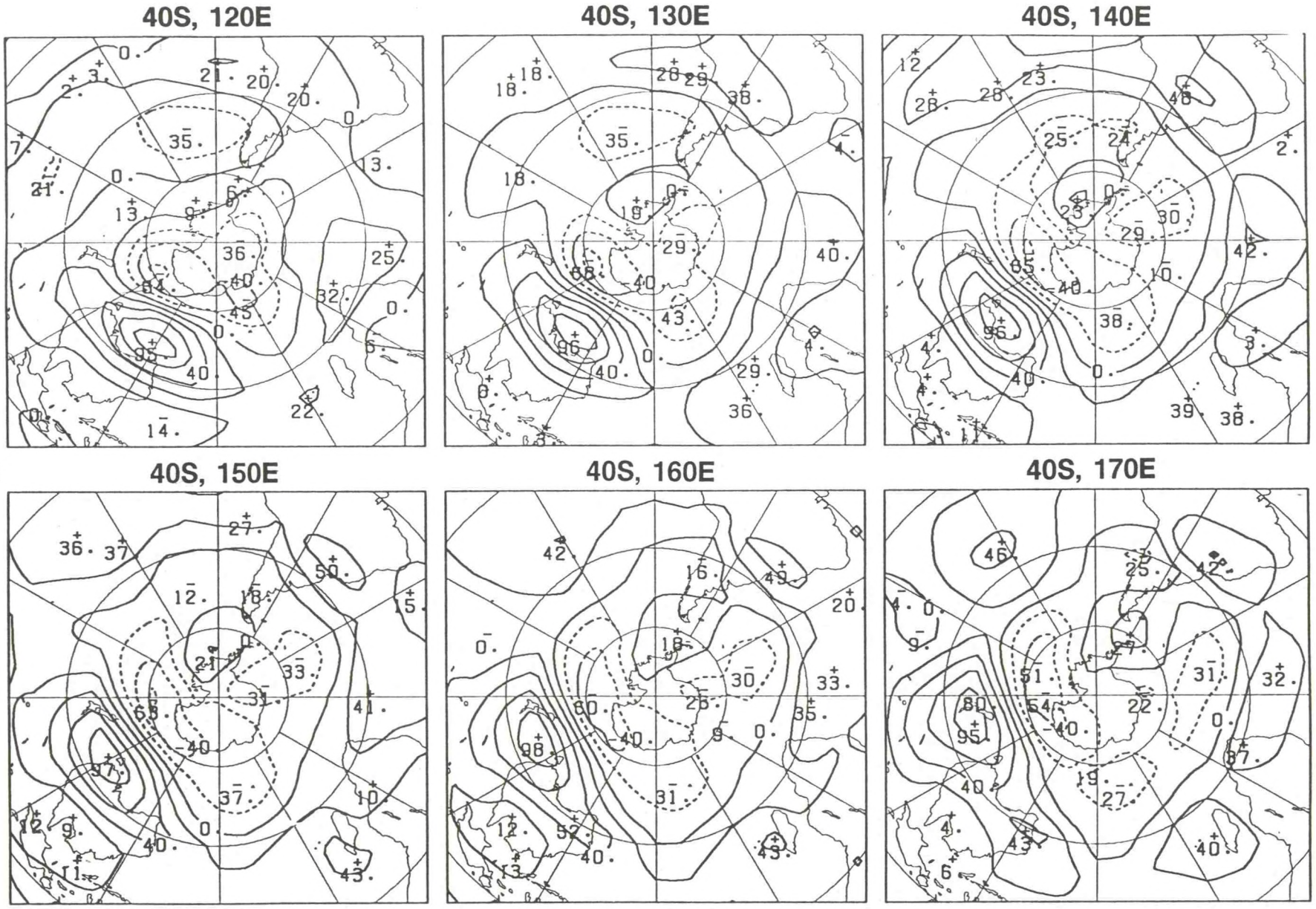
40S, 120E
40S, 130E
40S, 140E
40S, 150E
40S, 160E
40S, 170E

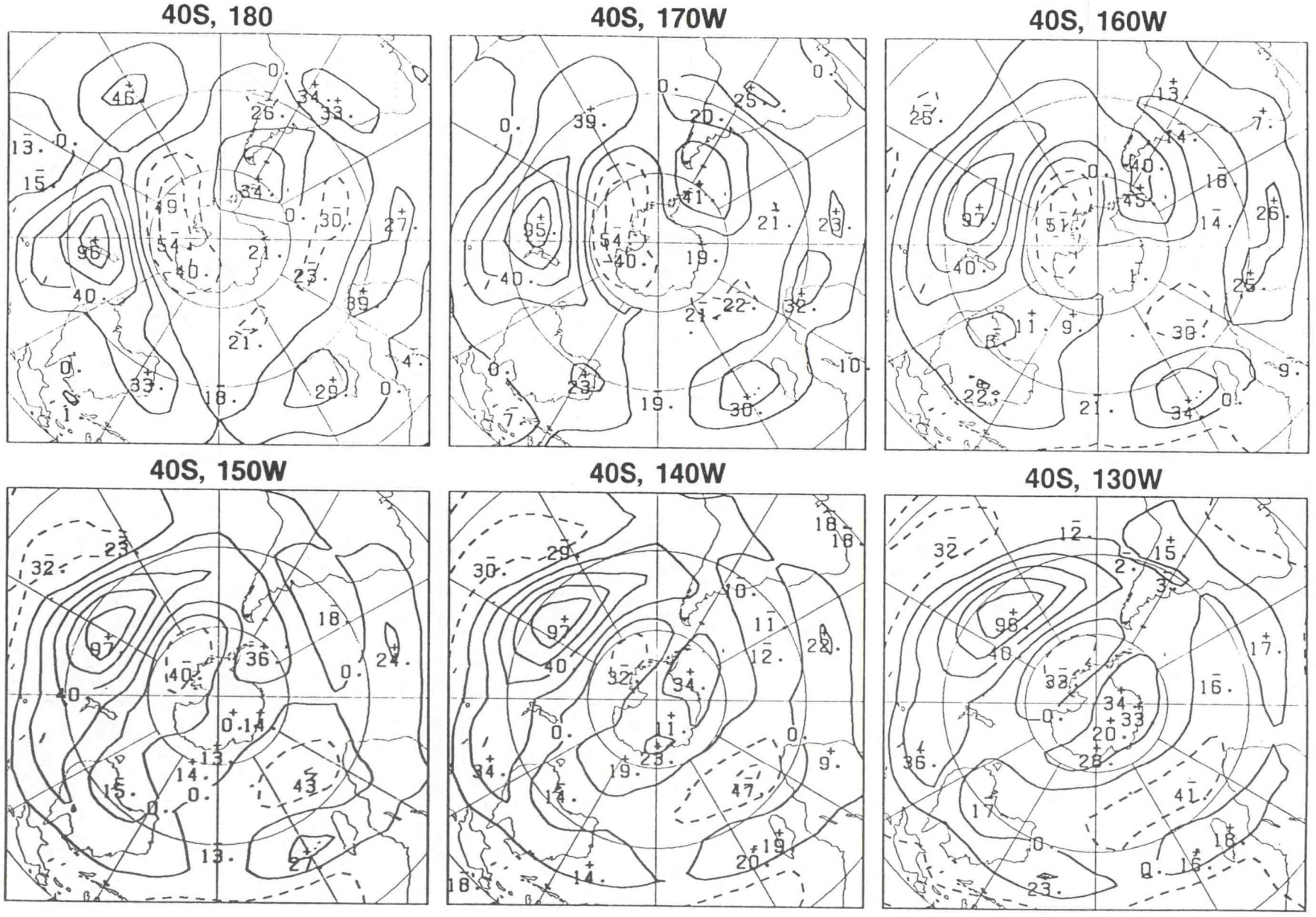
40S, 180
40S, 170W
40S, 160W
40S, 150W
40S, 140W
40S, 130W

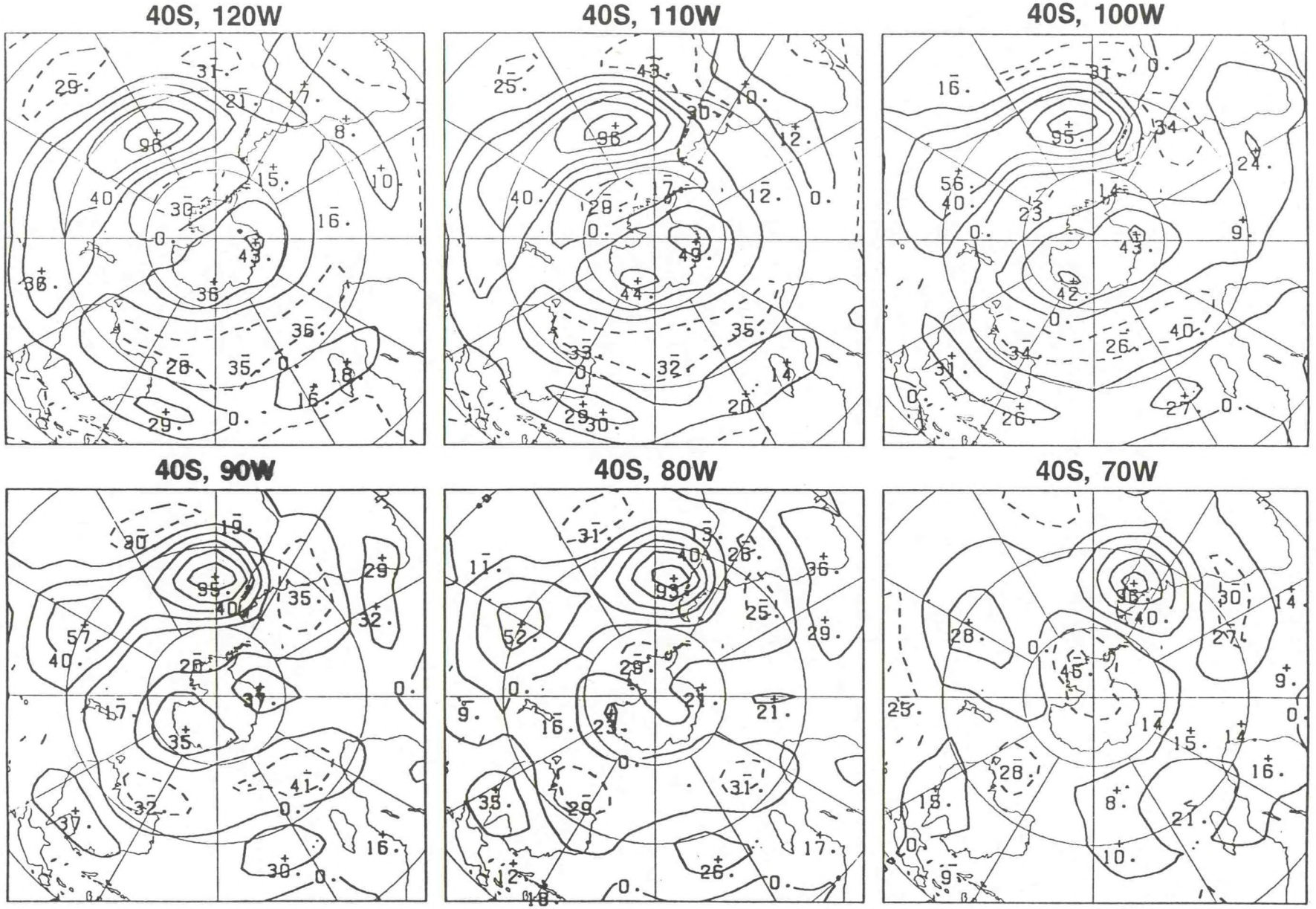
40S, 120W
40S, 110W
40S, 100W
40S, 90W
40S, 80W
40S, 70W

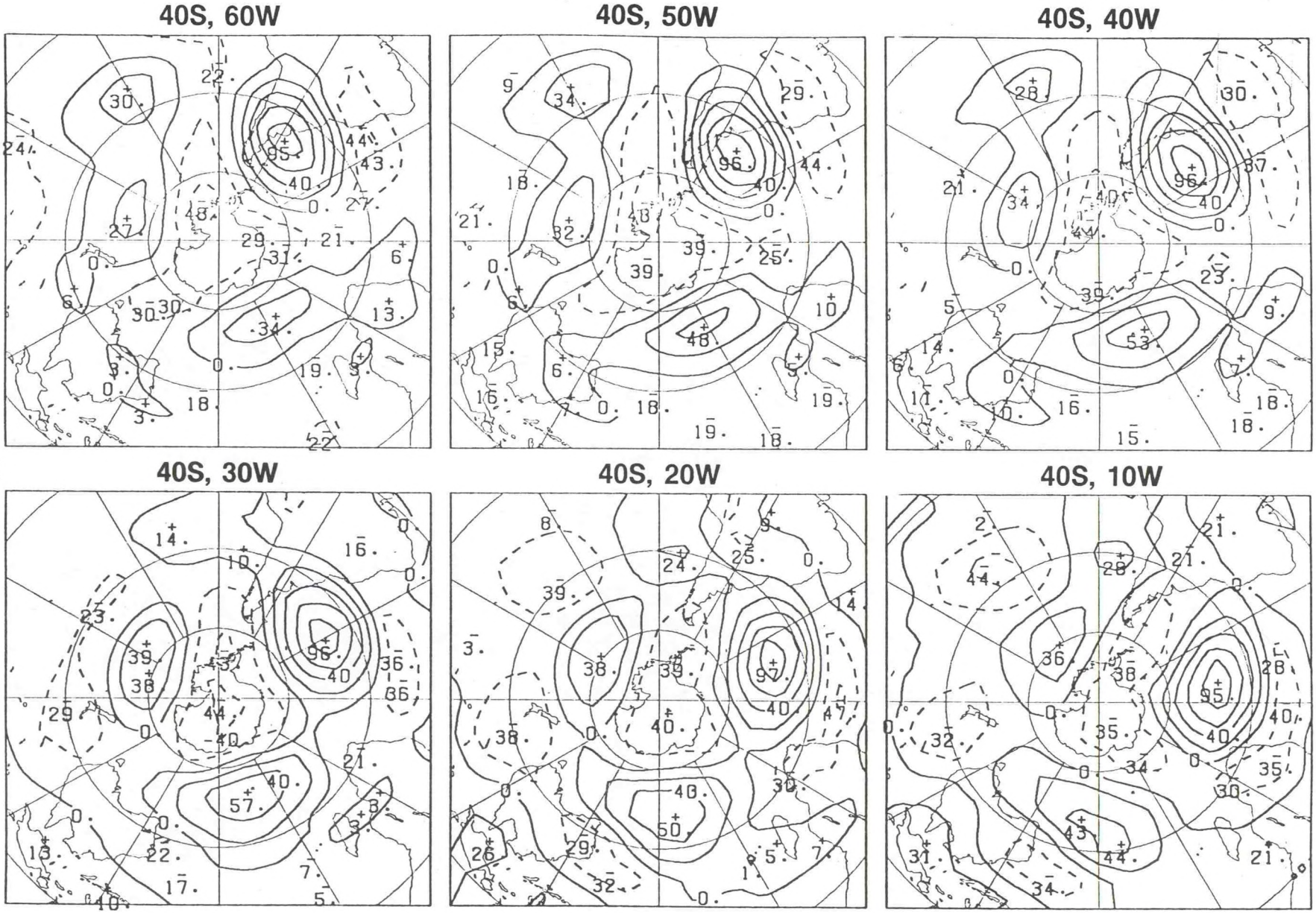
40S, 60W
40S, 50W
40S, 40W
40S, 30W
40S, 20W
40S, 10W

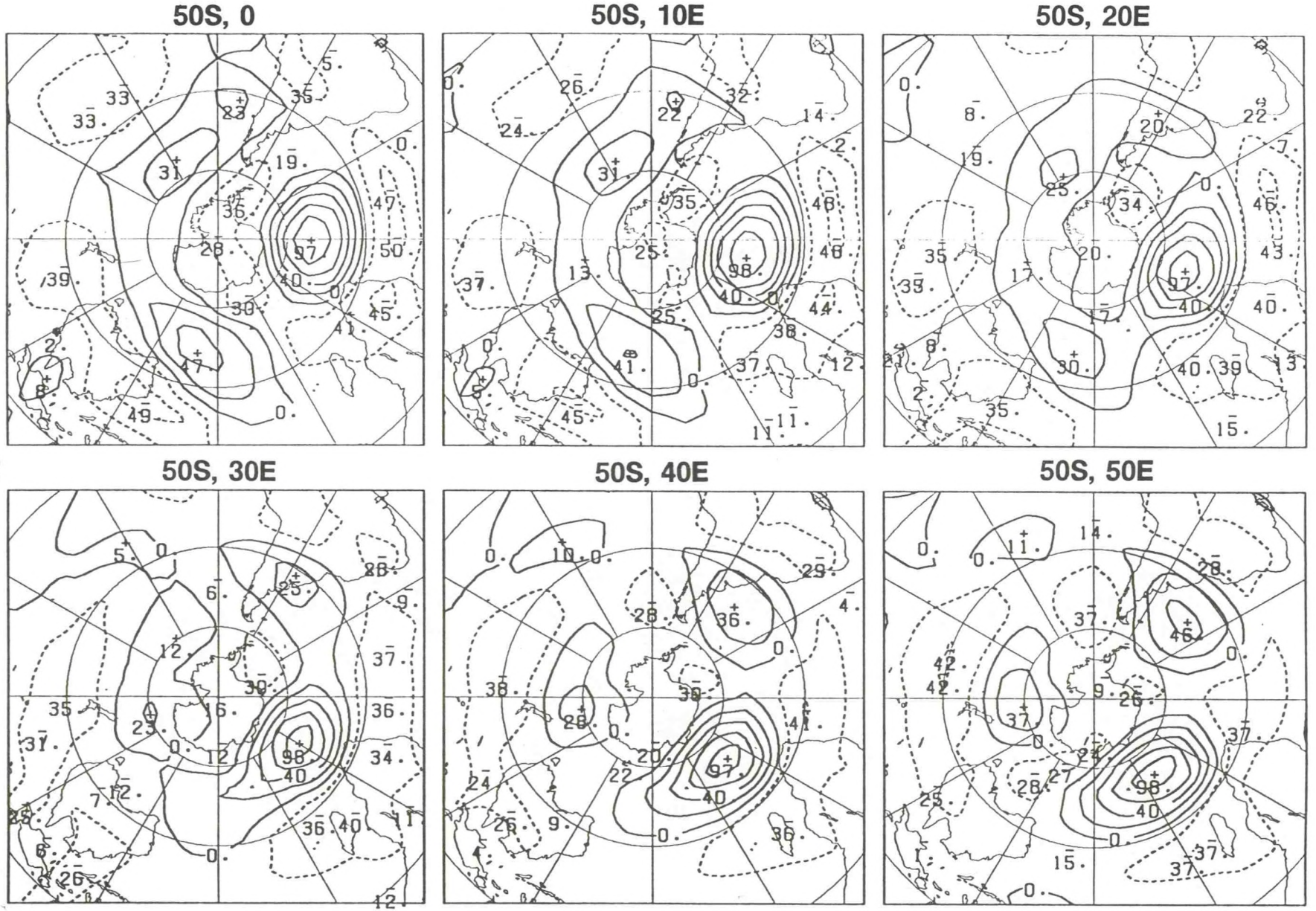
50S, 0
50S, 10E
50S, 20E
50S, 30E
50S, 40E
50S, 50E

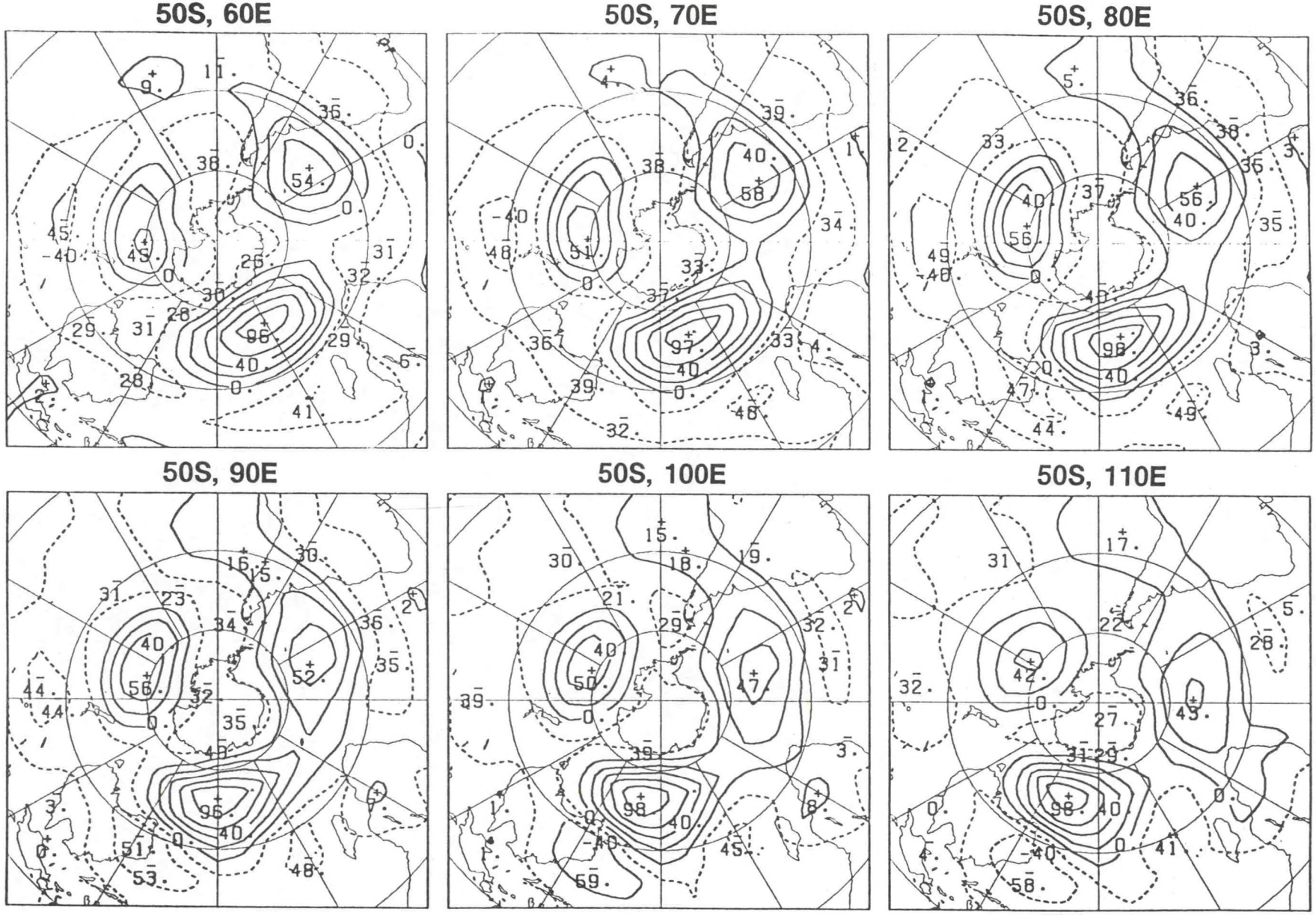
50S, 60E
50S, 70E
50S, 80E
50S, 90E
50S, 100E
50S, 110E

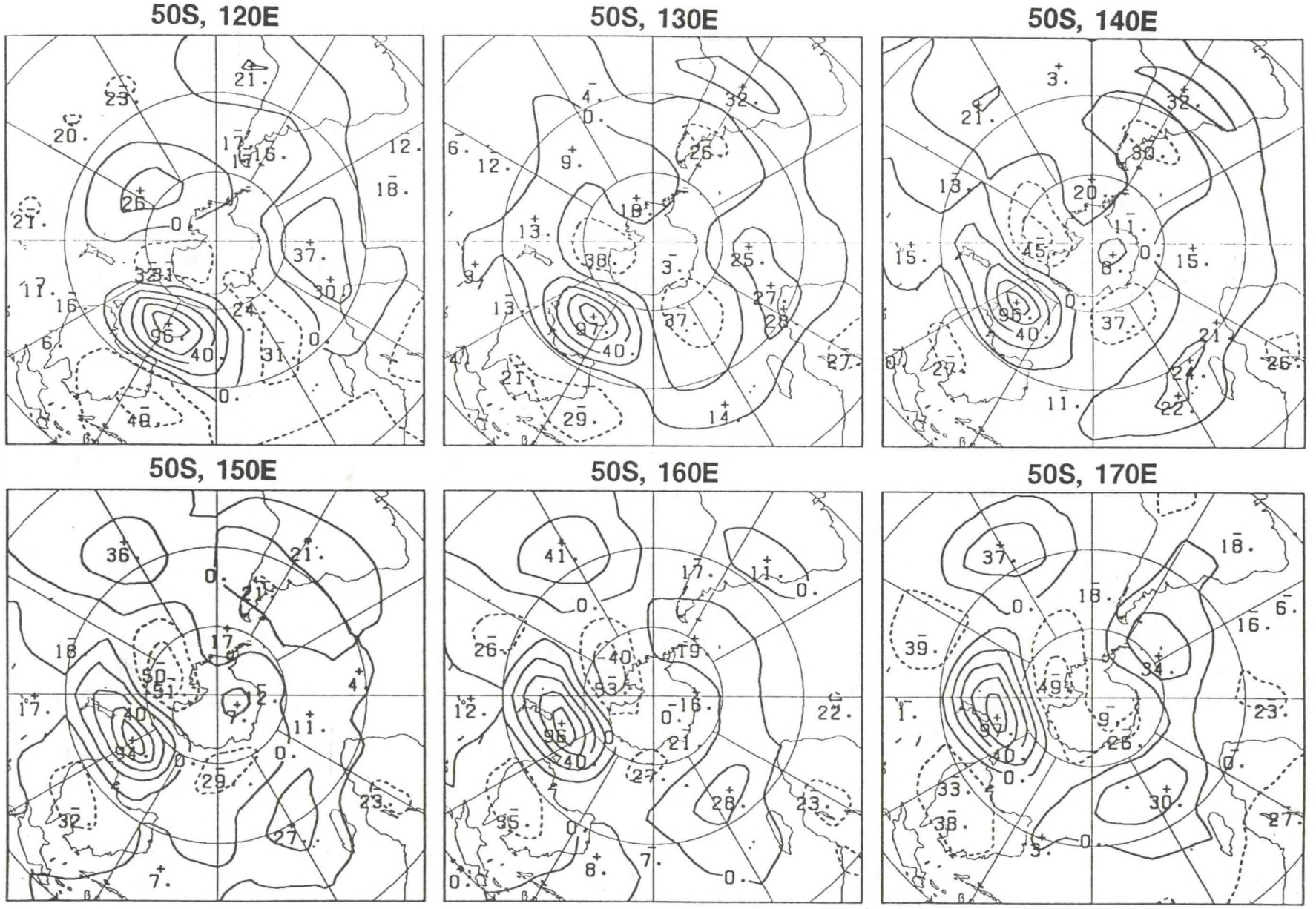
50S, 120E
50S, 130E
50S, 140E
50S, 150E
50S, 160E
50S, 170E

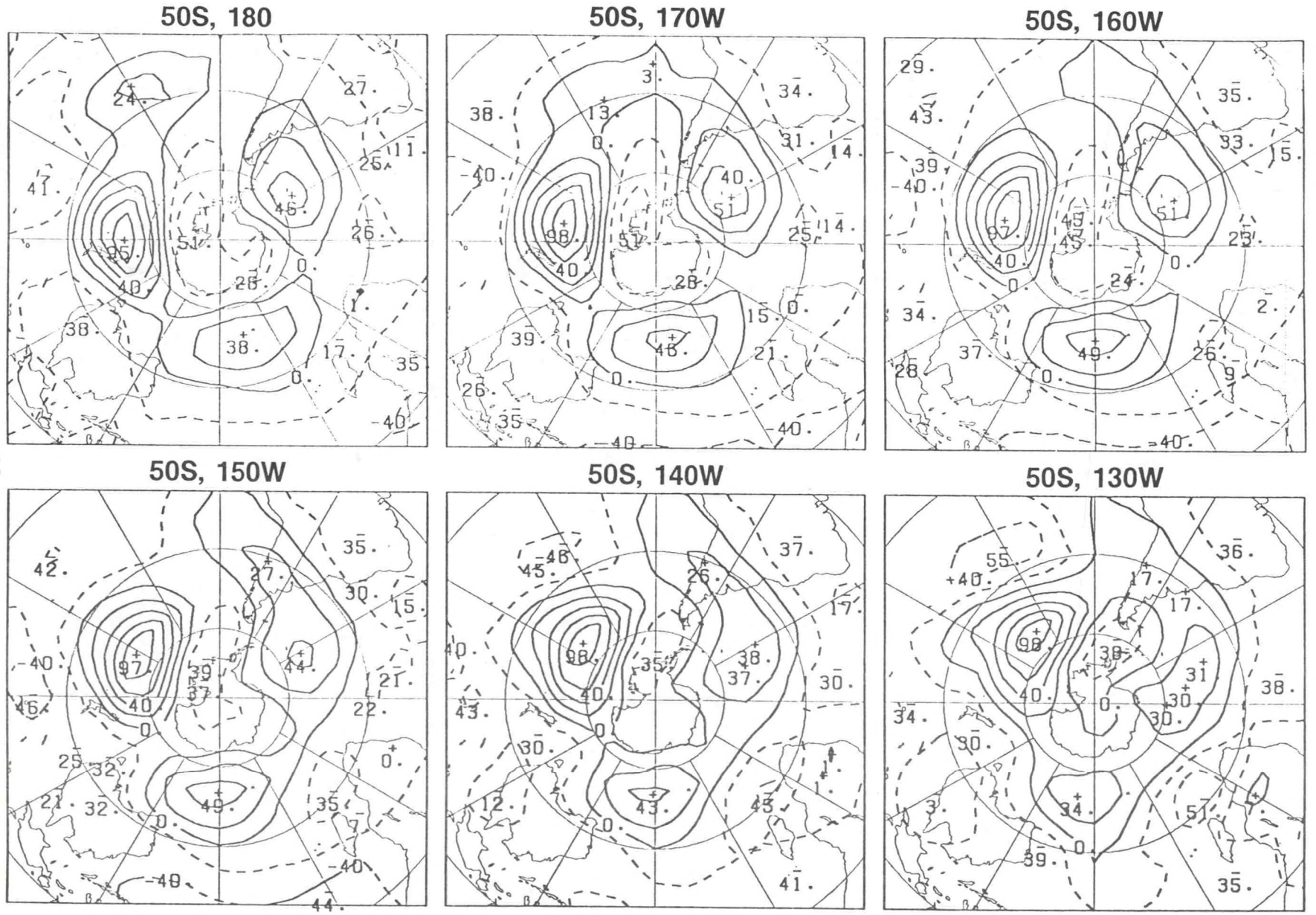
50S, 180
50S, 170W
50S, 160W
50S, 150W
50S, 140W
50S, 130W

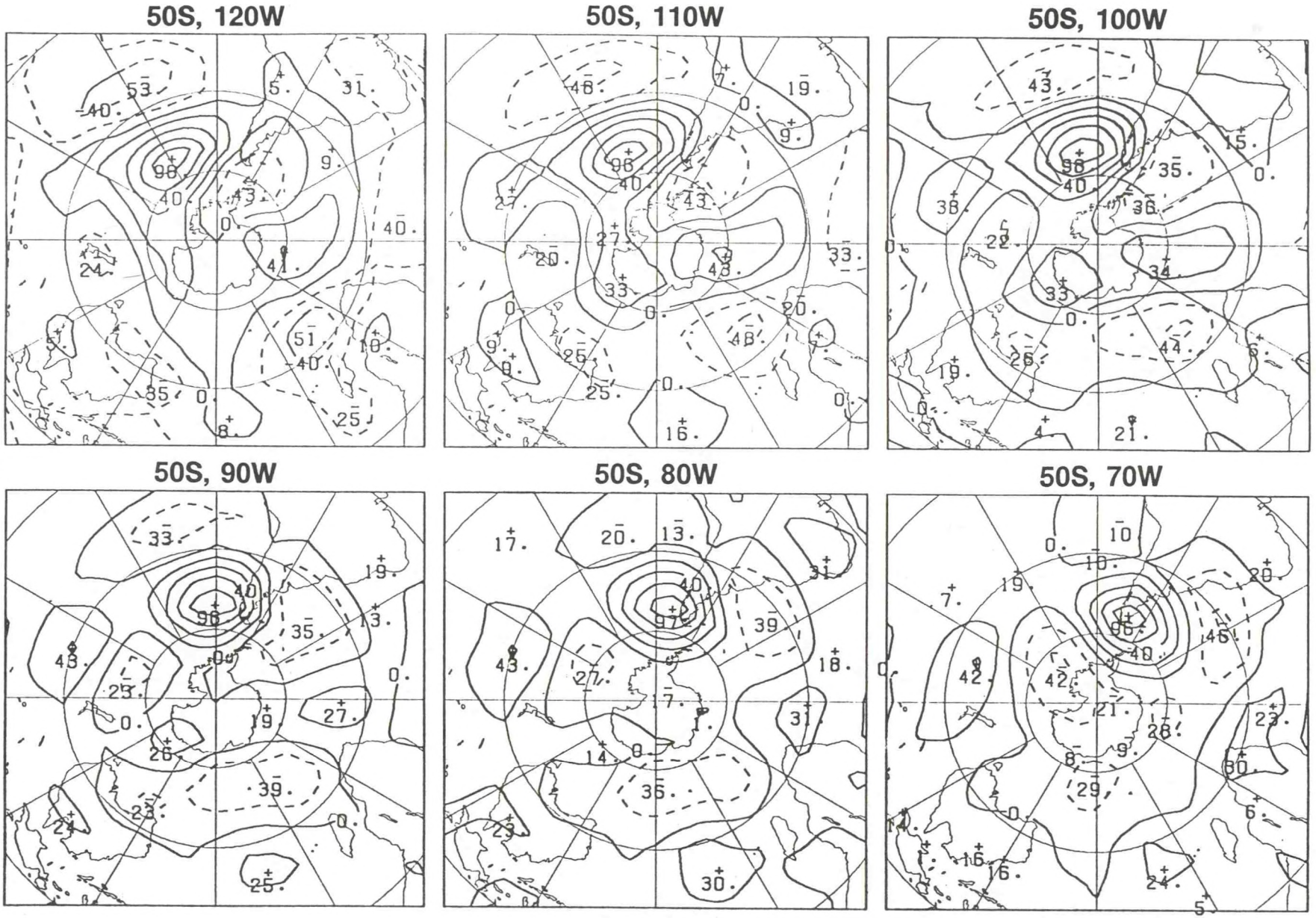
50S, 120W
50S, 110W
50S, 100W
50S, 90W
50S, 80W
50S, 70W

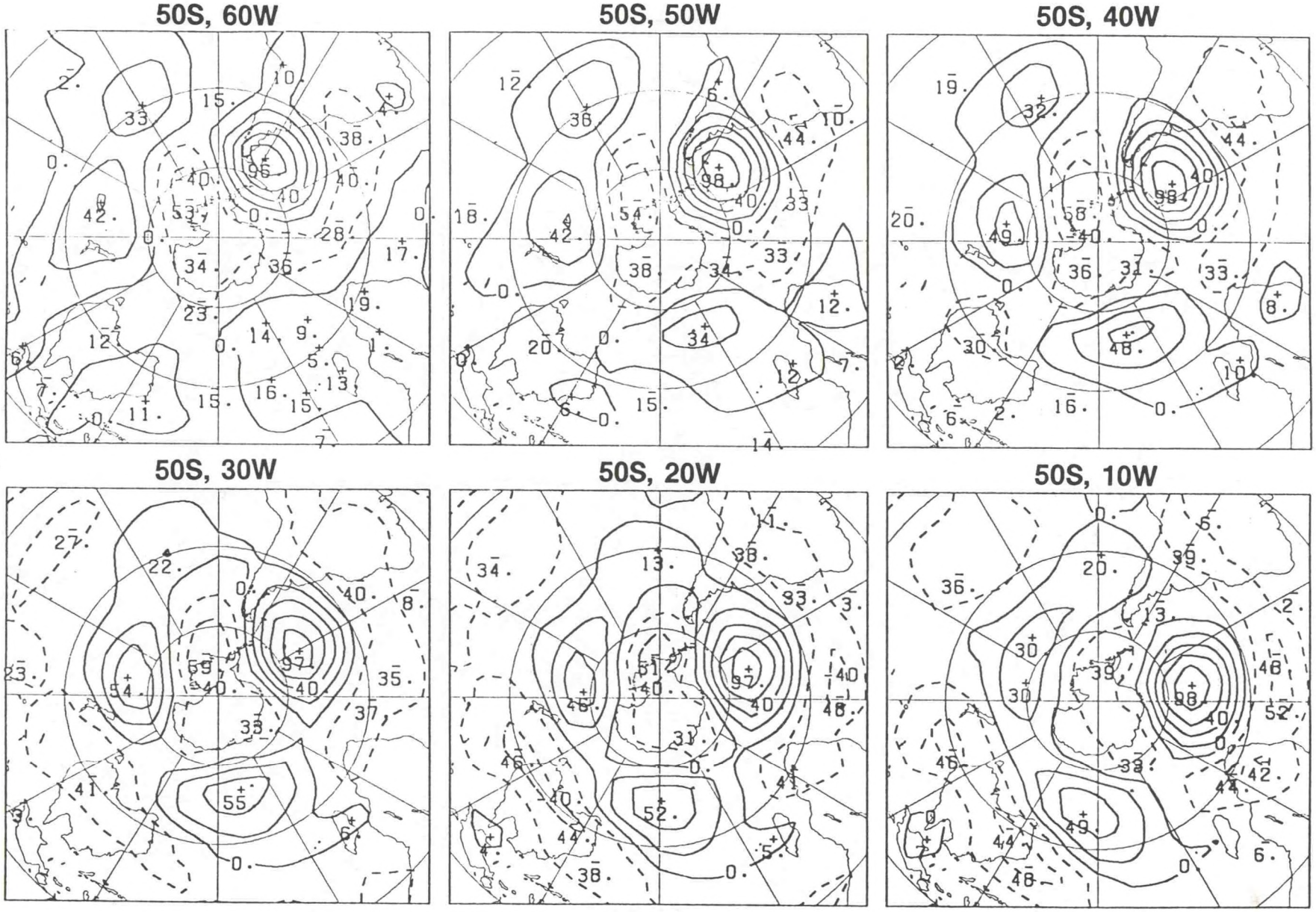
50S, 60W
50S, 50W
50S, 40W
50S, 30W
50S, 20W
50S, 10W

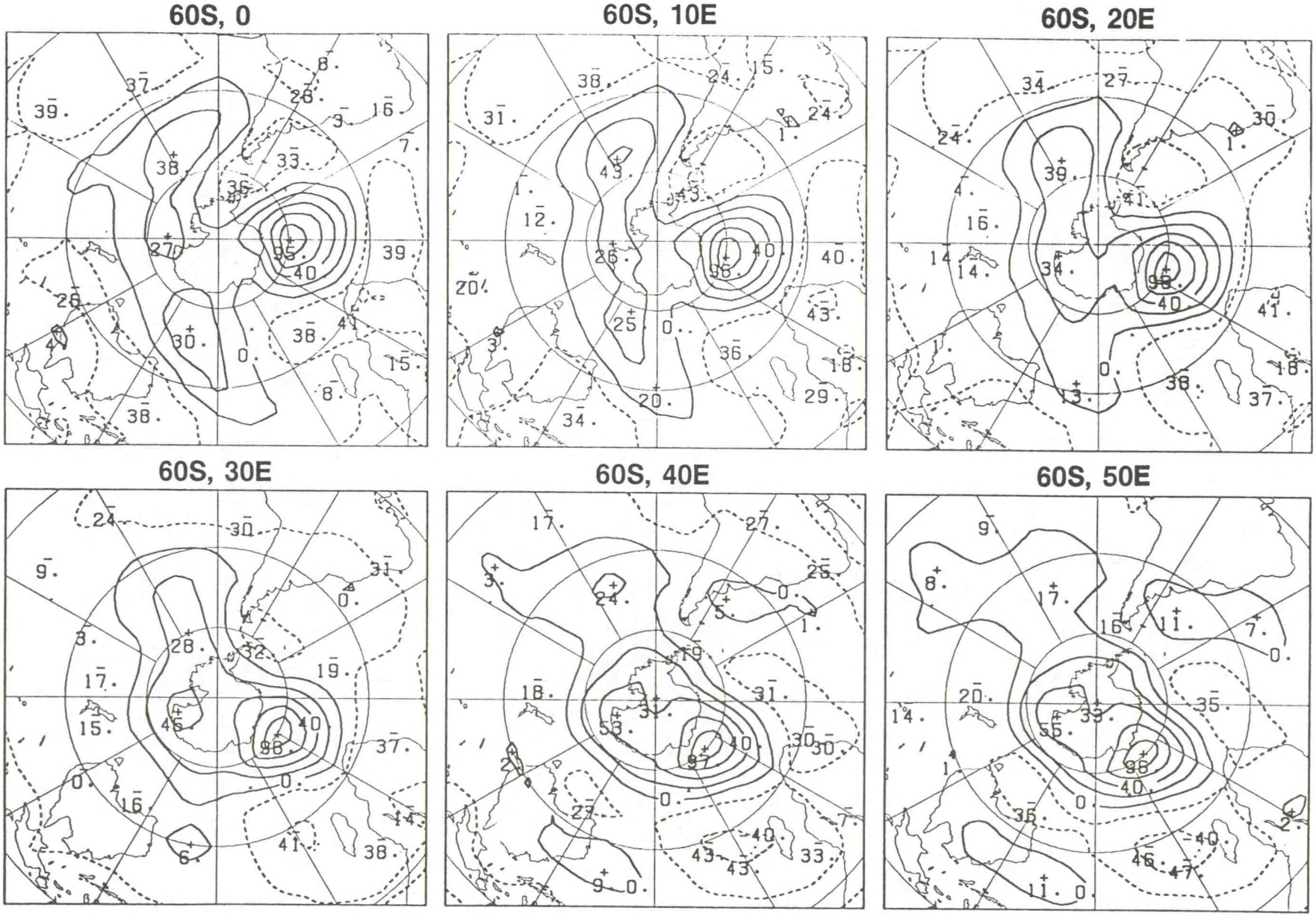
60S, 0
60S, 10E
60S, 20E
60S, 30E
60S, 40E
60S, 50E

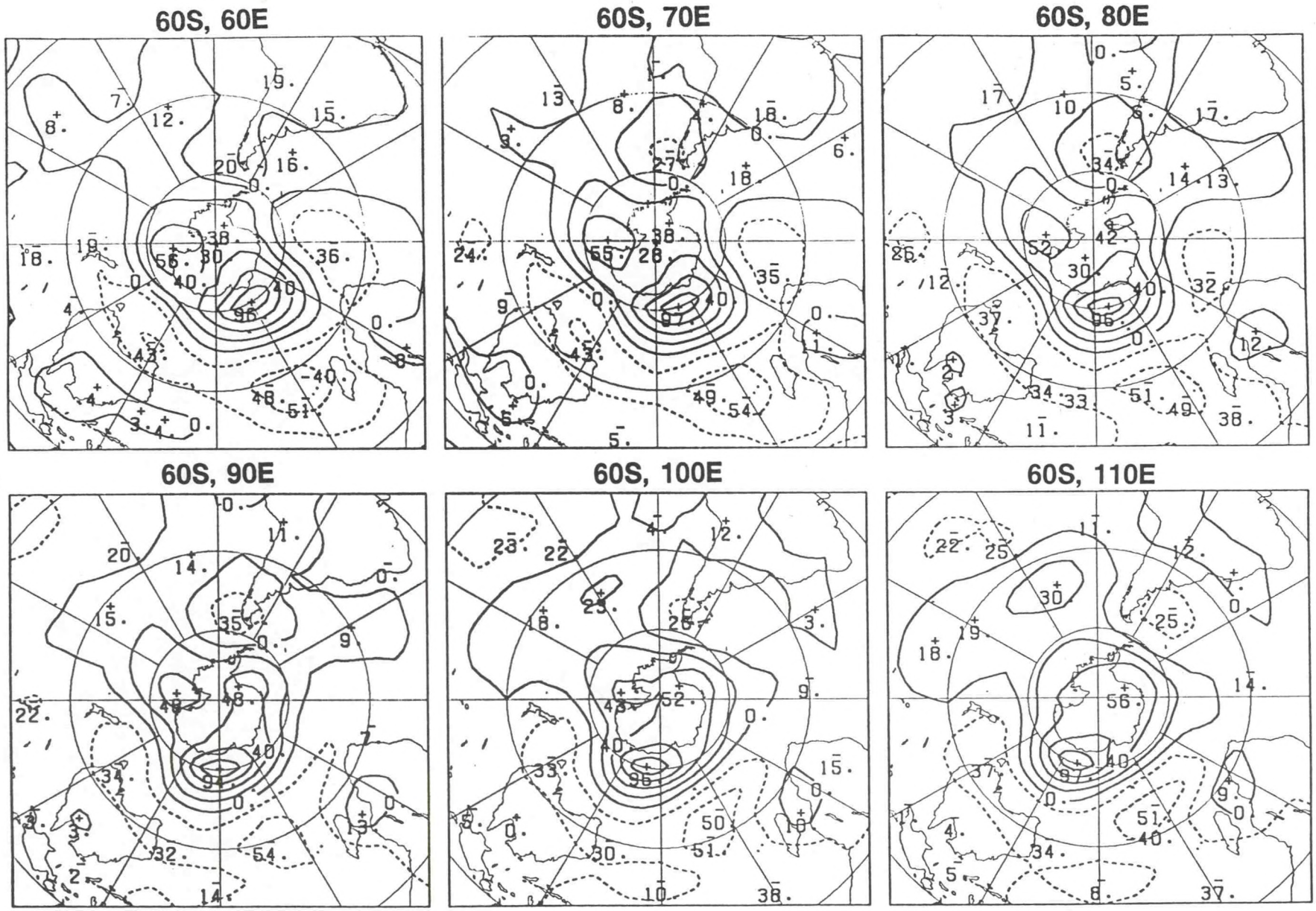
60S, 60E
60S, 70E
60S, 80E
60S, 90E
60S, 100E
60S, 110E

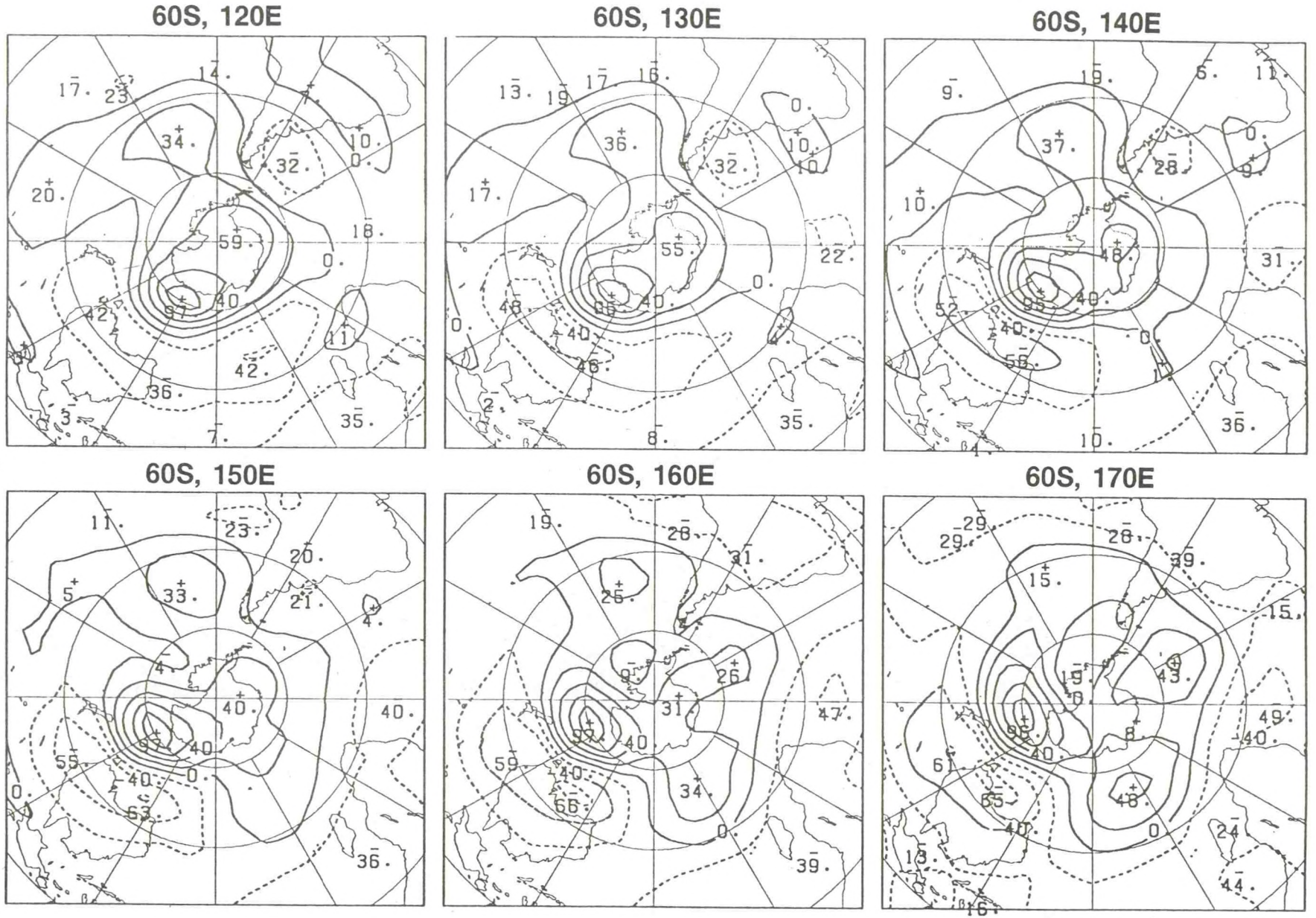
60S, 120E
60S, 130E
60S, 140E
60S, 150E
60S, 160E
60S, 170E

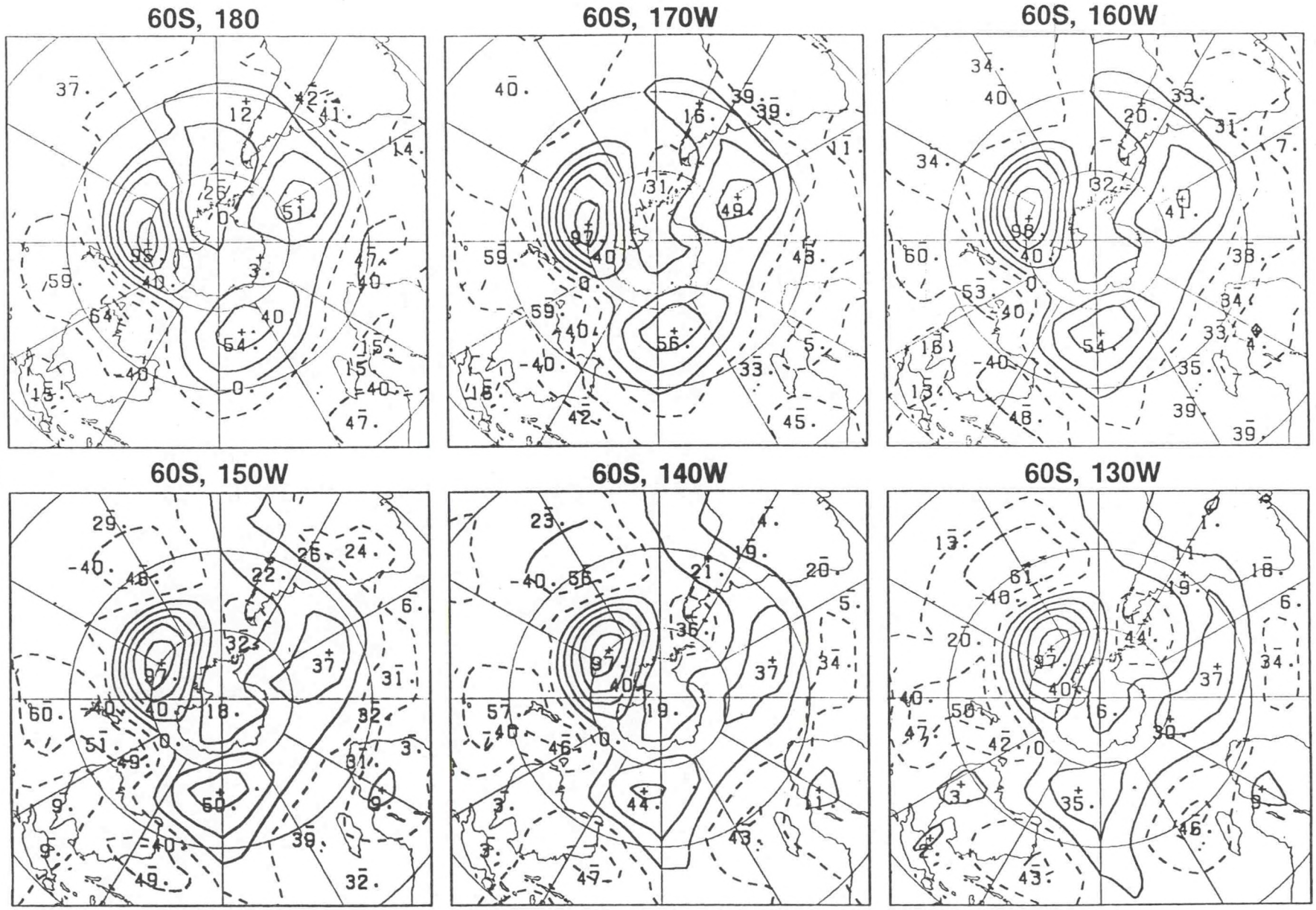
60S, 180
60S, 170W
60S, 160W
60S, 150W
60S, 140W
60S, 130W

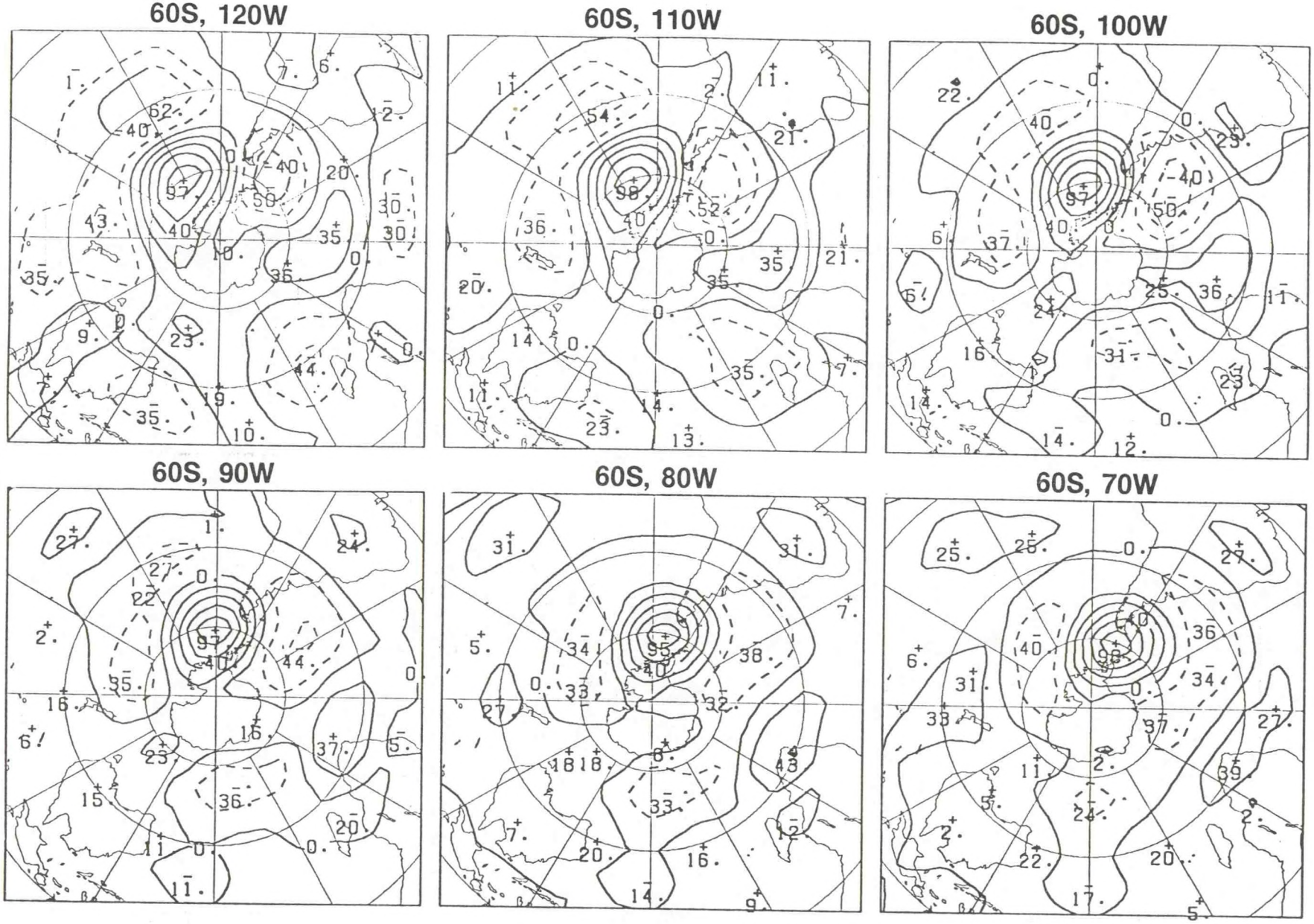
60S, 120W
60S, 110W
60S, 100W
60S, 90W
60S, 80W
60S, 70W

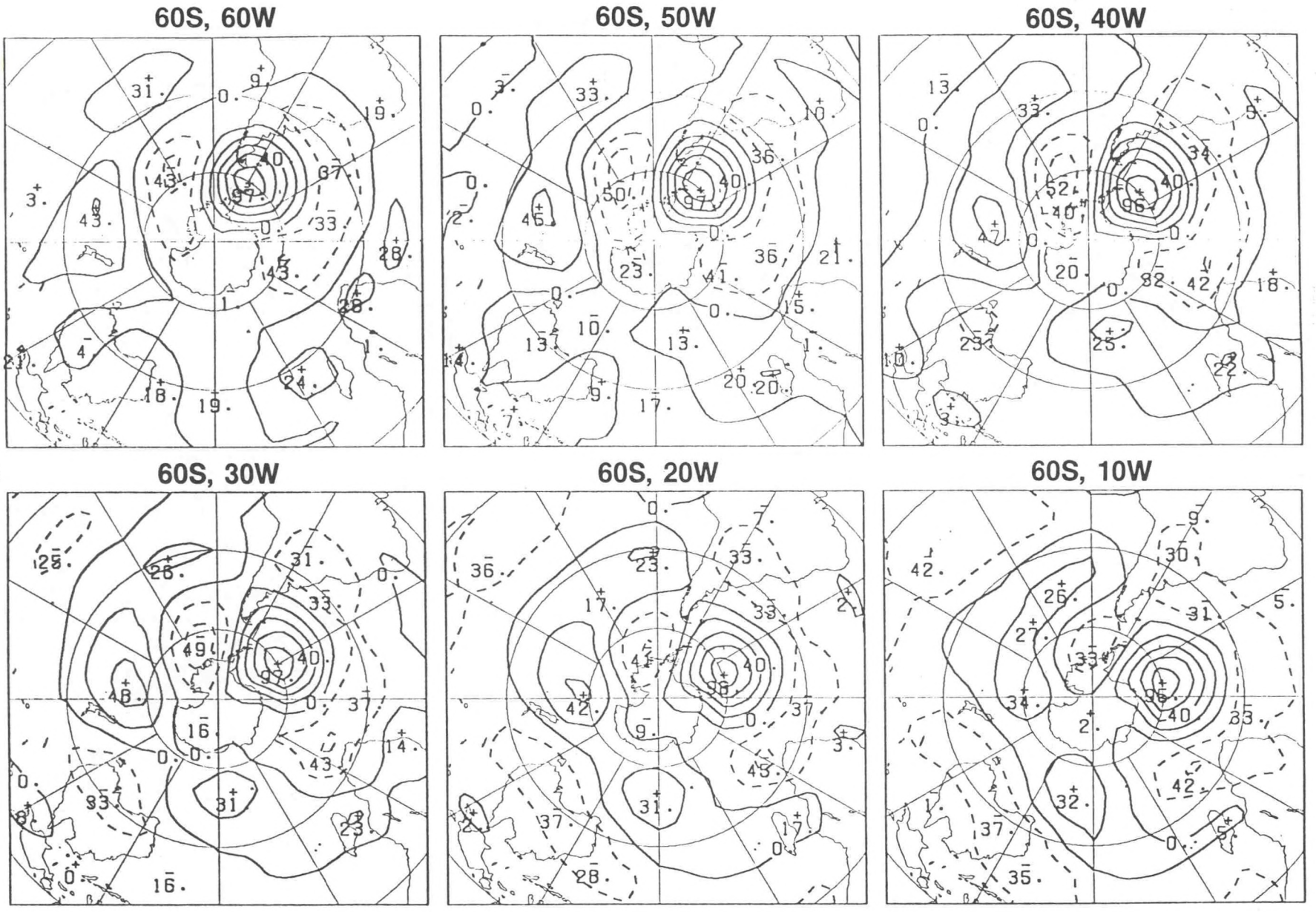
60S, 60W
60S, 50W
60S, 40W
60S, 30W
60S, 20W
60S, 10W

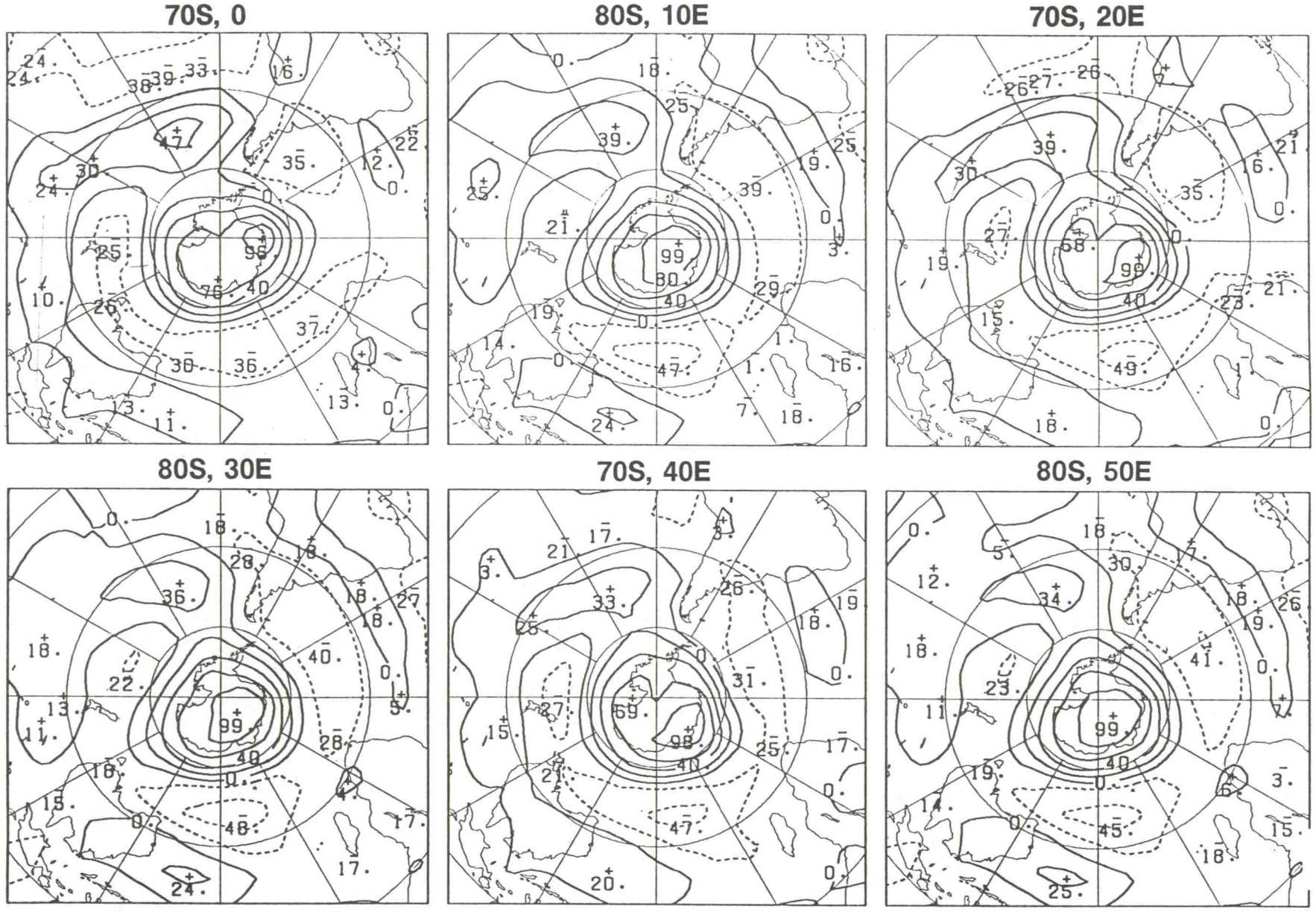
70S, 0
80S, 10E
70S, 20E
80S, 30E
70S, 40E
80S, 50E

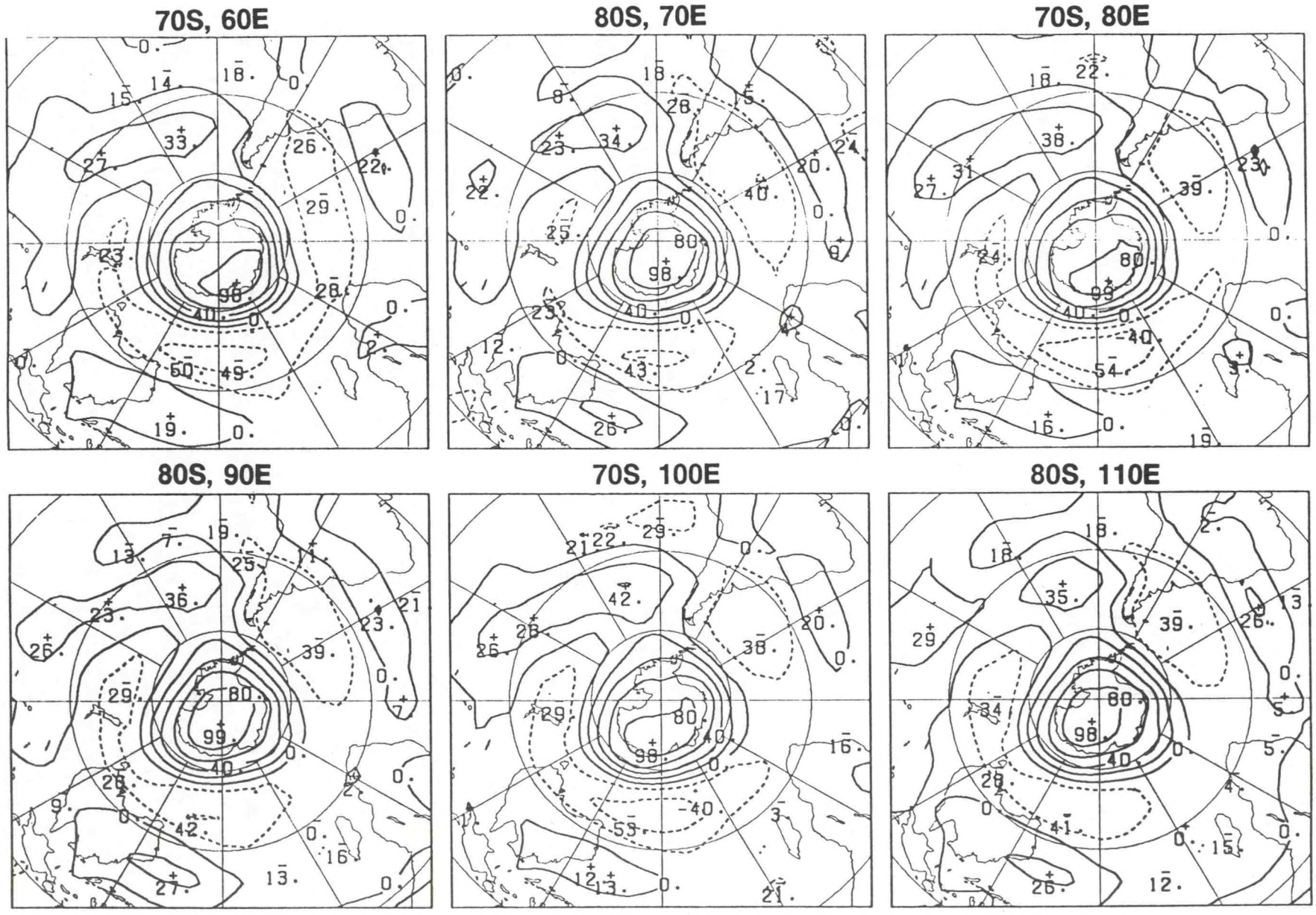
70S, 60E
80S, 70E
70S, 80E
80S, 90E
70S, 100E
80S, 110E

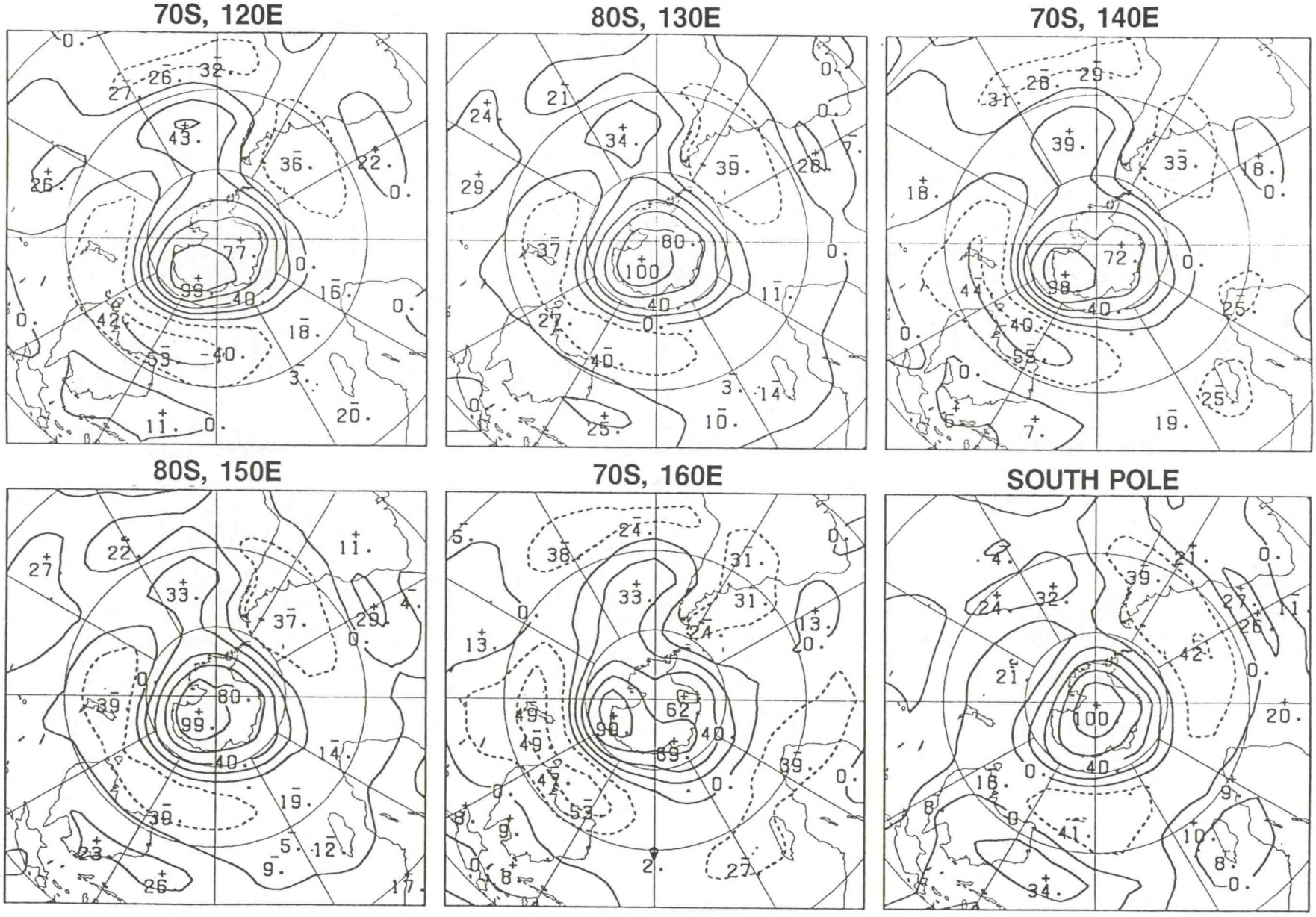
70S, 120E
80S, 130E
70S, 140E
80S, 150E
70S, 160E
SOUTH POLE

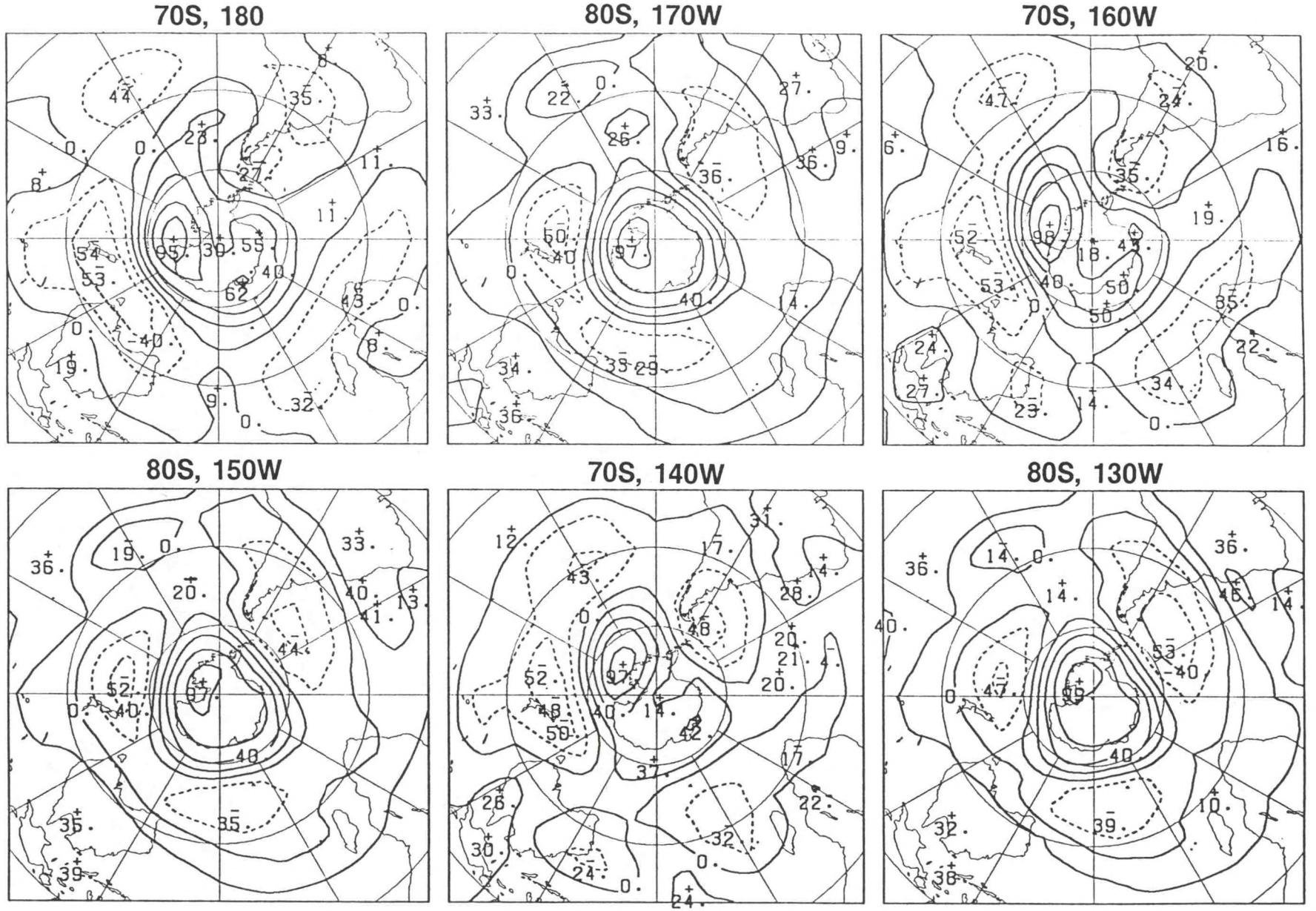
70S, 180
80S, 170W
70S, 160W
80S, 150W
70S, 140W
80S, 130W

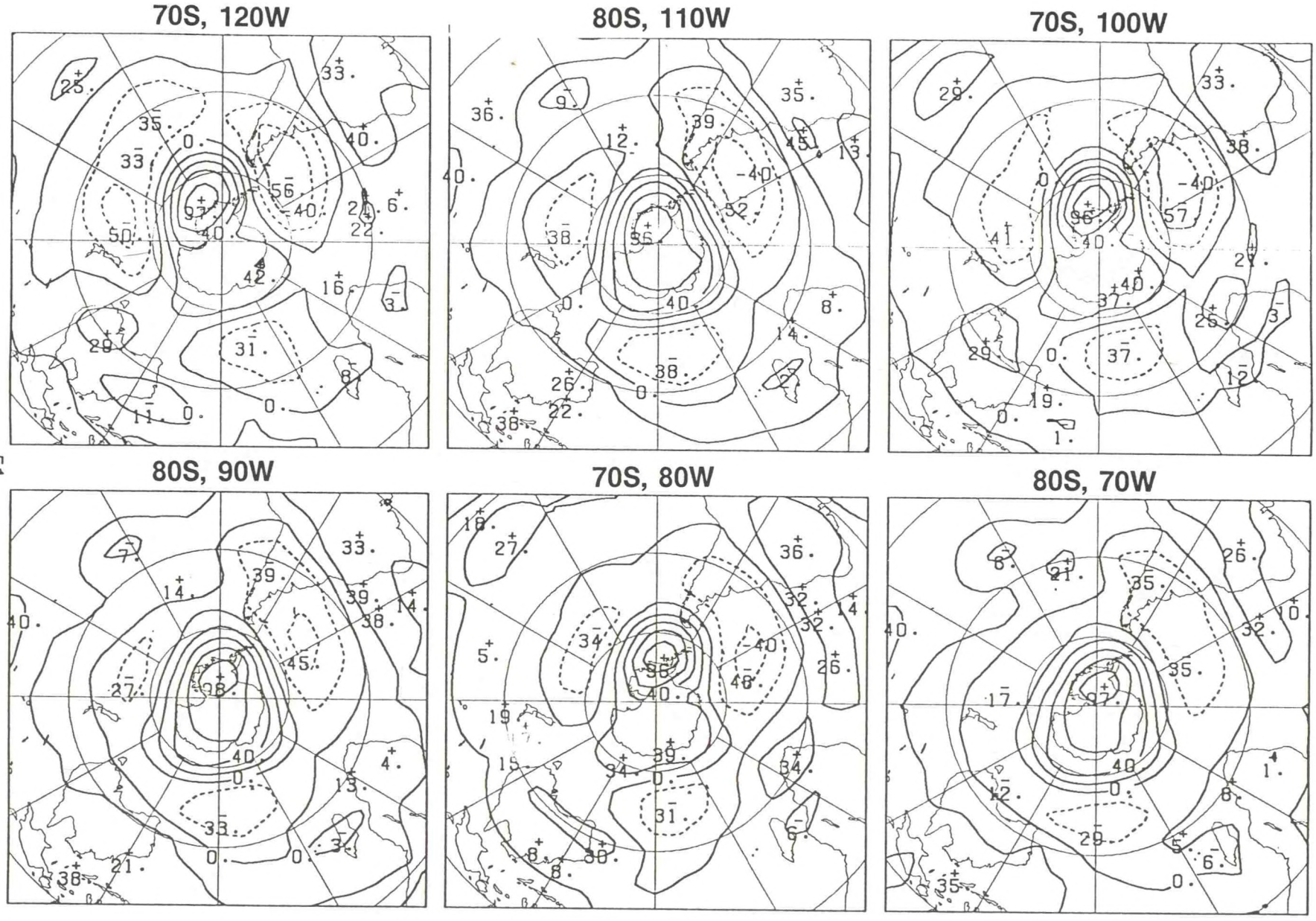
70S, 120W
80S, 110W
70S, 100W
80S, 90W
70S, 80W
80S, 70W

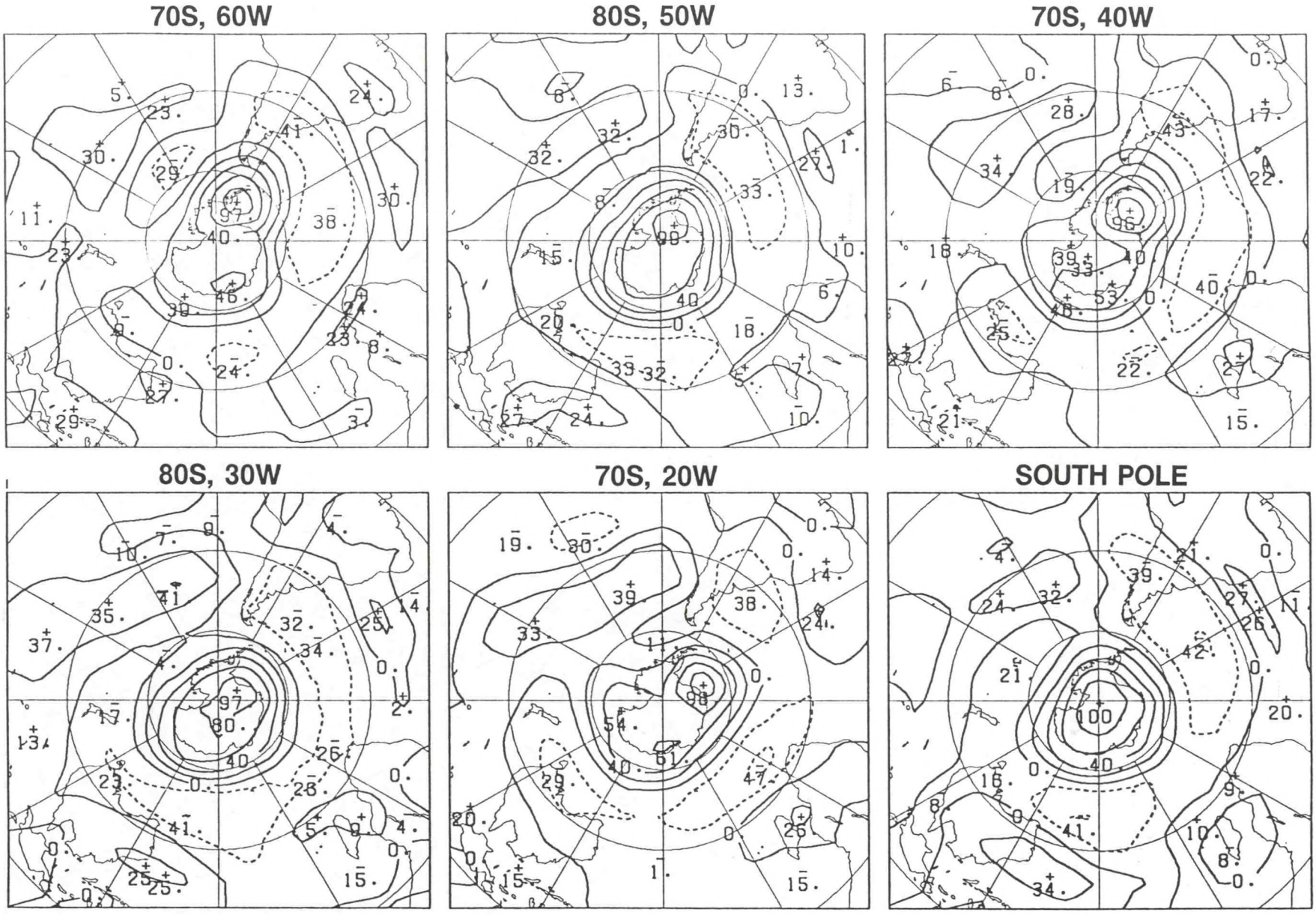
70S, 60W
80S, 50W
70S, 40W
80S, 30W
70S, 20W
SOUTH POLE

SUMMER (NOV–MAR)

<table>
<tr><th>LATITUDE (S)</th><th>SOUTH ATLANTIC</th><th>INDIAN OCEAN</th><th>WESTERN S. PAC</th><th>CENTRAL, EASTERN S. PAC</th></tr>
<tr><td>20</td><td colspan="4">MERIDIONAL DIPOLE, ZONALLY ELONGATED
WEAK WAVE 4 PATTERN</td></tr>
<tr><td>30</td><td colspan="2">MERIDIONAL DIPOLE, ZONALLY ELONGATED</td><td colspan="2">ZONALLY ELONGATED
WEAK WAVE 3 PATTERN</td></tr>
<tr><td>40</td><td>WAVES 3&4</td><td colspan="3" rowspan="2">WAVES 3&4
SOME ZONAL SYMMETRY</td></tr>
<tr><td>50</td></tr>
<tr><td>60</td><td colspan="2">ISOLATED ANOMALY</td><td colspan="2">MERIDIONAL DIPOLE, ZONALLY ELONGATED
EAST CENTRAL: ISOLATED ANOMALY</td></tr>
<tr><td>70, 80</td><td colspan="4">MERIDIONAL DIPOLE, ZONALLY ELONGATED</td></tr>
<tr><td>S. POLE</td><td colspan="4">NEGATIVE CORRELATIONS MOST PRONOUNCED NEAR 45S OVER INDIAN AND ATLANTIC OCEANS</td></tr>
</table>

TABLE 2: Summary of summertime (October - April) teleconnection patterns determined subjectively from one-point teleconnection maps computed from monthly mean 500 mb height anomalies for the period 1979-1990. Patterns are identified at 10^{o} latitude increments for five primary regions: The South Atlantic, the Indian Ocean, the western South Pacific, the central and eastern South Pacific, and the polar region. See Introduction for a description of terms.

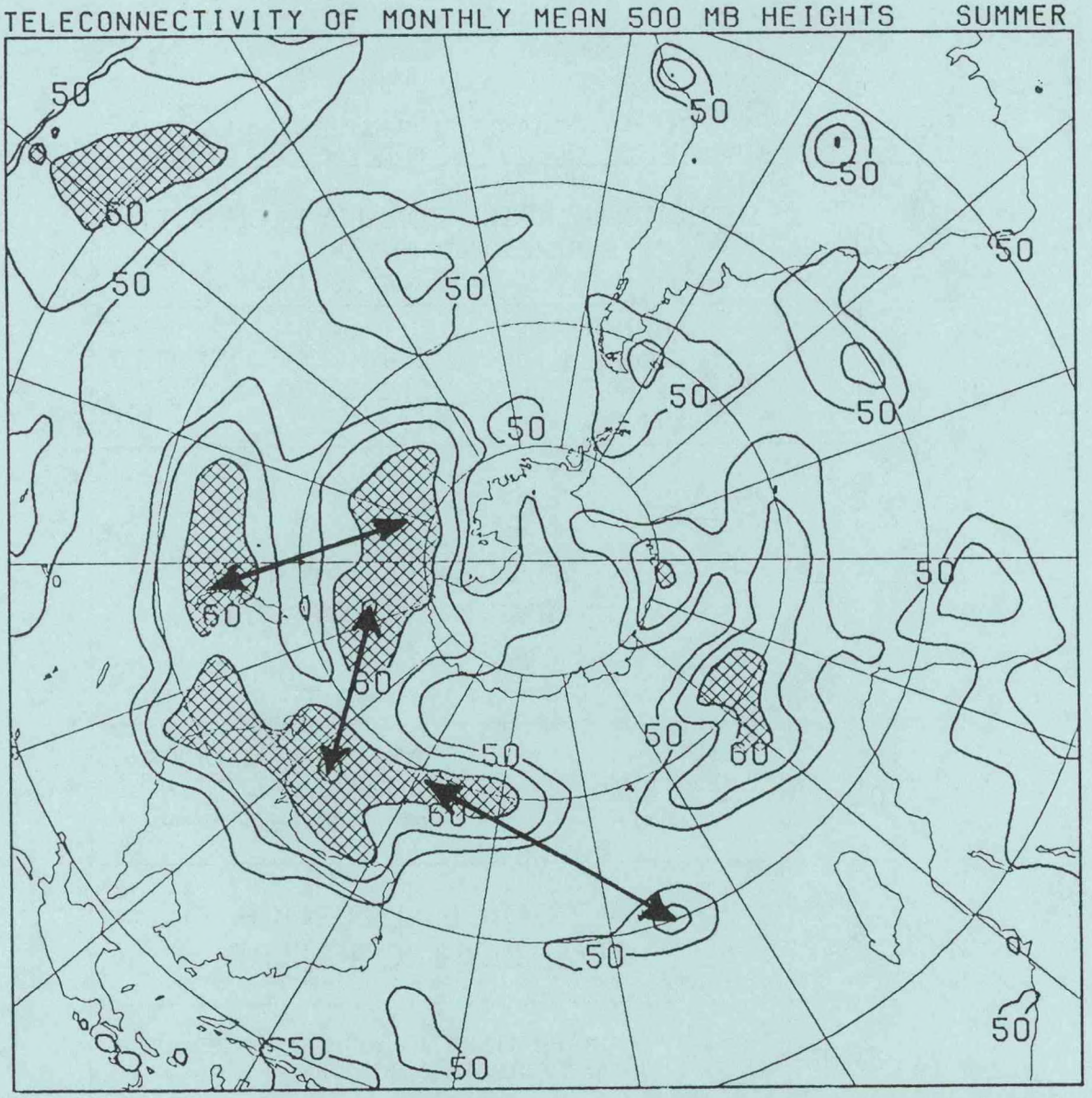

Teleconnectivity of monthly mean 500 mb geopotential height anomalies for the Southern Hemisphere warm season (November - March). Values are strongest negative correlations (negative signs omitted) for each one-point correlation map plotted at the base grid point. Correlations are multiplied by 100 and are only contoured for values less than -0.5. Values less than -0.6 are shaded. Arrows connect centers of strongest teleconnectivity with grid points which show strongest negative correlation on their respective one-point correlation maps. High teleconnectivity values in the vicinity of elevated terrain are due to changes in model resolution and/or changes in analysis procedures. For those regions the values should be ignored.

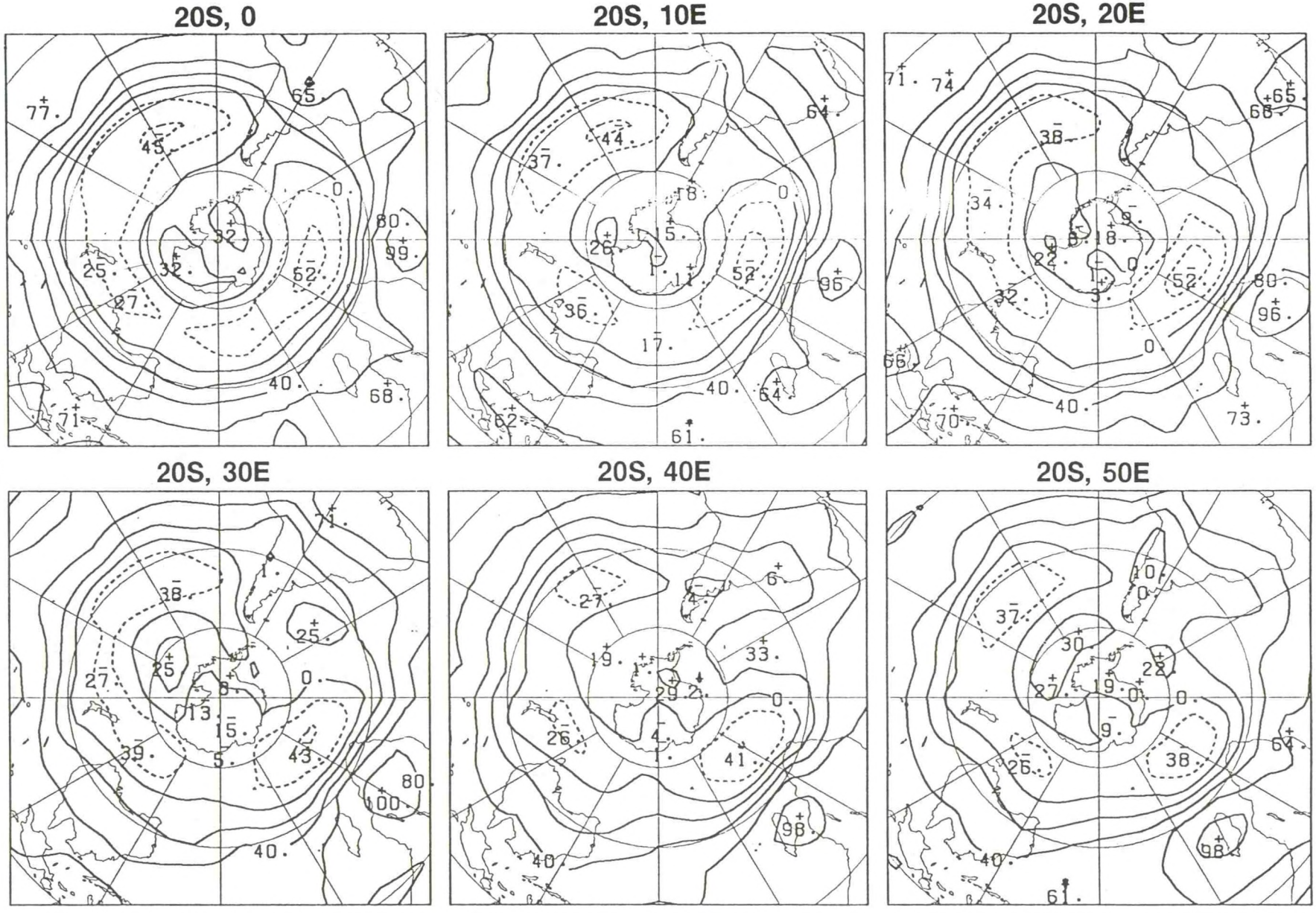
20S, 0
20S, 10E
20S, 20E
20S, 30E
20S, 40E
20S, 50E

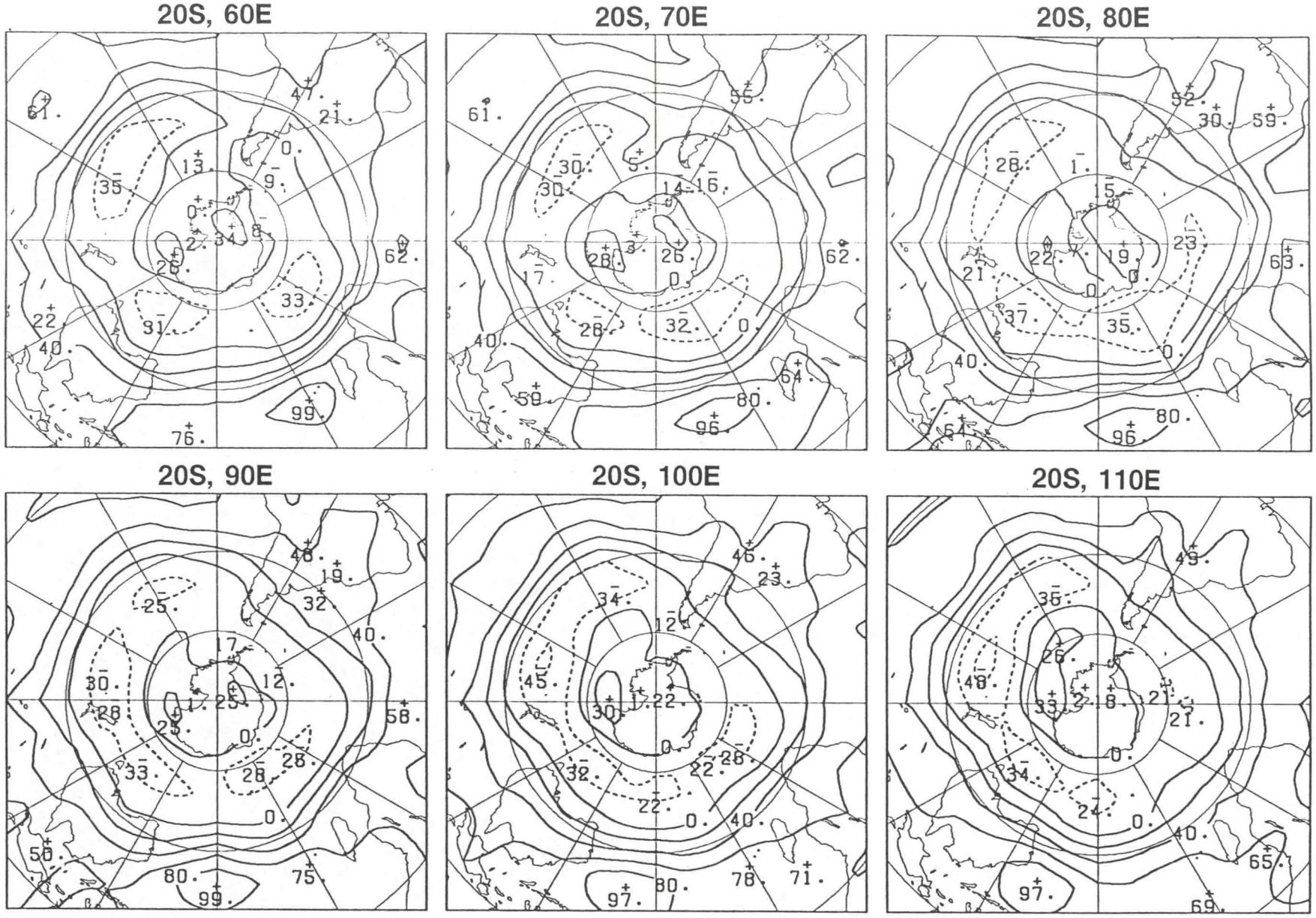
20S, 60E
20S, 70E
20S, 80E
20S, 90E
20S, 100E
20S, 110E

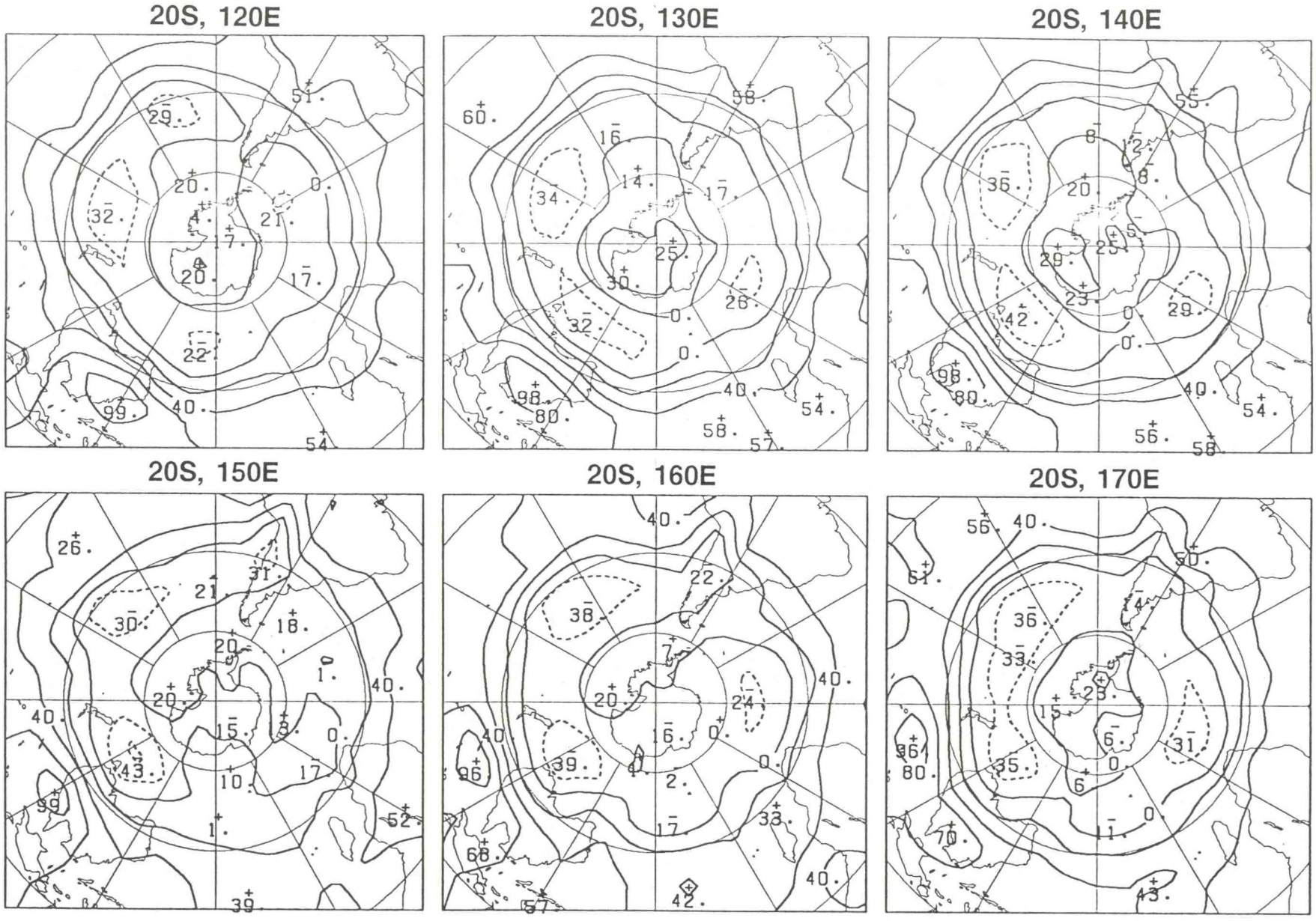
20S, 120E
20S, 130E
20S, 140E
20S, 150E
20S, 160E
20S, 170E

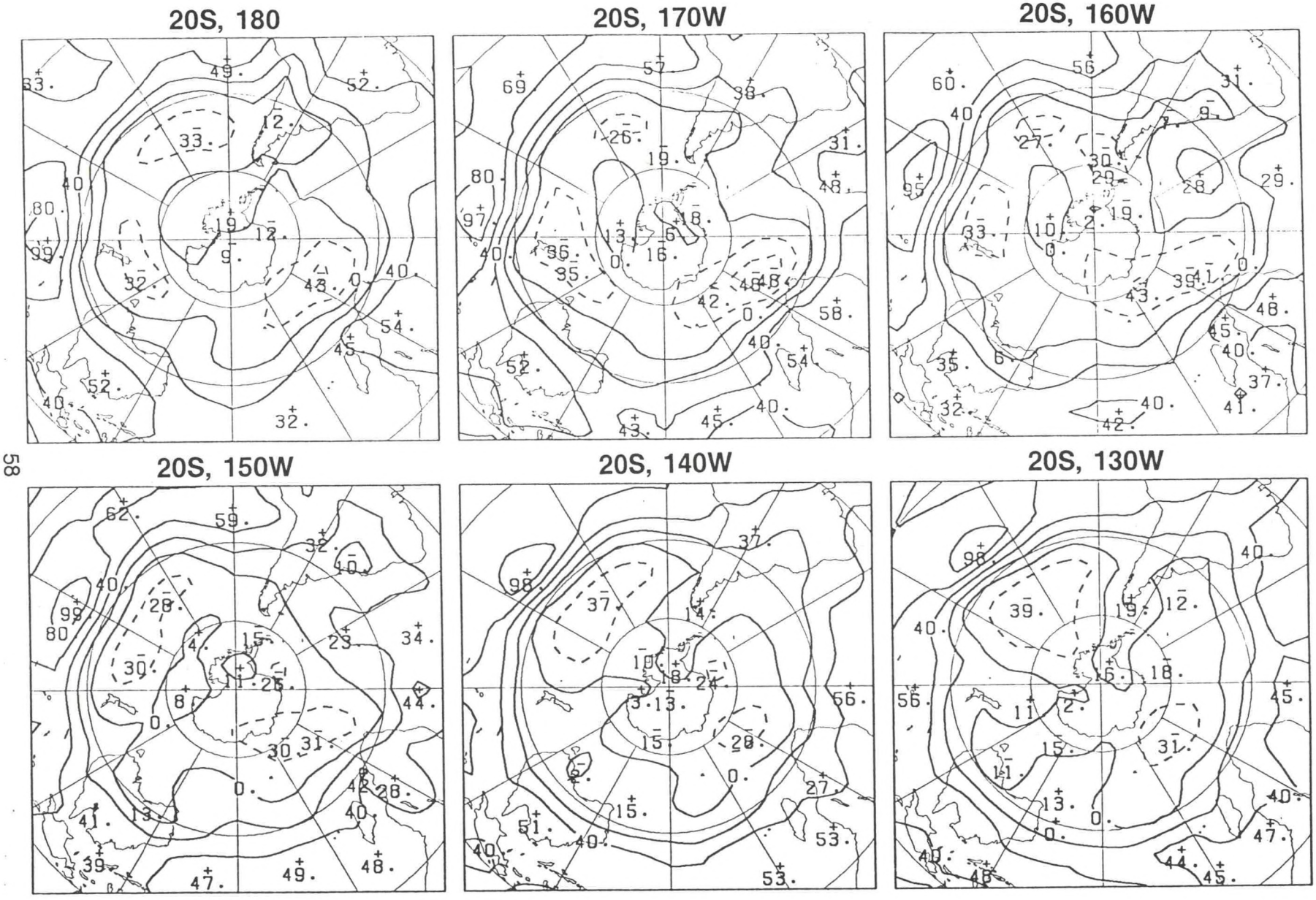
20S, 180
20S, 170W
20S, 160W
20S, 150W
20S, 140W
20S, 130W

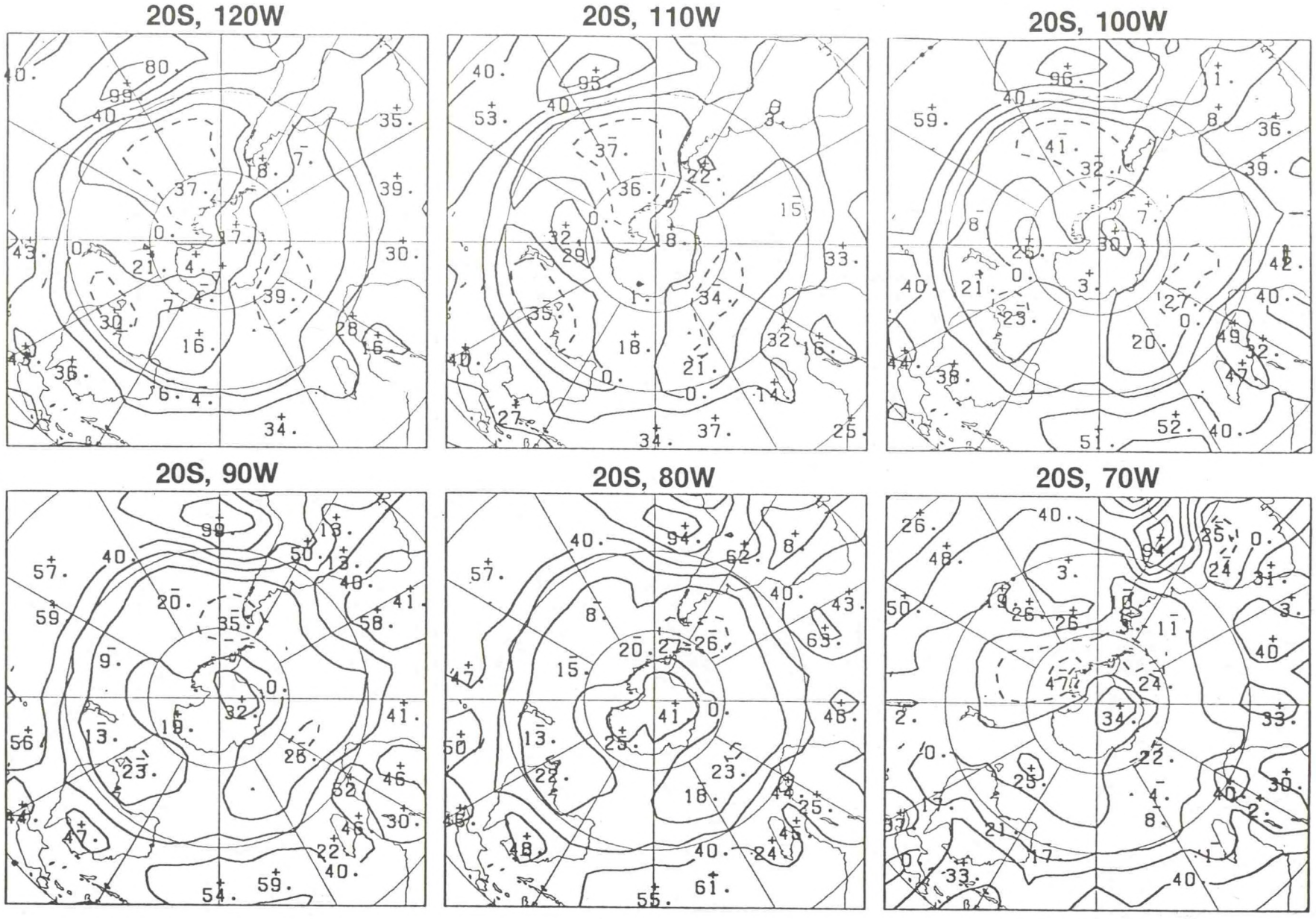
20S, 120W
20S, 110W
20S, 100W
20S, 90W
20S, 80W
20S, 70W

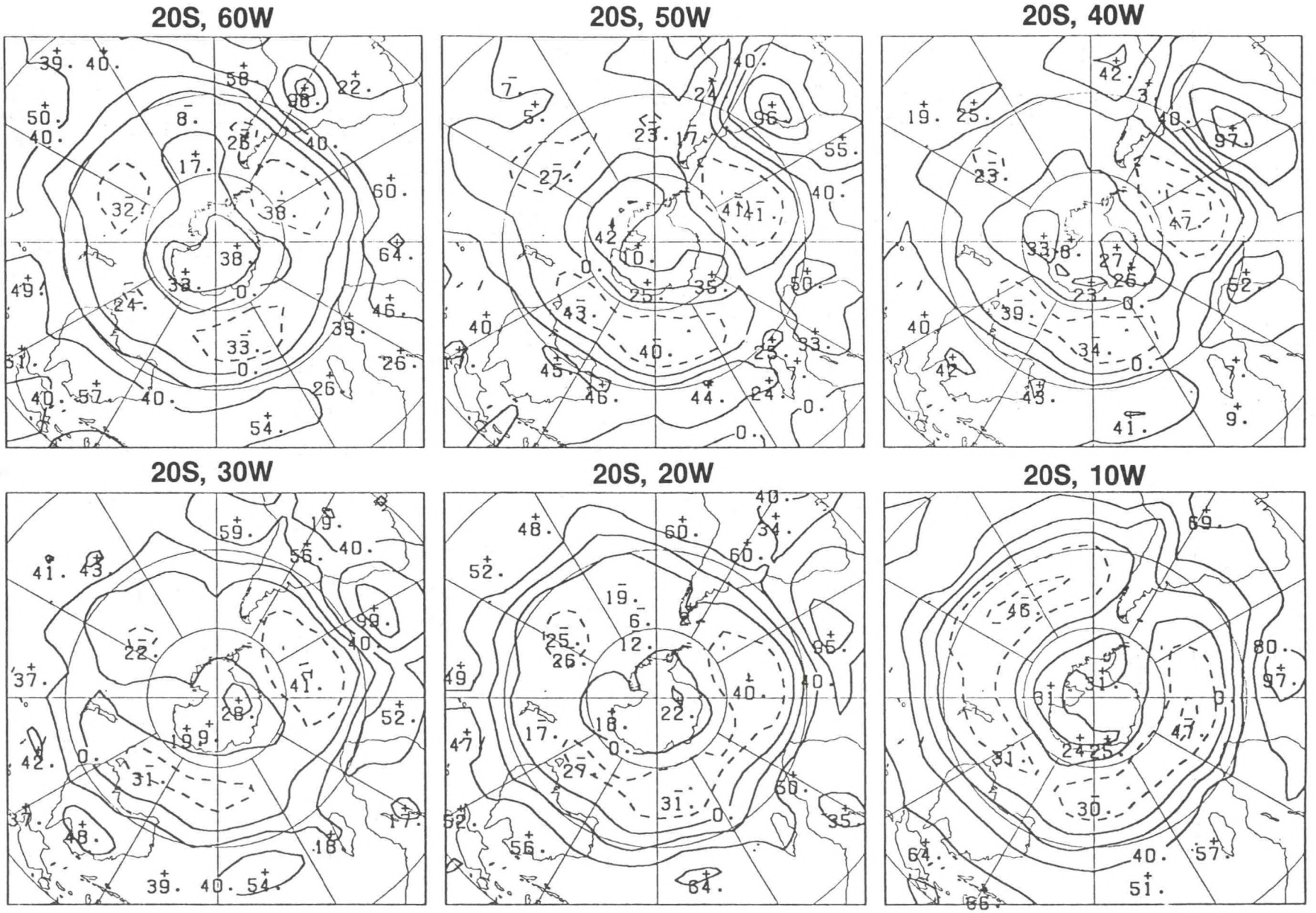
20S, 60W
20S, 50W
20S, 40W
20S, 30W
20S, 20W
20S, 10W

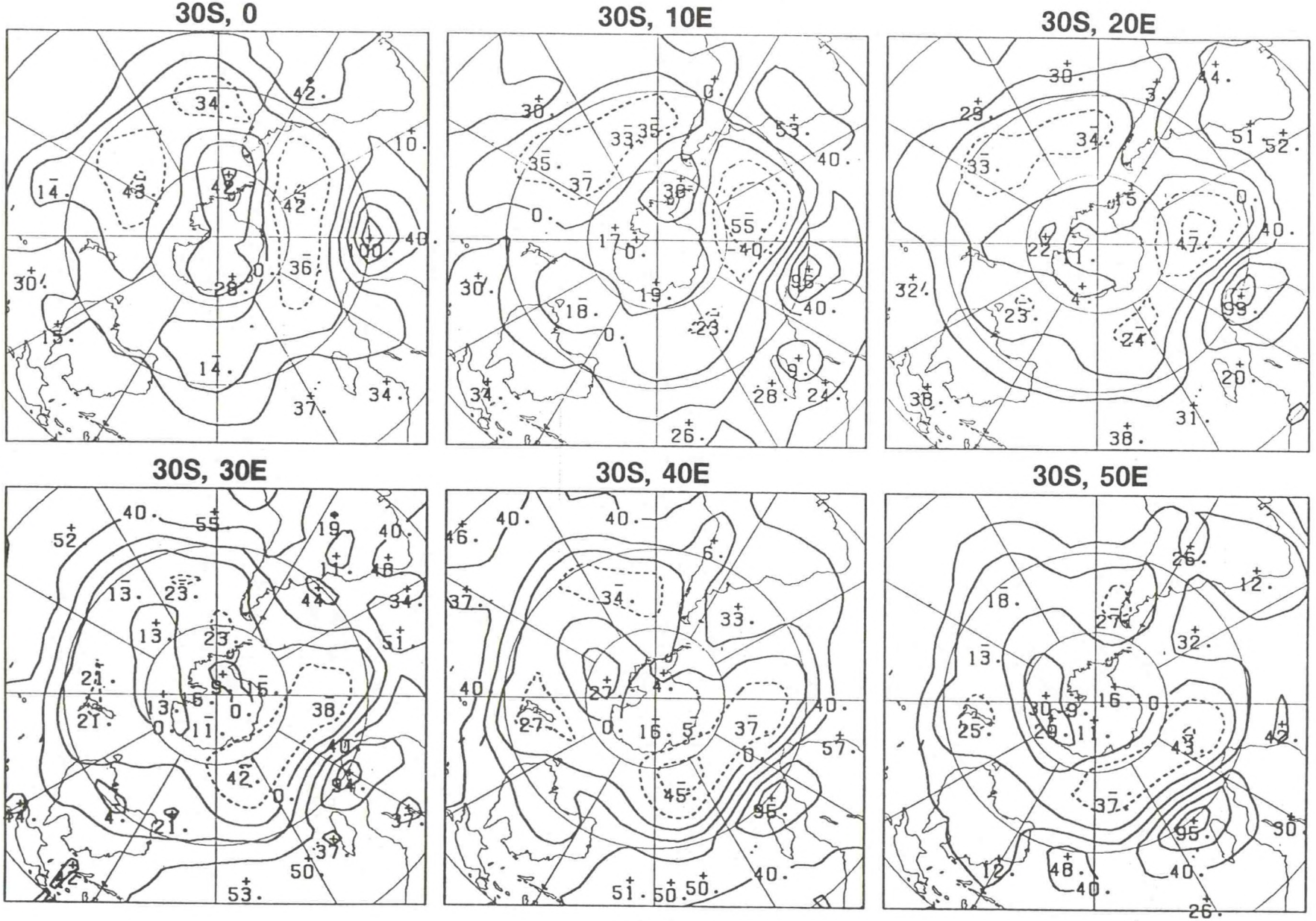
30S, 0
30S, 10E
30S, 20E
30S, 30E
30S, 40E
30S, 50E

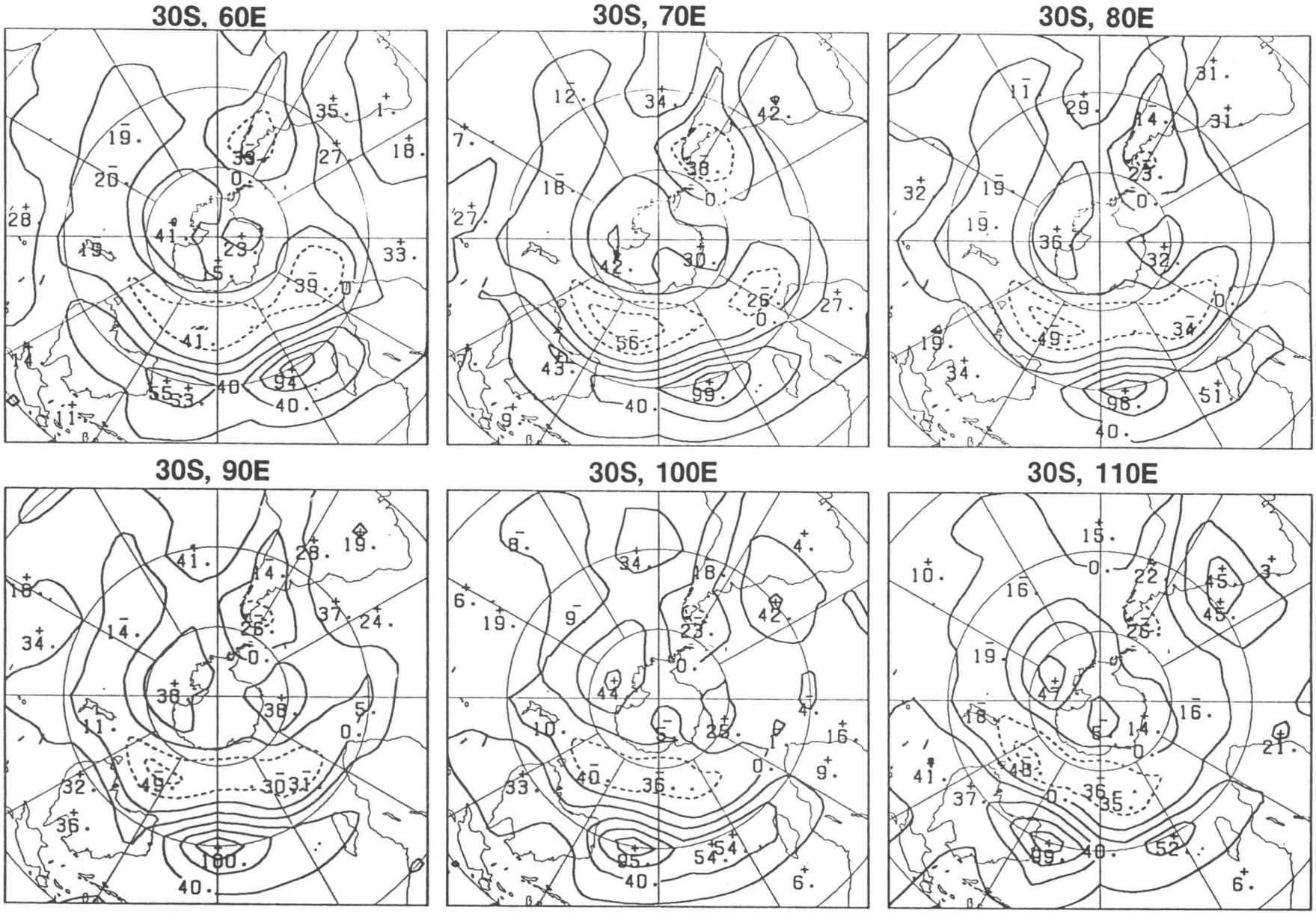
30S, 60E
30S, 70E
30S, 80E
30S, 90E
30S, 100E
30S, 110E

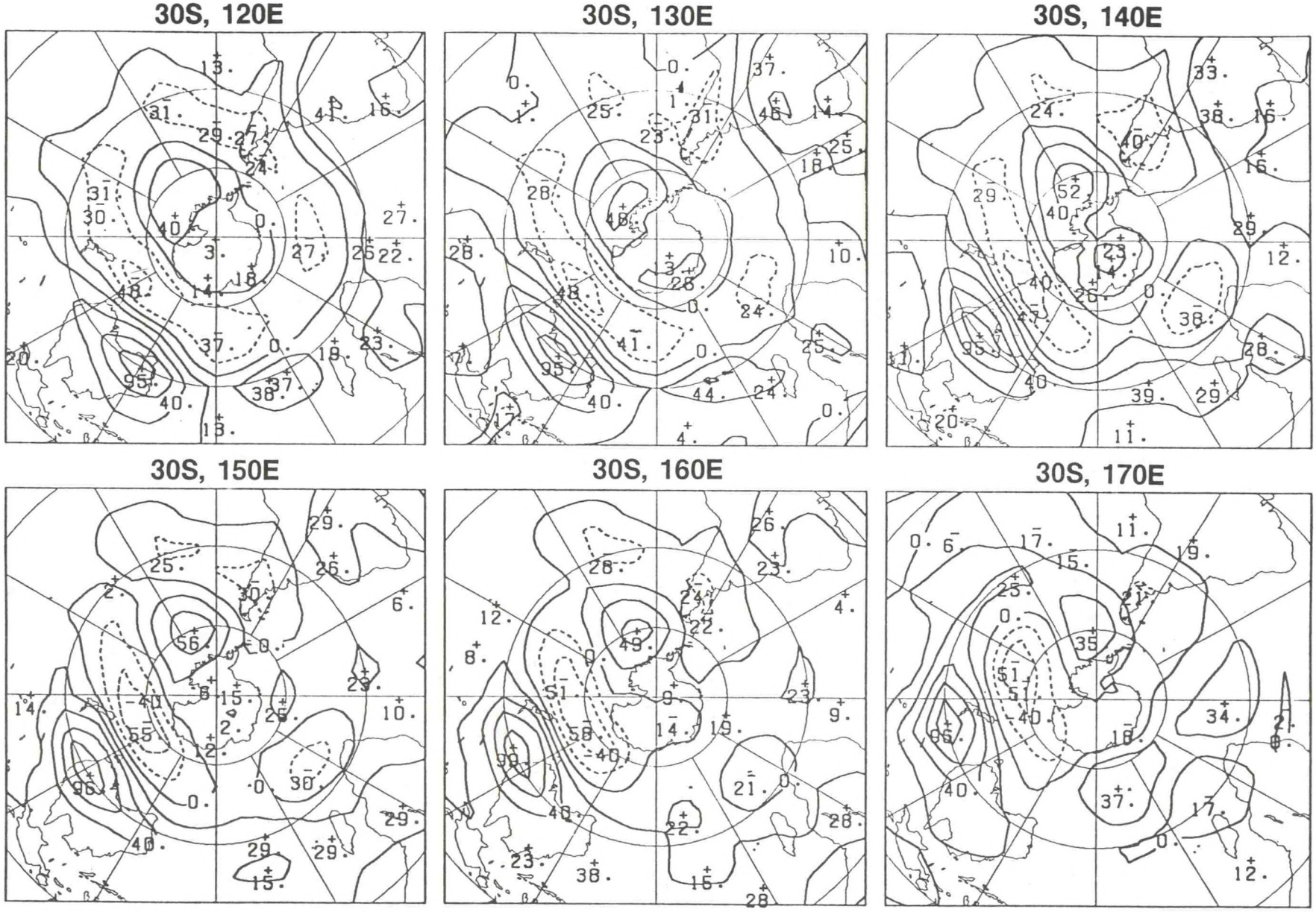
30S, 120E
30S, 130E
30S, 140E
30S, 150E
30S, 160E
30S, 170E

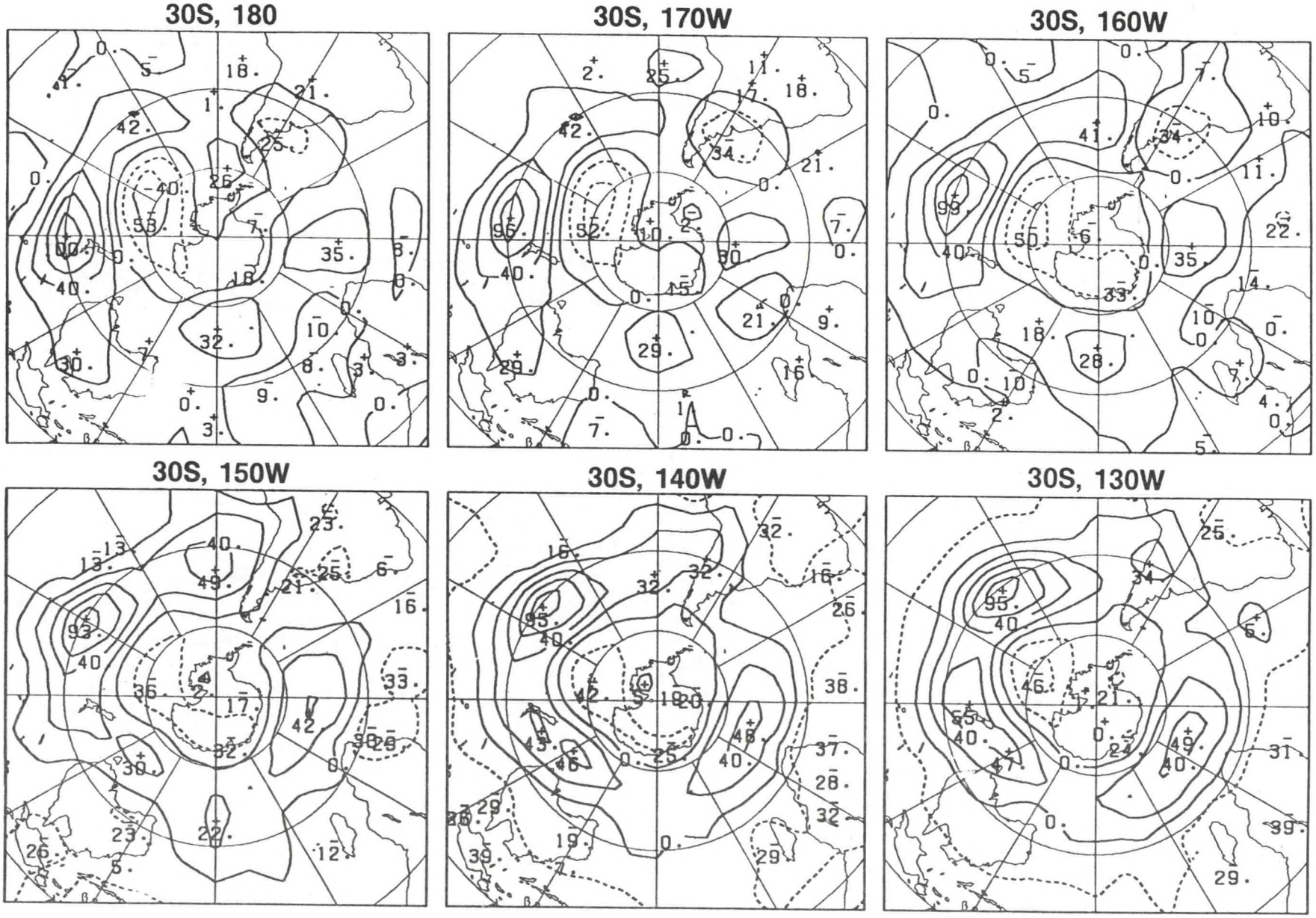
30S, 180
30S, 170W
30S, 160W
30S, 150W
30S, 140W
30S, 130W

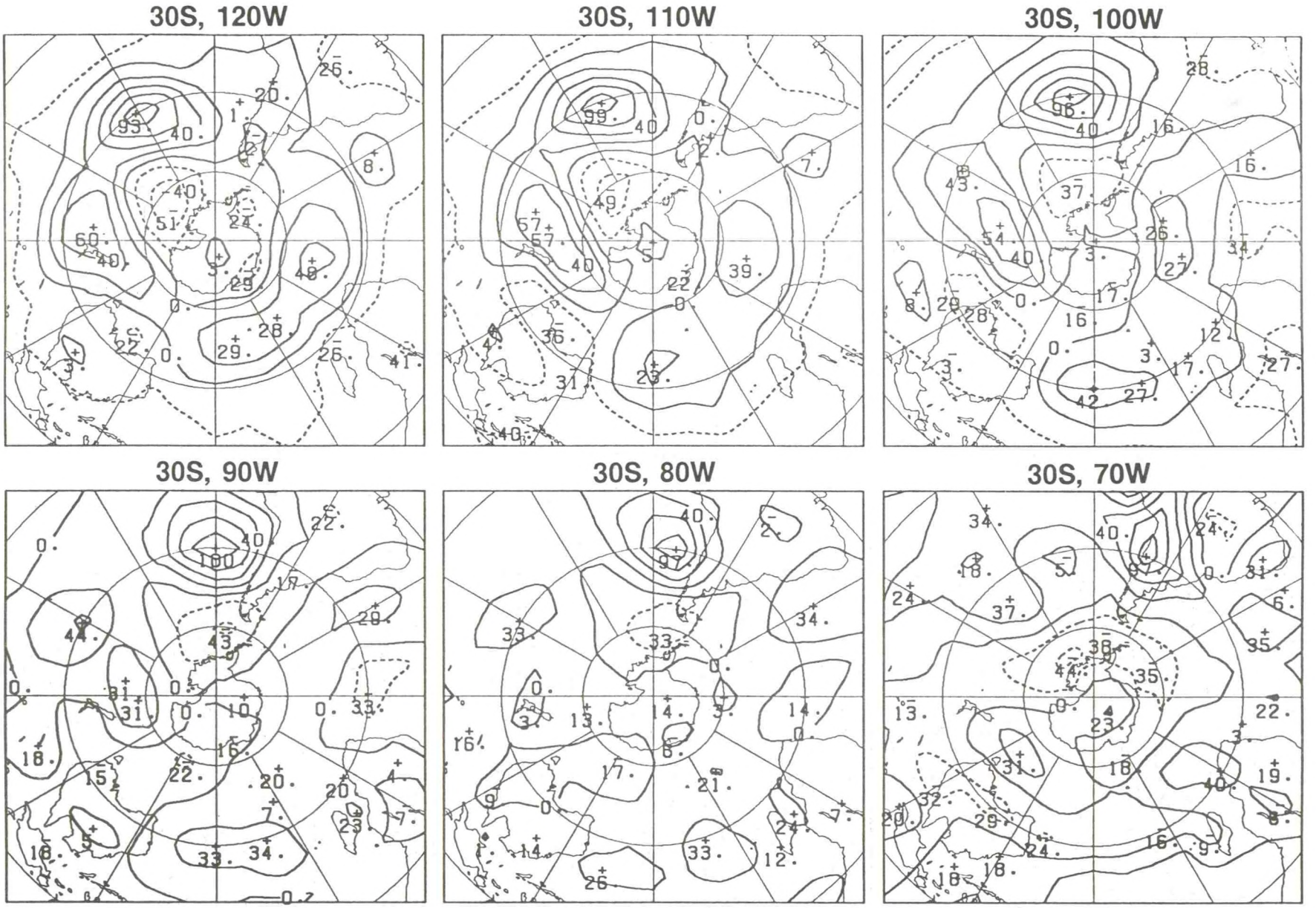
30S, 120W
30S, 110W
30S, 100W
30S, 90W
30S, 80W
30S, 70W

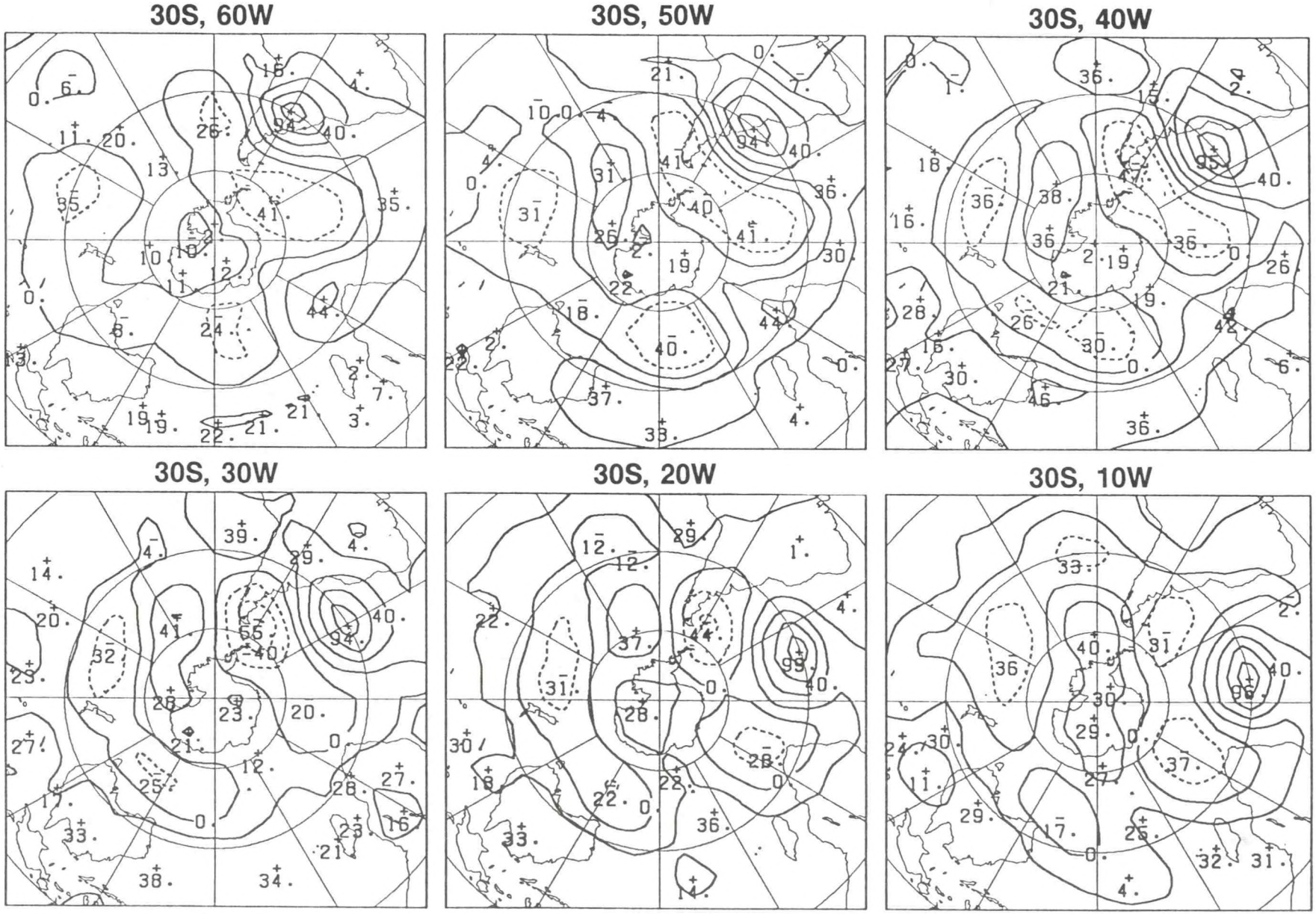
30S, 60W
30S, 50W
30S, 40W
30S, 30W
30S, 20W
30S, 10W

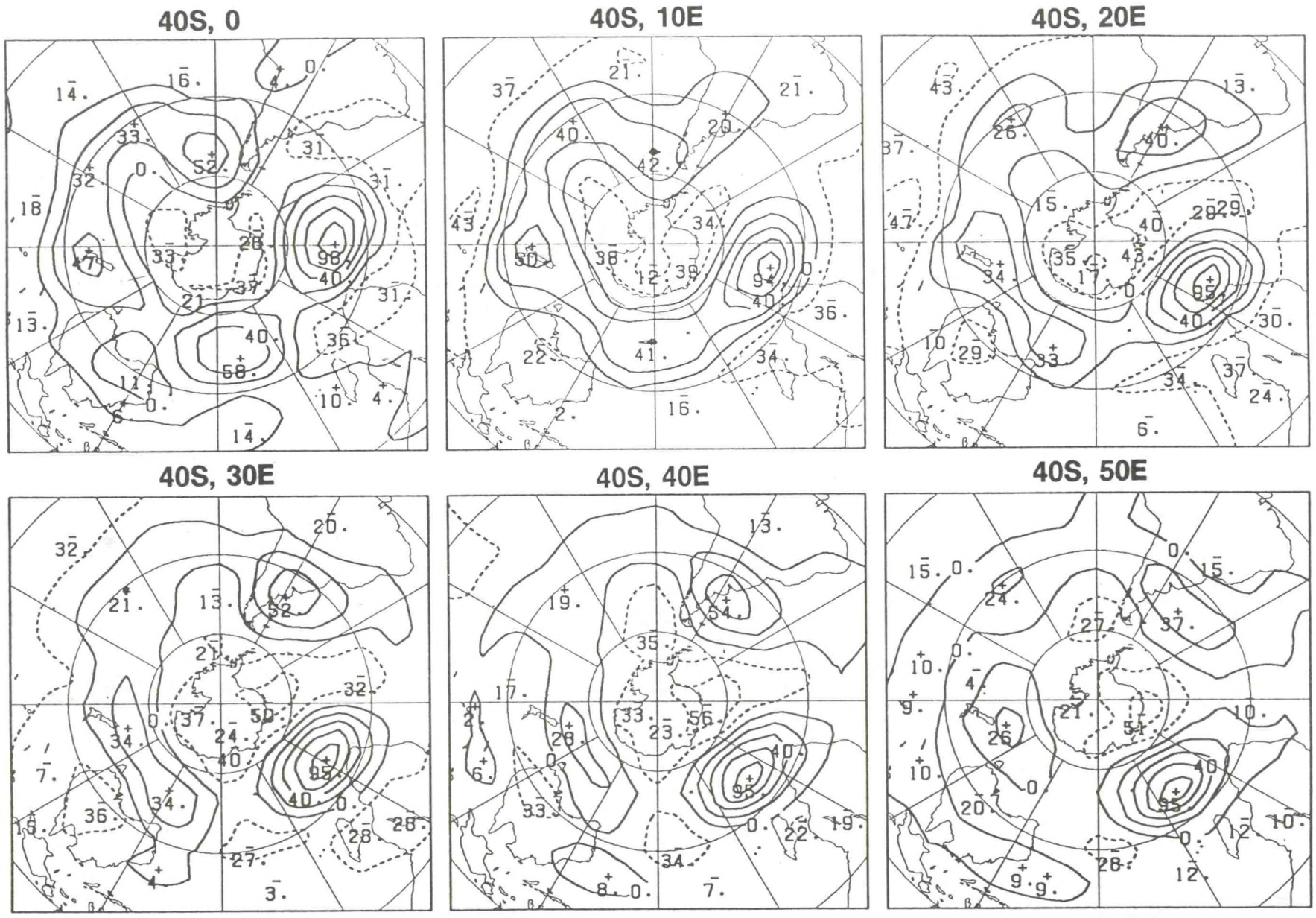
40S, 0
40S, 10E
40S, 20E
40S, 30E
40S, 40E
40S, 50E

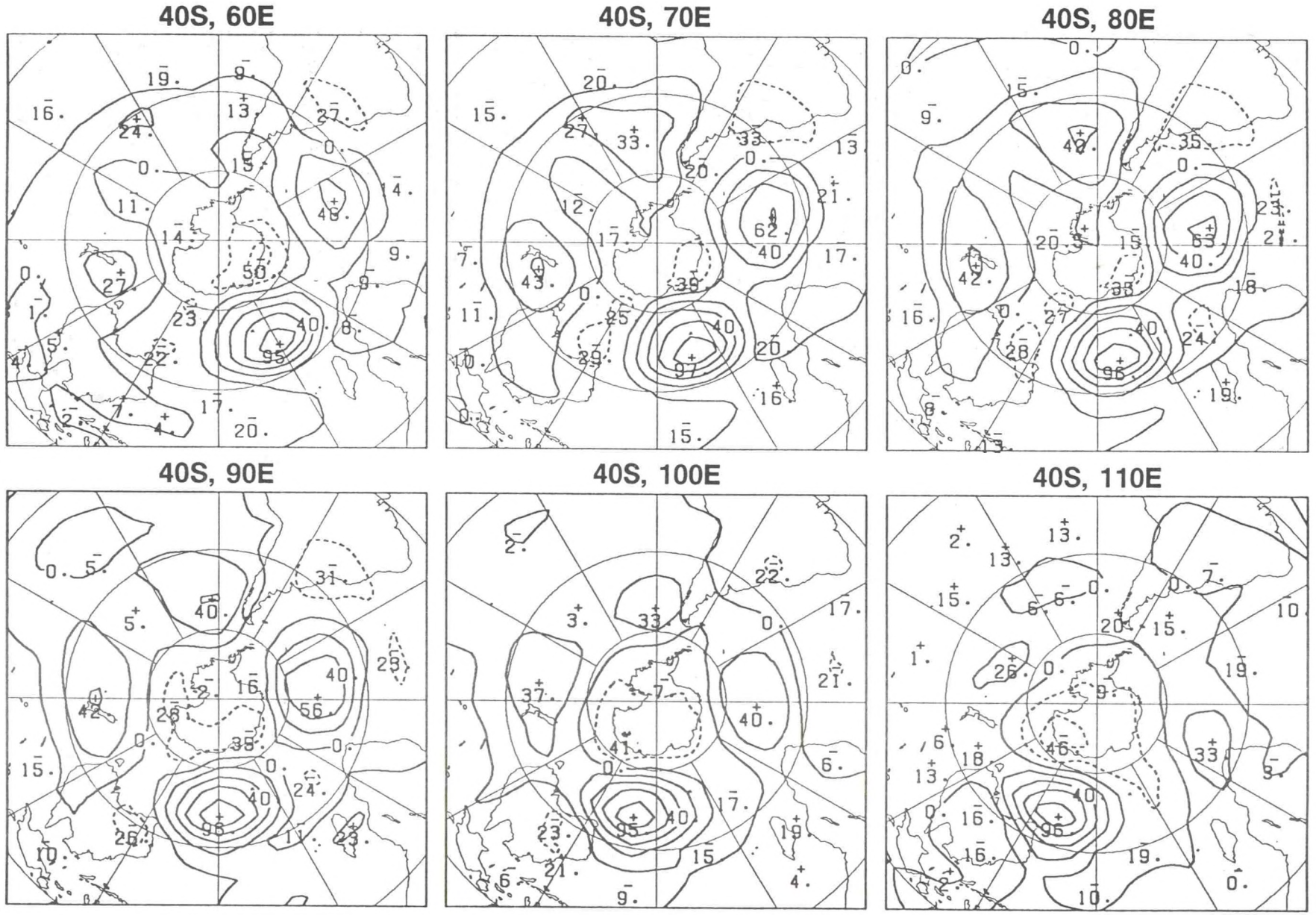
40S, 60E
40S, 70E
40S, 80E
40S, 90E
40S, 100E
40S, 110E

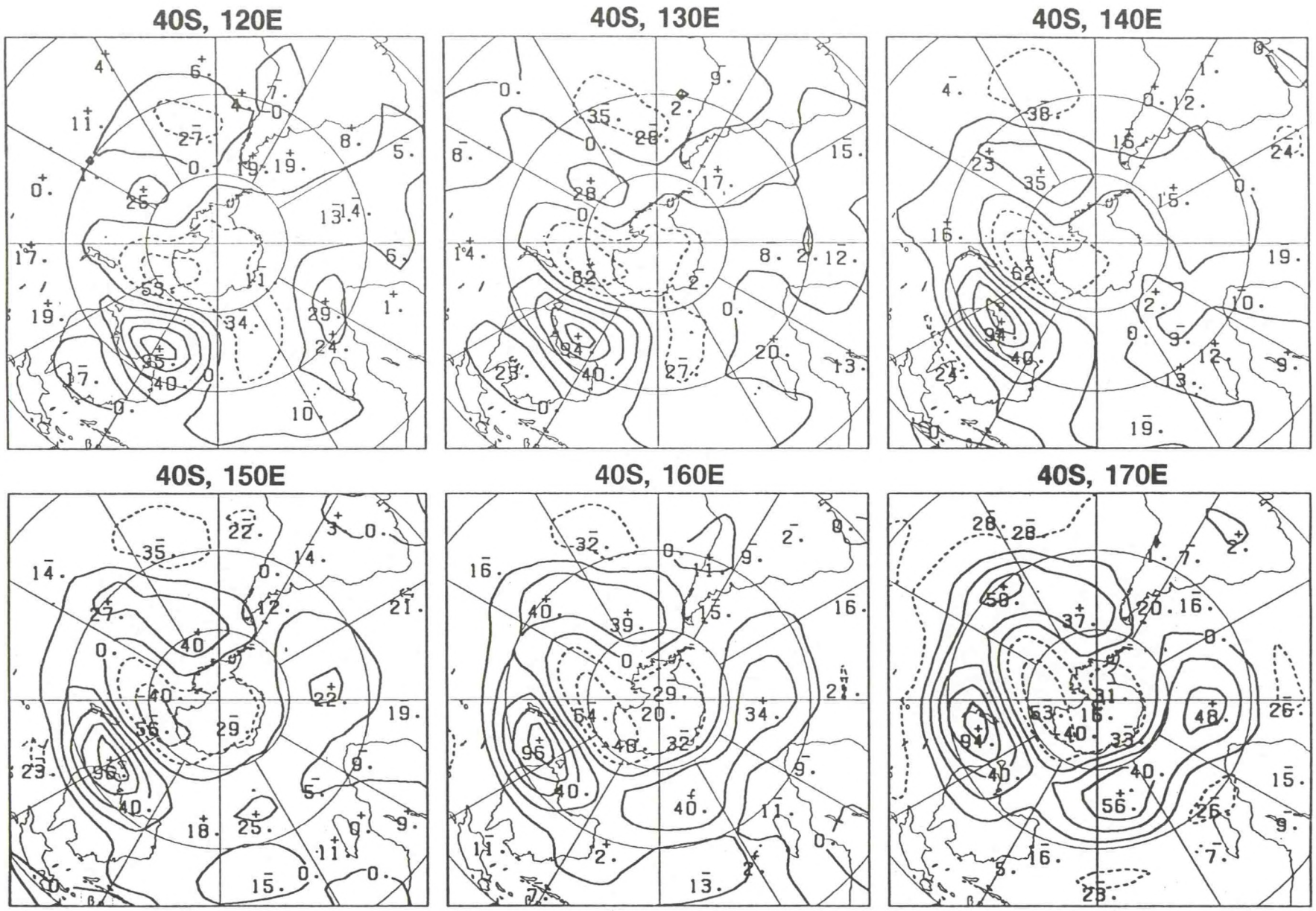
40S, 120E
40S, 130E
40S, 140E
40S, 150E
40S, 160E
40S, 170E

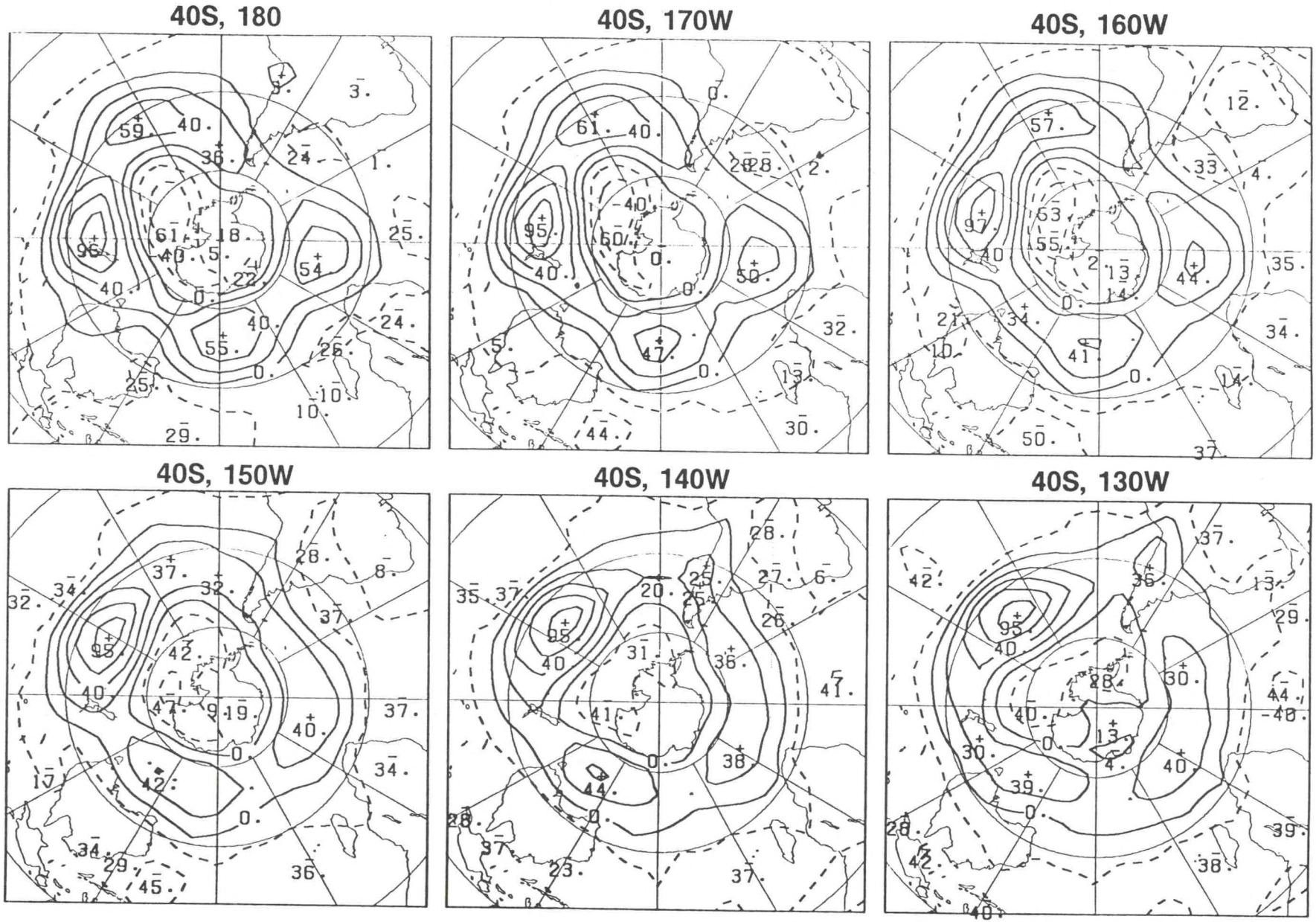
40S, 180
40S, 170W
40S, 160W
40S, 150W
40S, 140W
40S, 130W

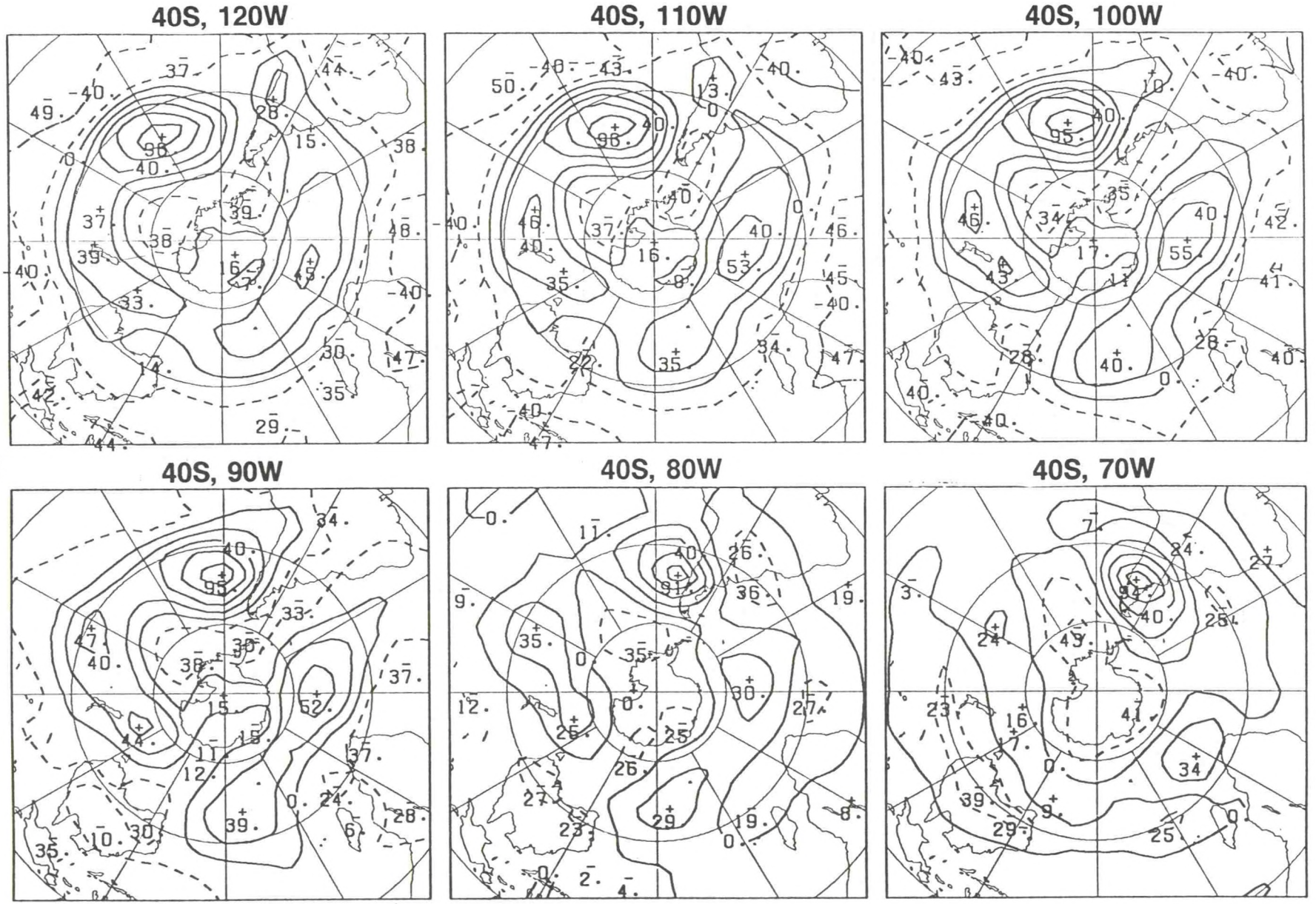
40S, 120W
40S, 110W
40S, 100W
40S, 90W
40S, 80W
40S, 70W

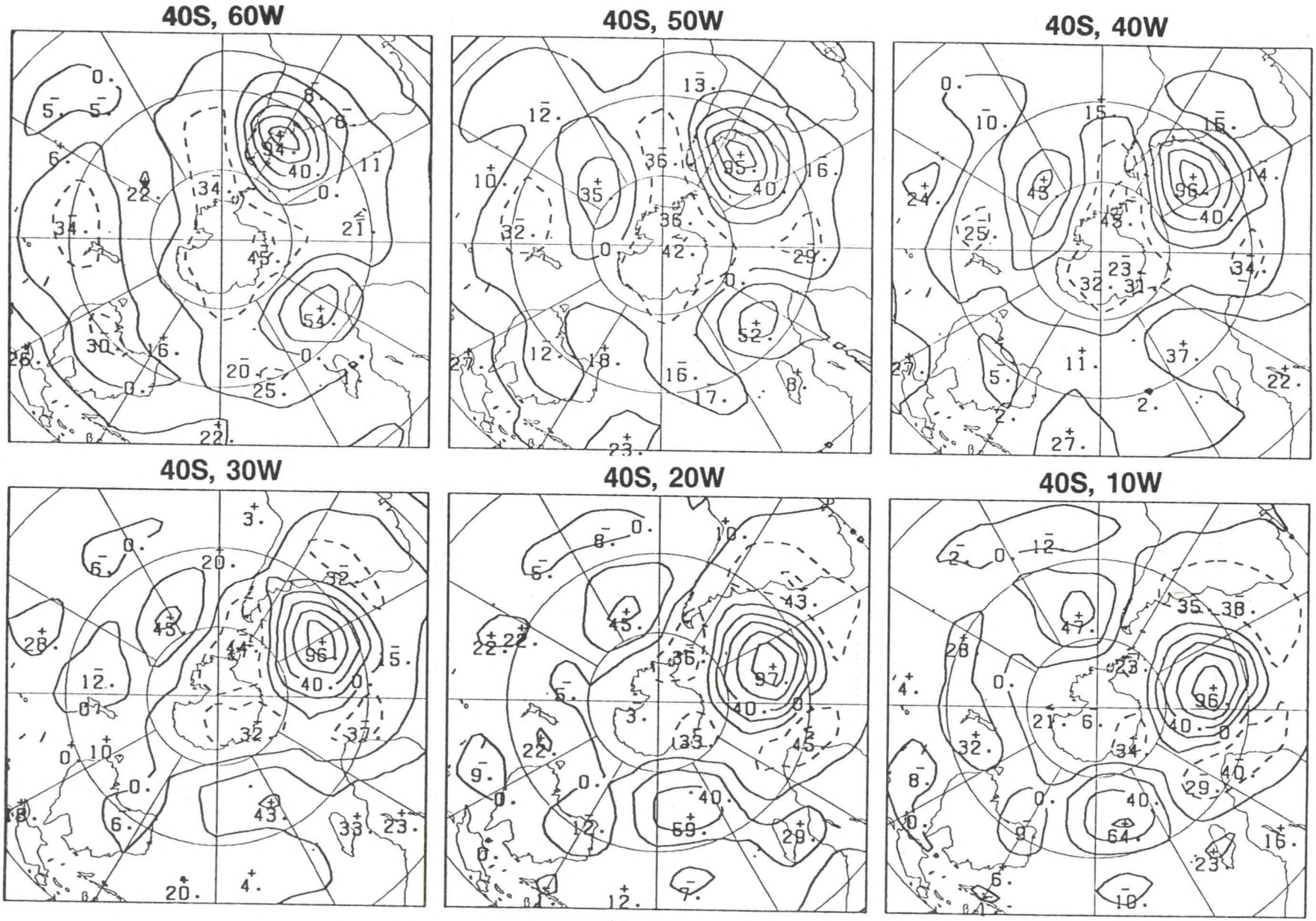
40S, 60W
40S, 50W
40S, 40W
40S, 30W
40S, 20W
40S, 10W

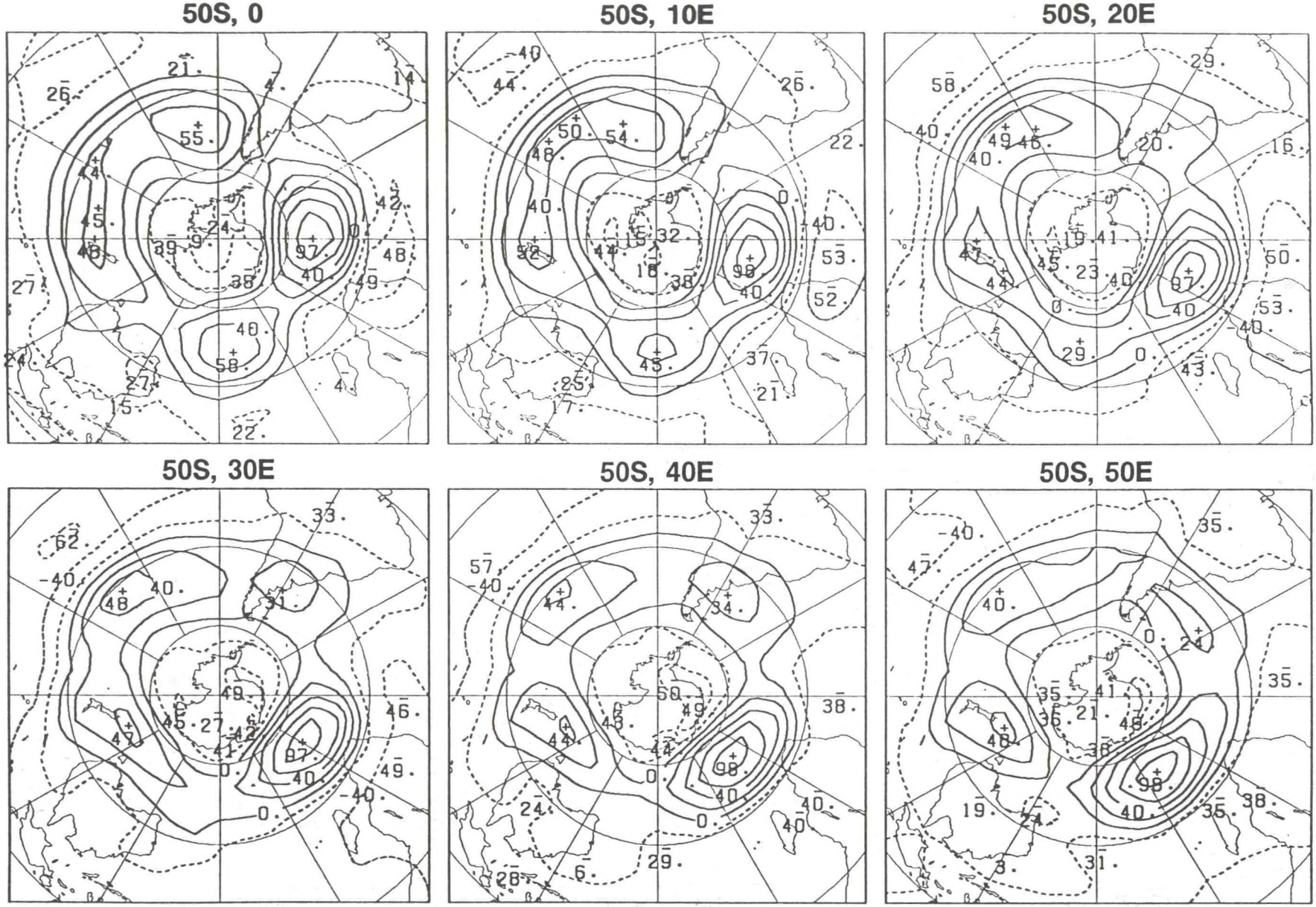
50S, 0
50S, 10E
50S, 20E
50S, 30E
50S, 40E
50S, 50E

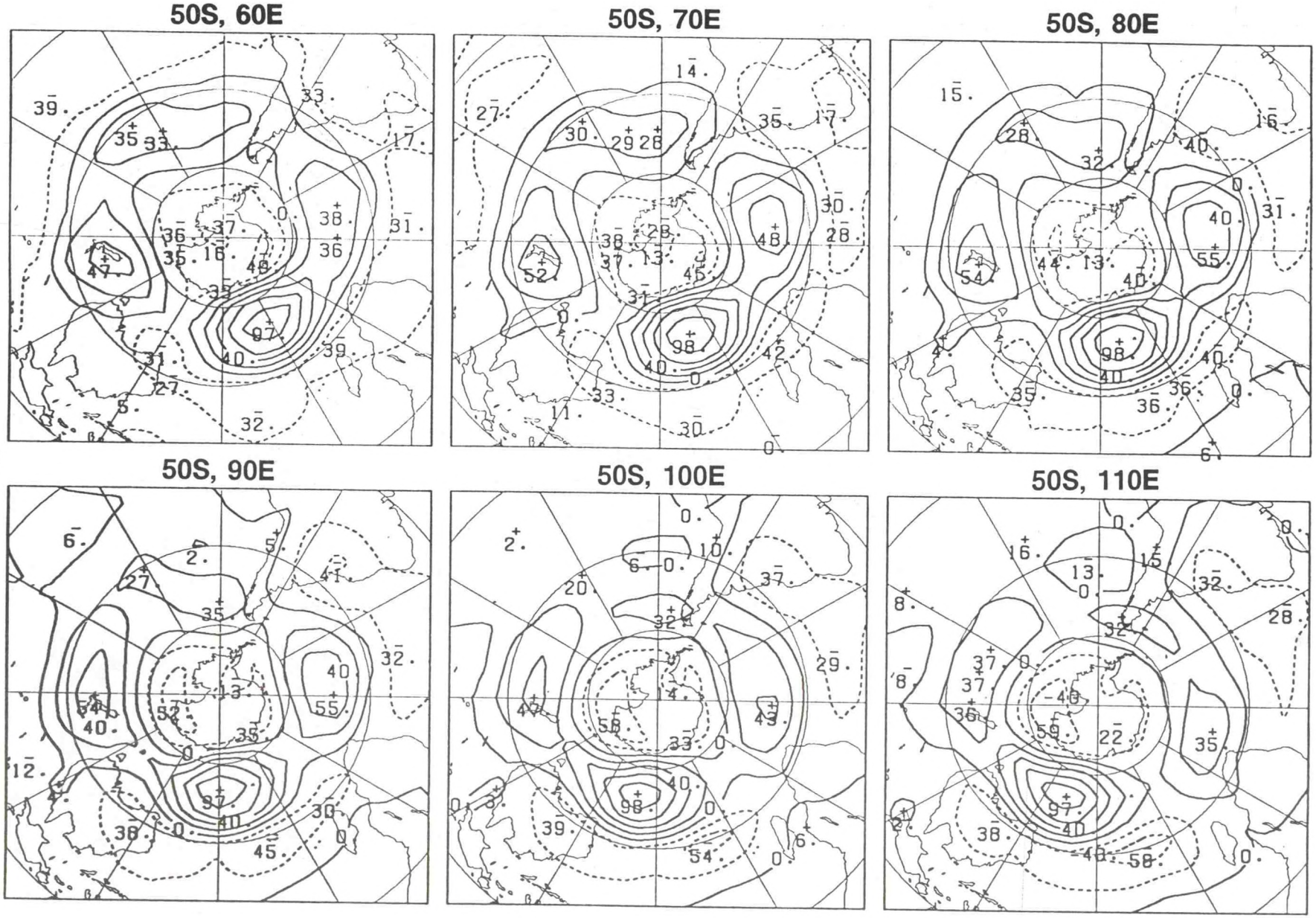
50S, 60E
50S, 70E
50S, 80E
50S, 90E
50S, 100E
50S, 110E

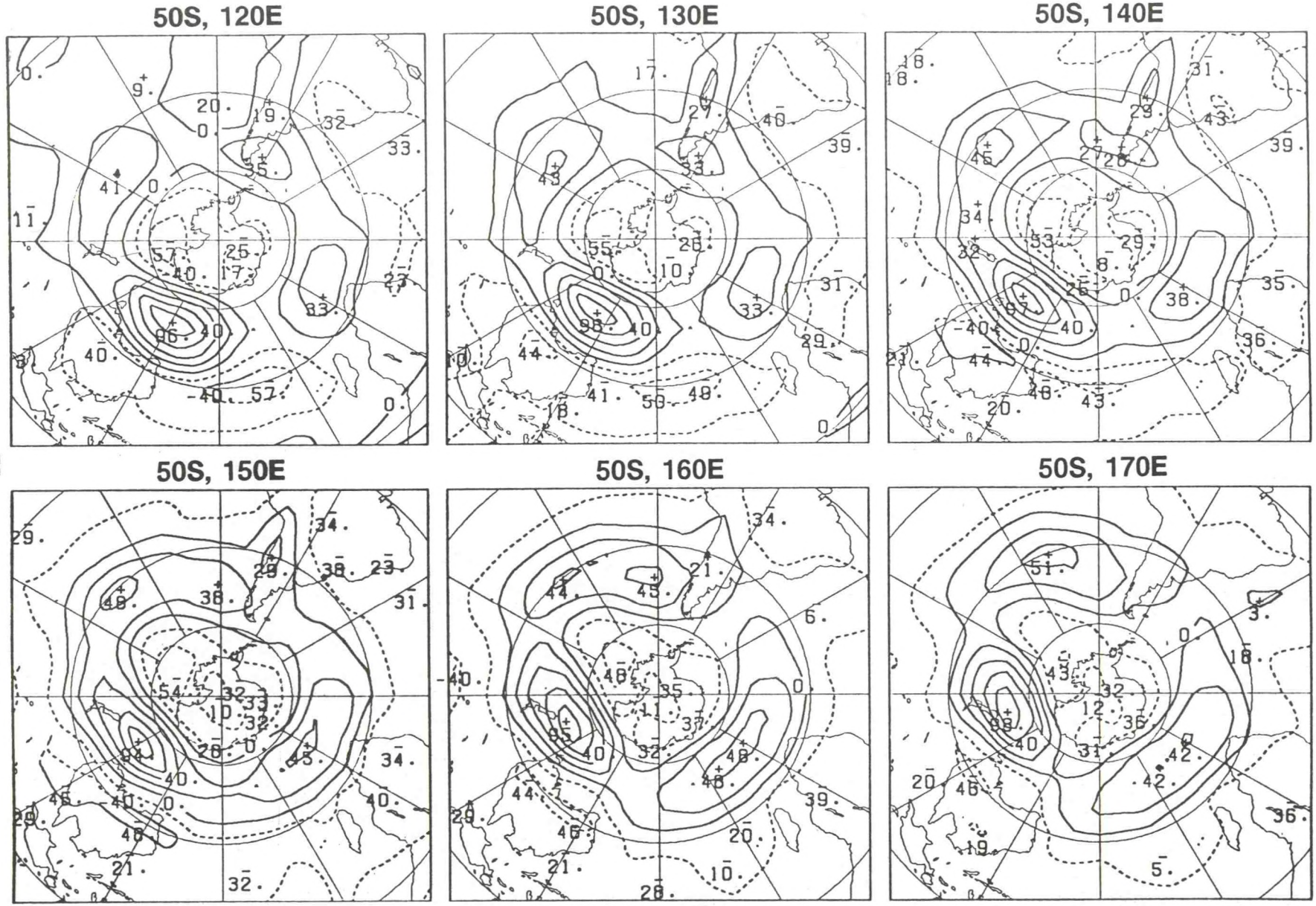
50S, 120E
50S, 130E
50S, 140E
50S, 150E
50S, 160E
50S, 170E

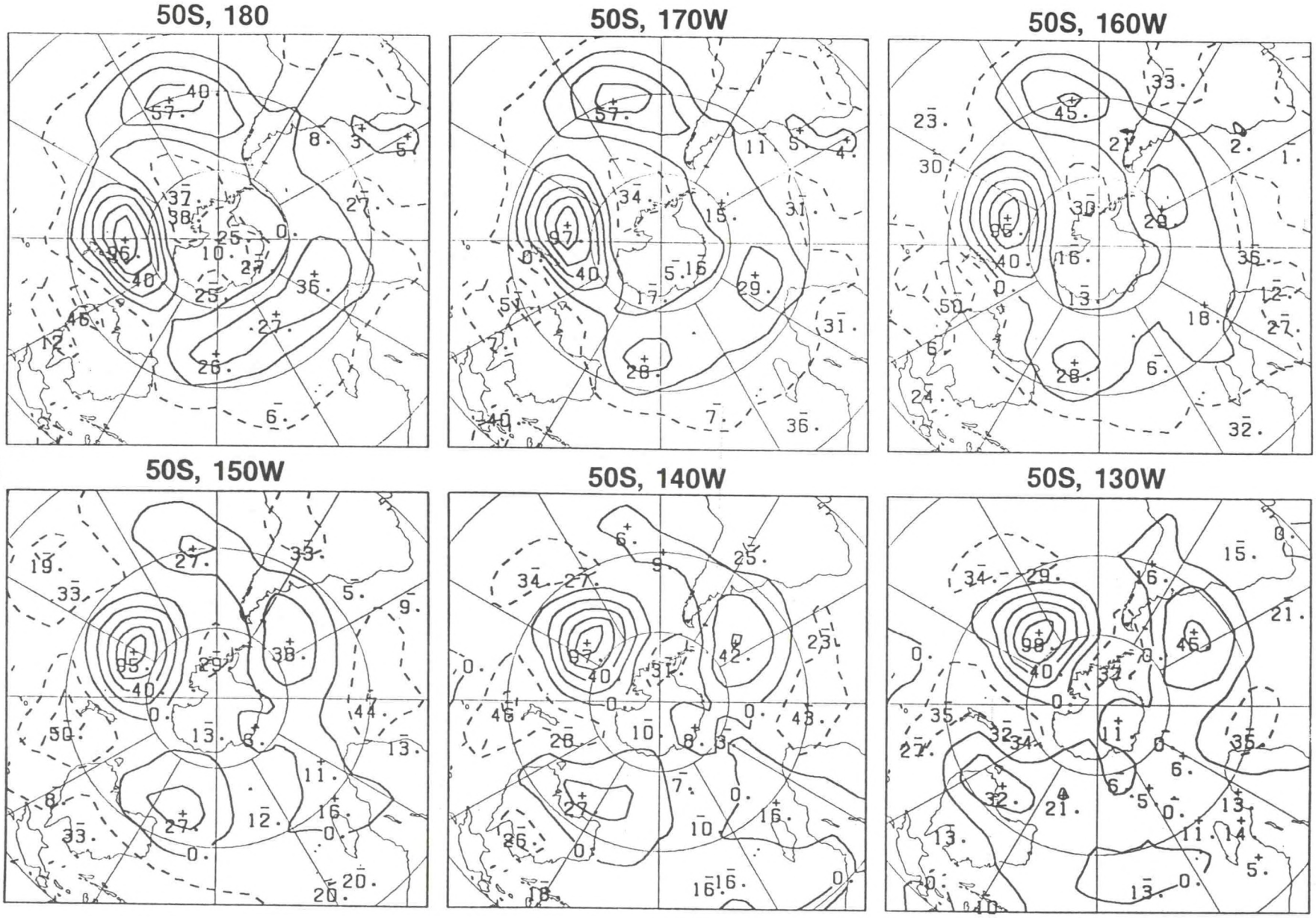
50S, 180
50S, 170W
50S, 160W
50S, 150W
50S, 140W
50S, 130W

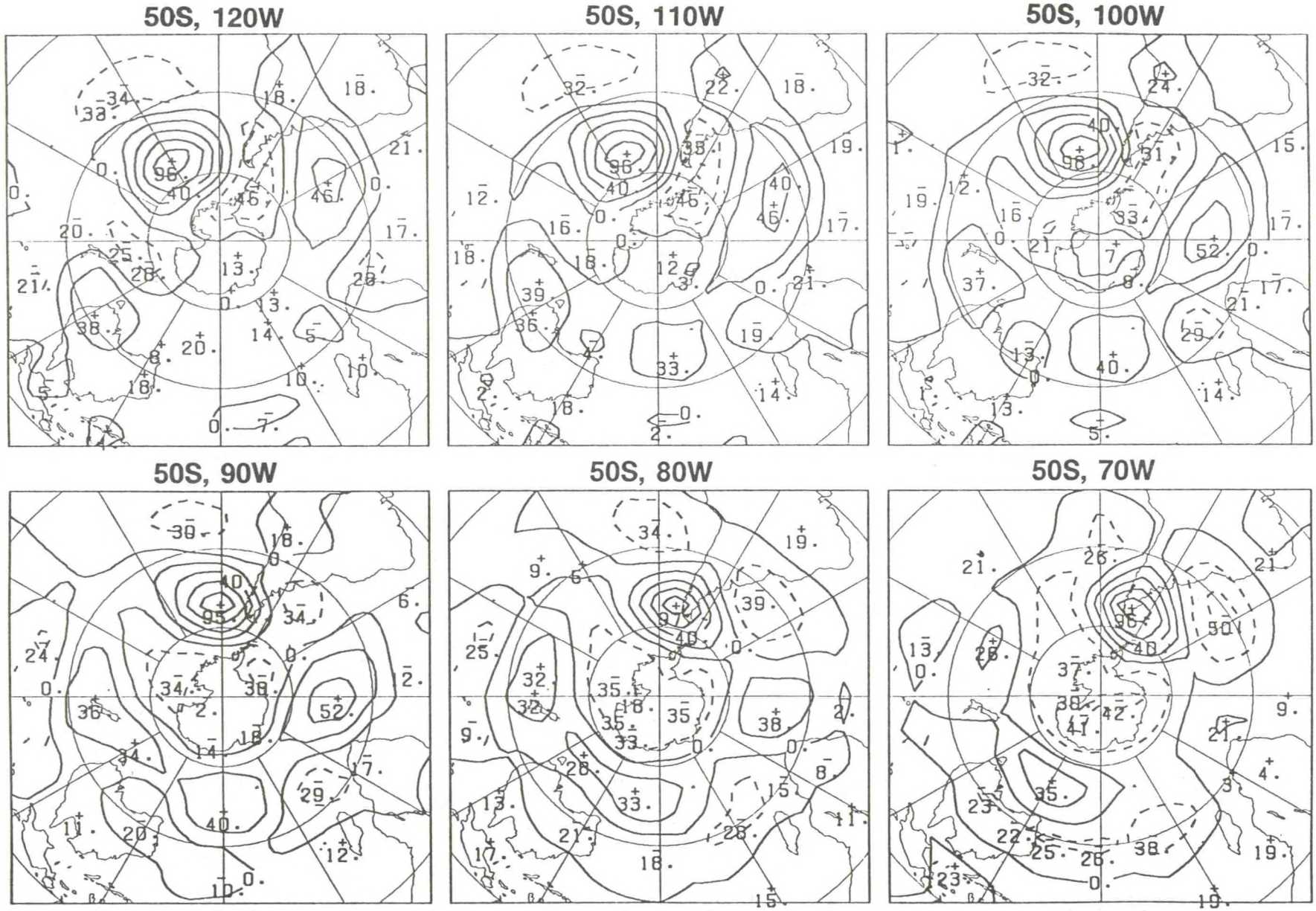
50S, 120W
50S, 110W
50S, 100W
50S, 90W
50S, 80W
50S, 70W

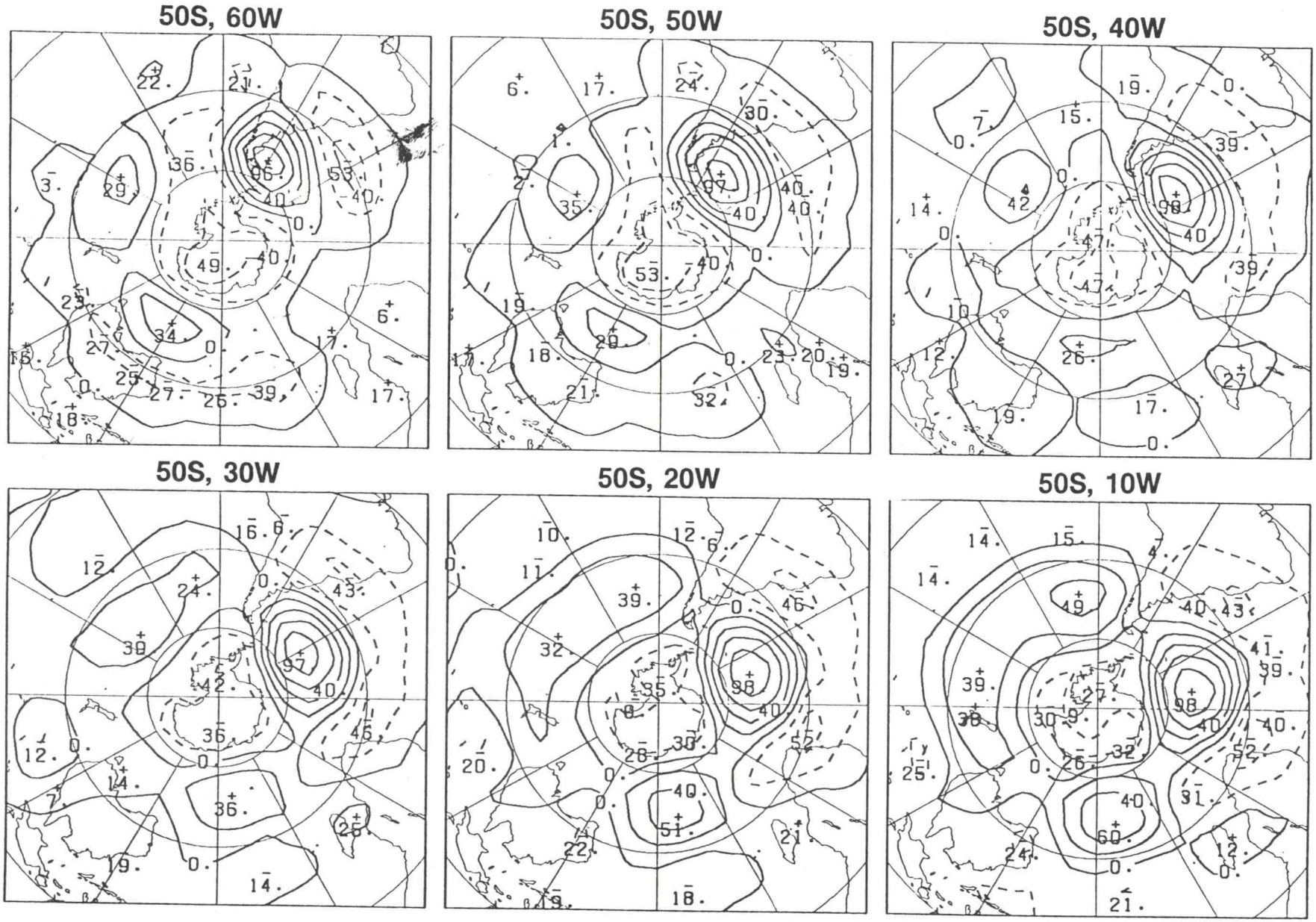
50S, 60W
50S, 50W
50S, 40W
50S, 30W
50S, 20W
50S, 10W

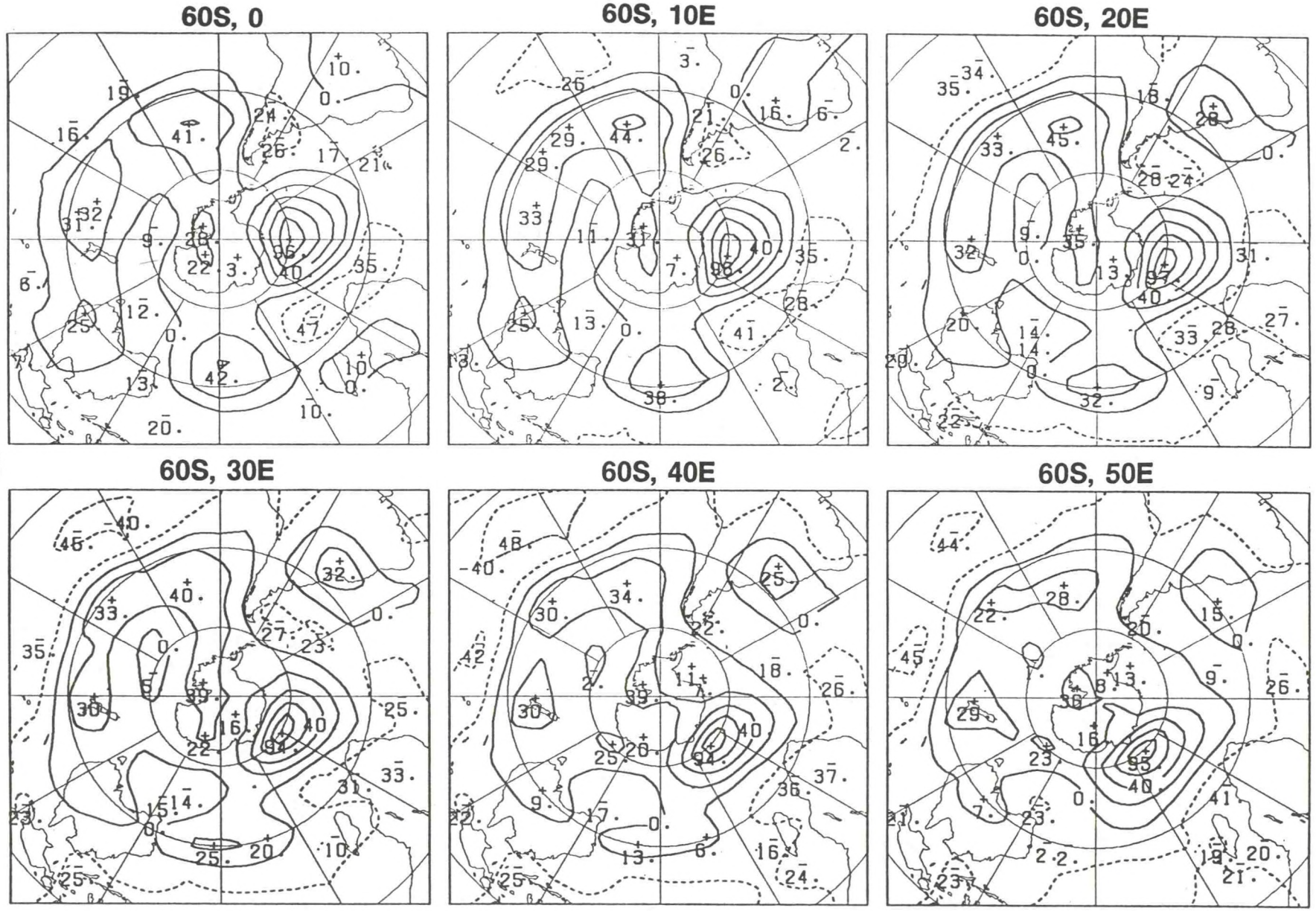
60S, 0
60S, 10E
60S, 20E
60S, 30E
60S, 40E
60S, 50E

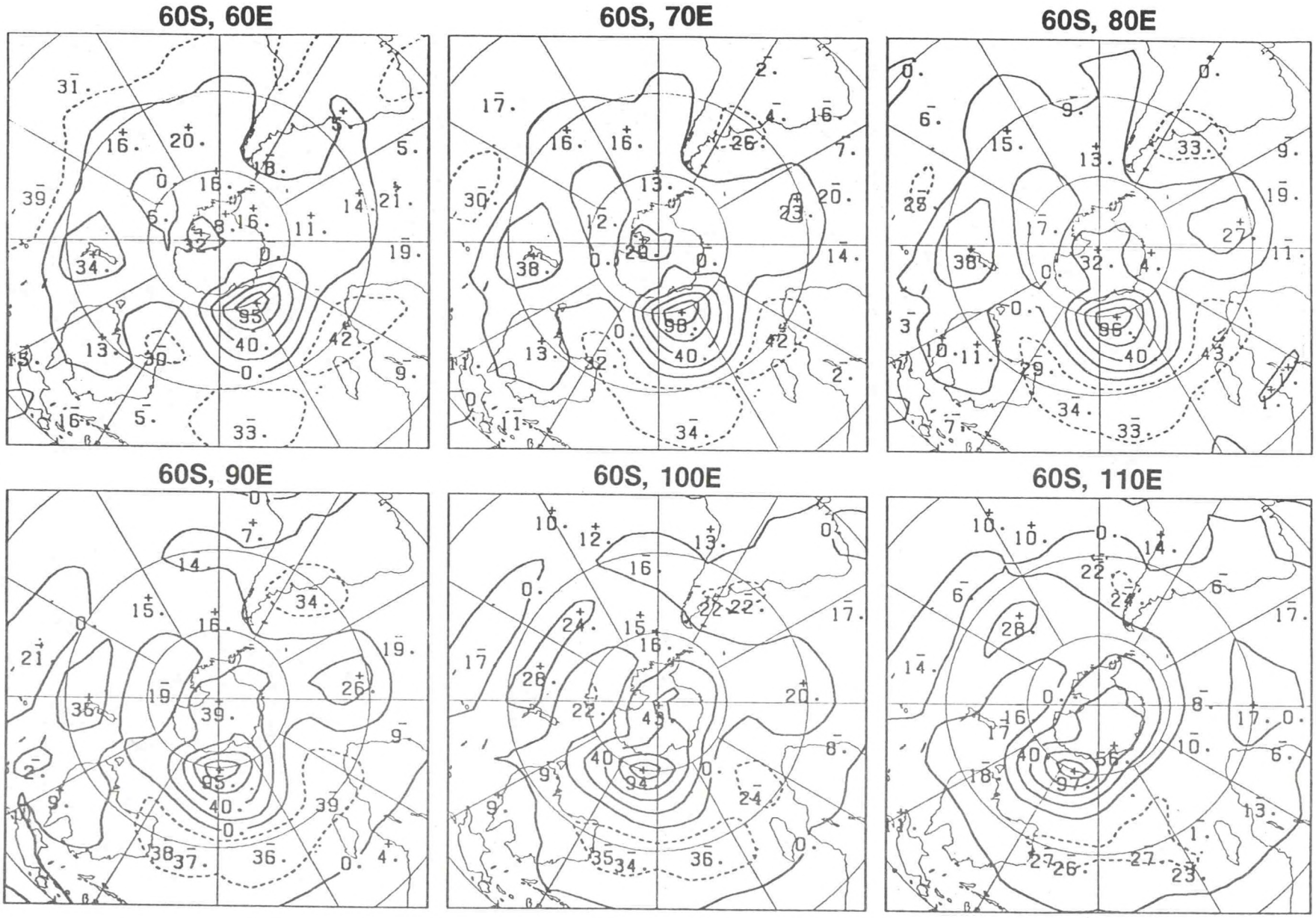
60S, 60E
60S, 70E
60S, 80E
60S, 90E
60S, 100E
60S, 110E

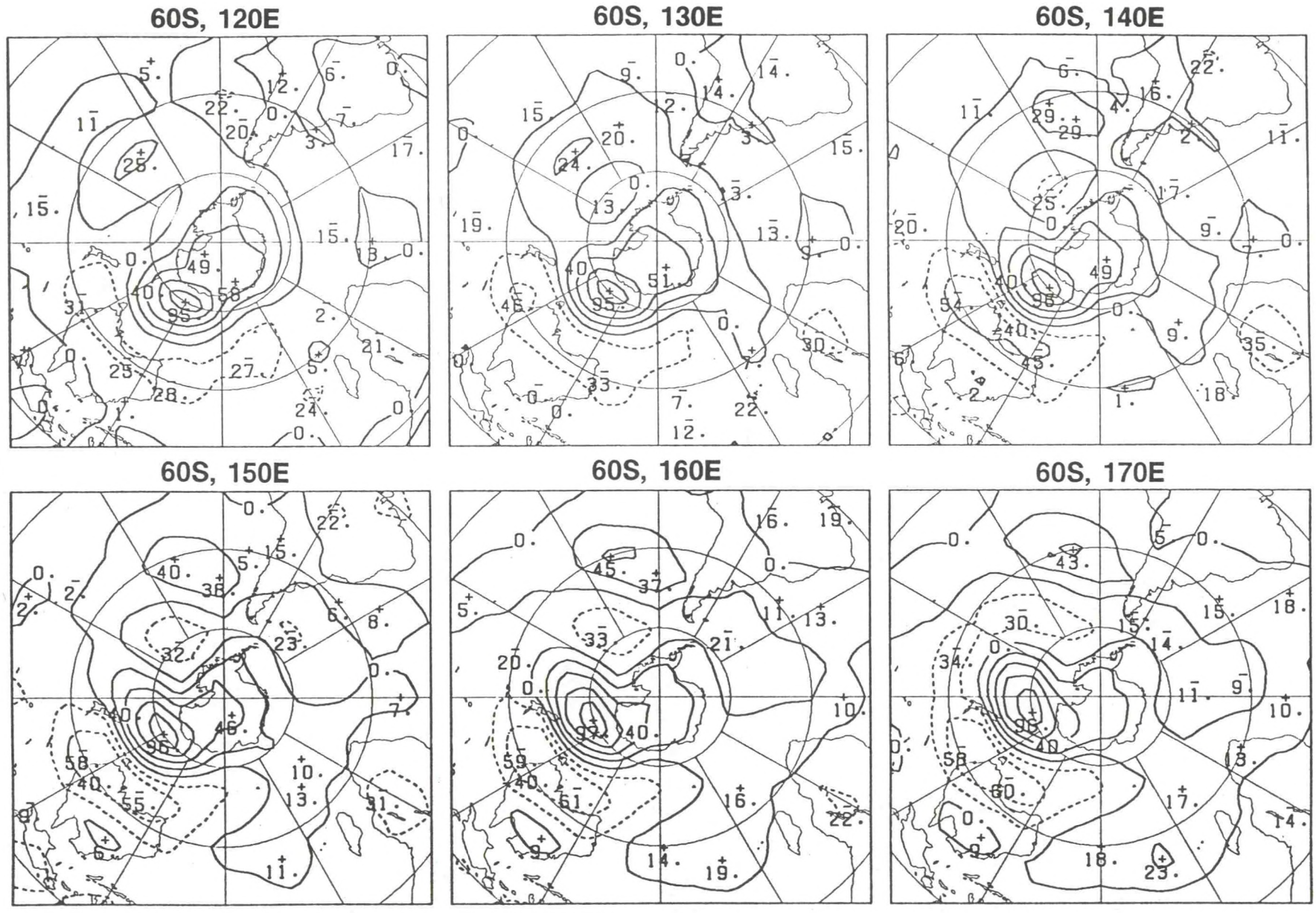
60S, 120E
60S, 130E
60S, 140E
60S, 150E
60S, 160E
60S, 170E

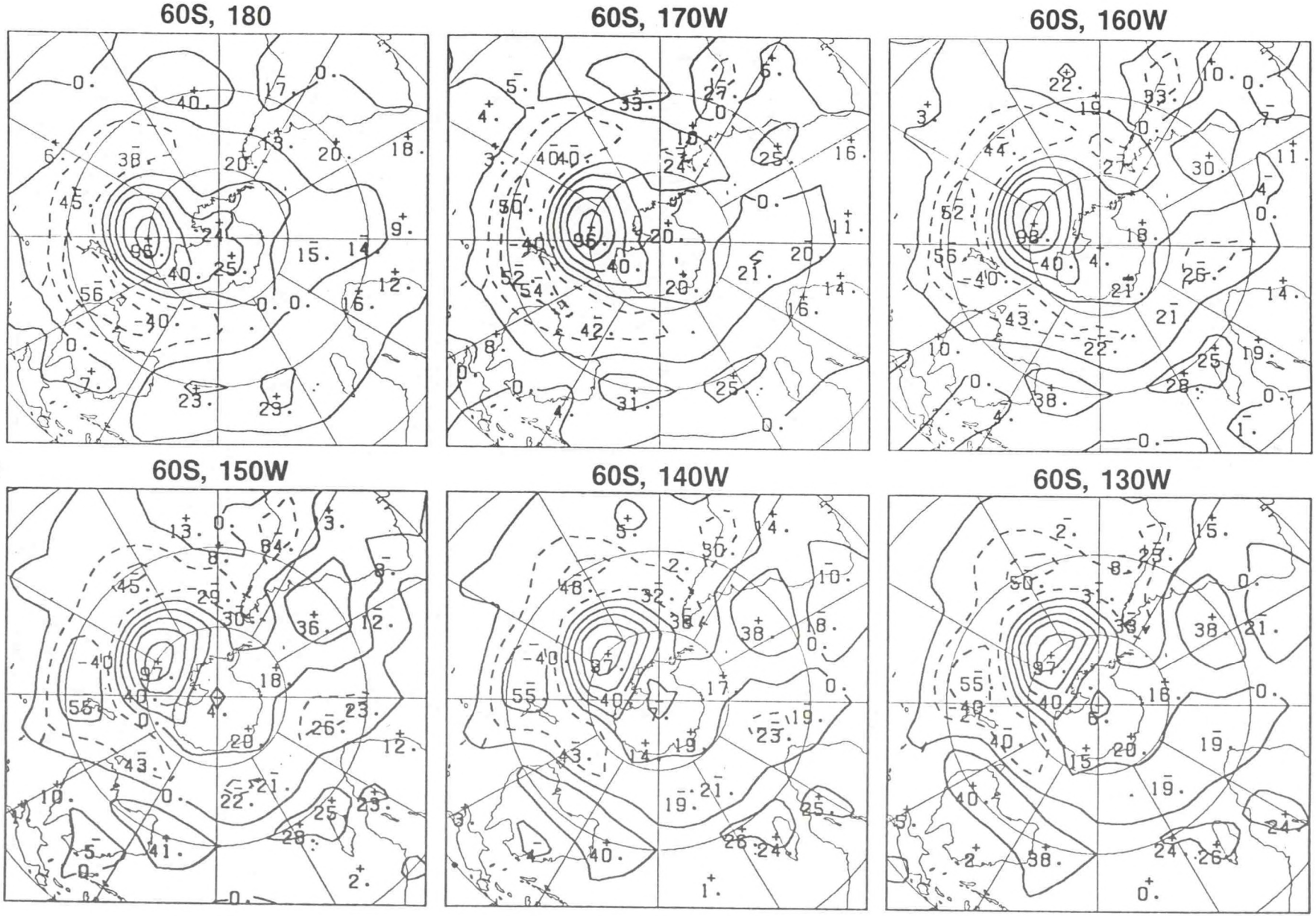
60S, 180
60S, 170W
60S, 160W
60S, 150W
60S, 140W
60S, 130W

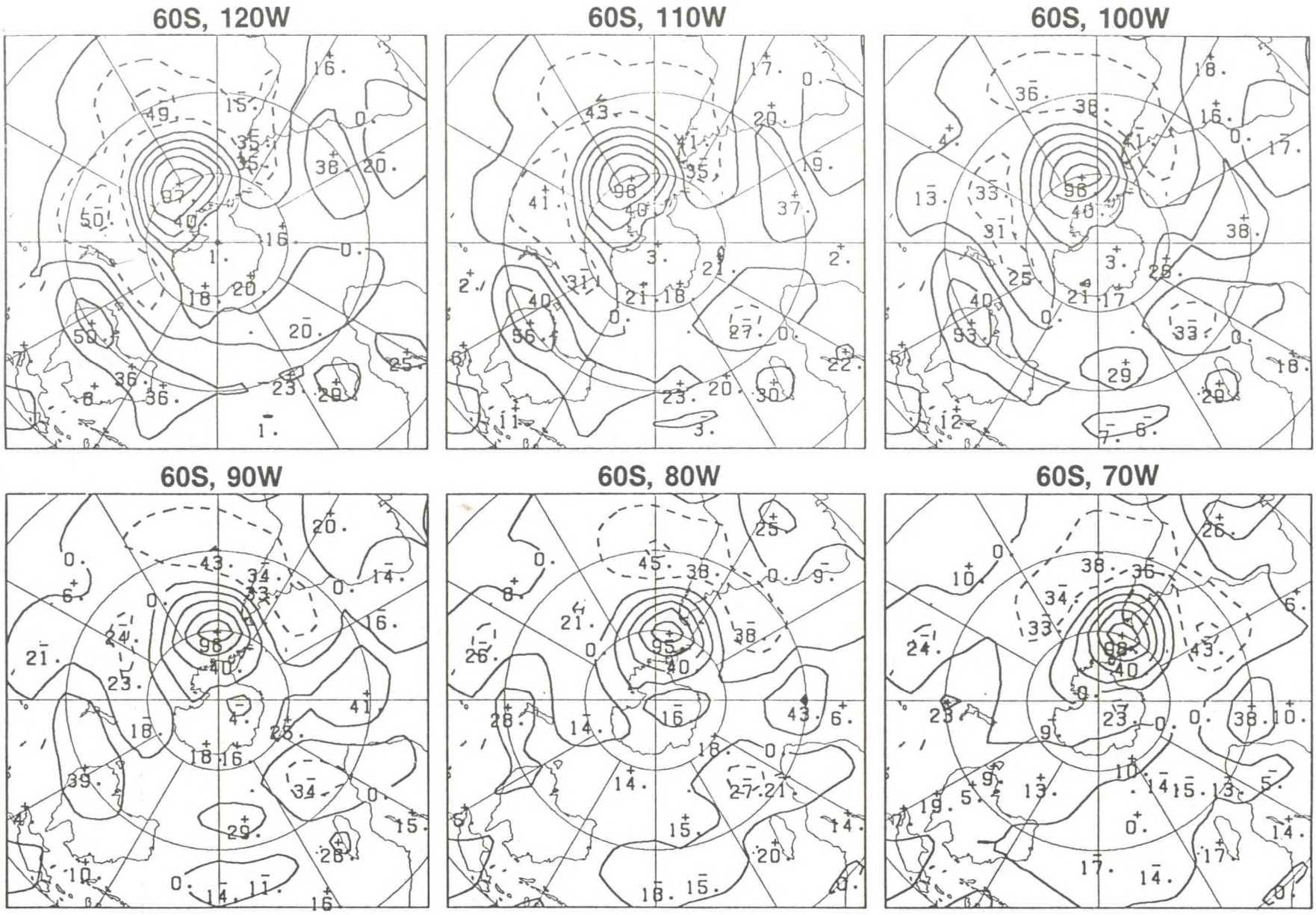
60S, 120W
60S, 110W
60S, 100W
60S, 90W
60S, 80W
60S, 70W

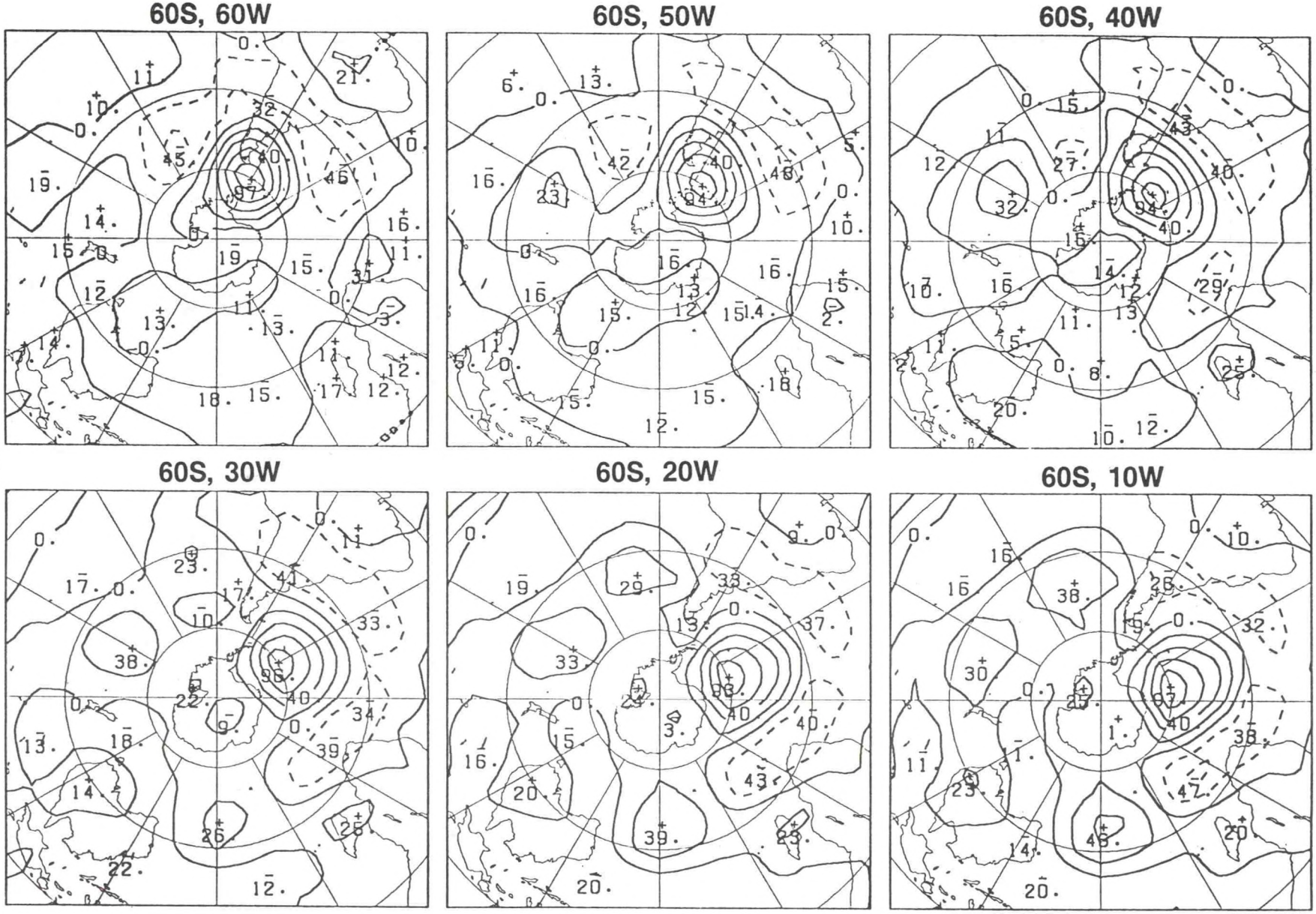
60S, 60W
60S, 50W
60S, 40W
60S, 30W
60S, 20W
60S, 10W

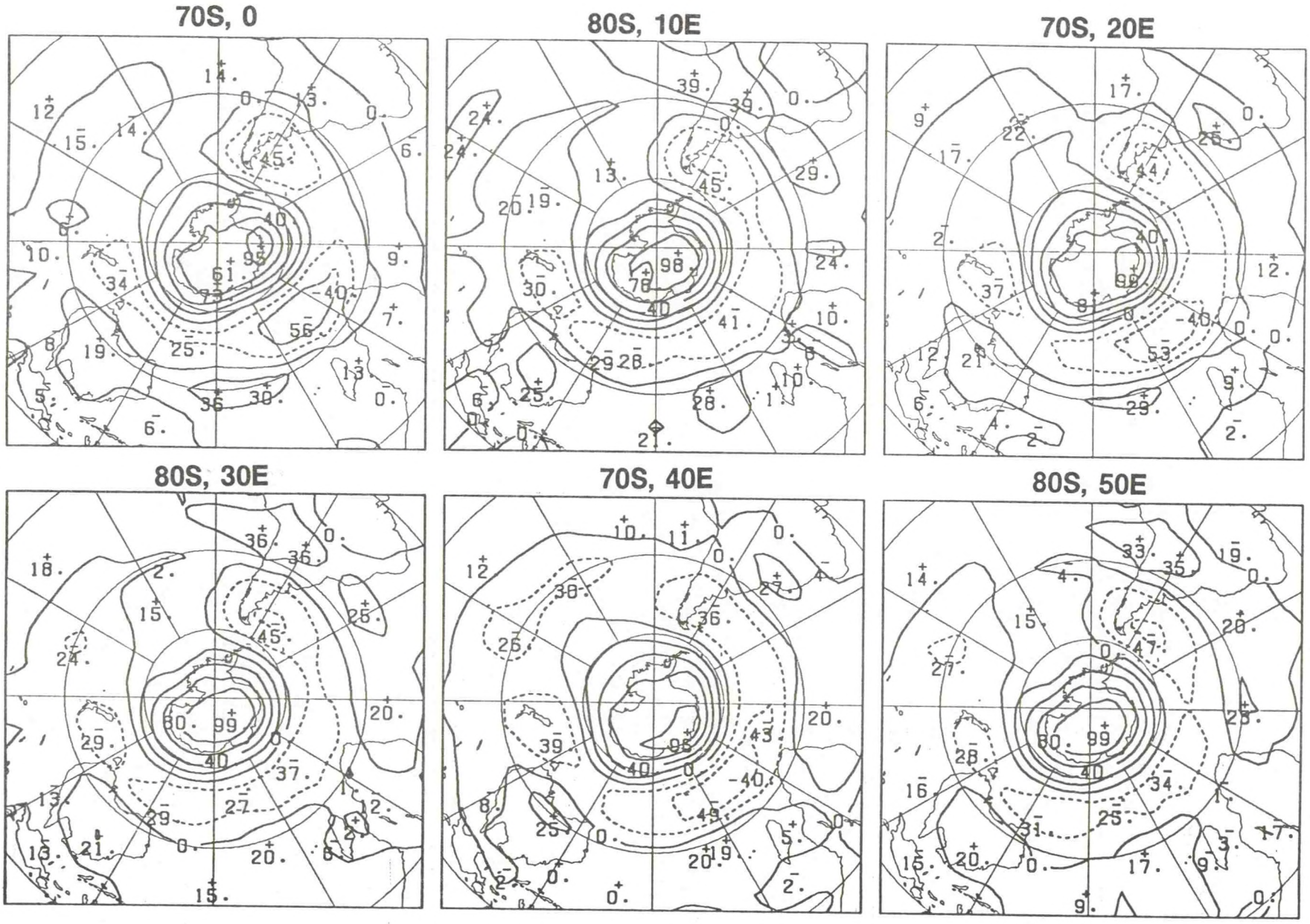
70S, 0
80S, 10E
70S, 20E
80S, 30E
70S, 40E
80S, 50E

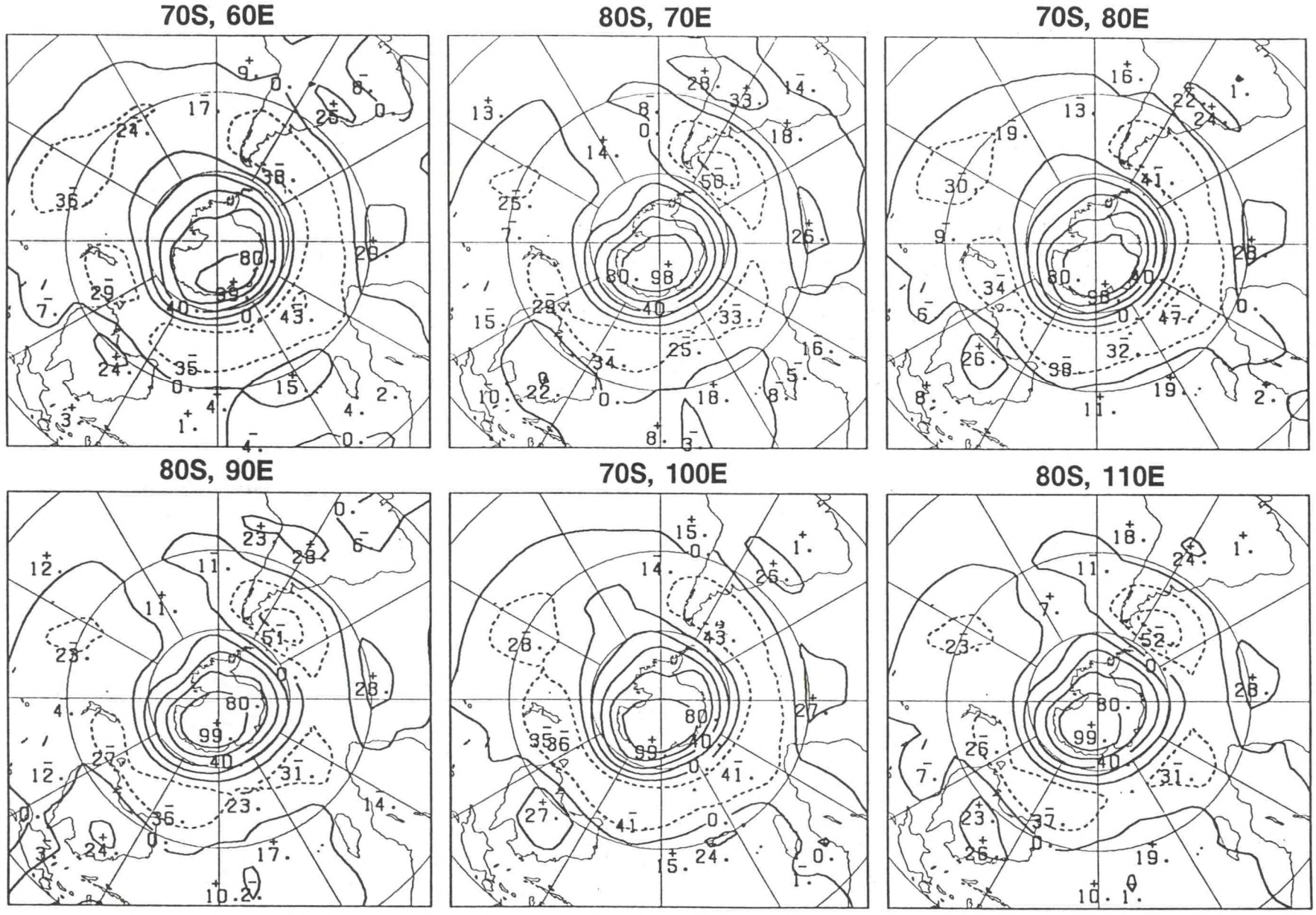
70S, 60E
80S, 70E
70S, 80E
80S, 90E
70S, 100E
80S, 110E

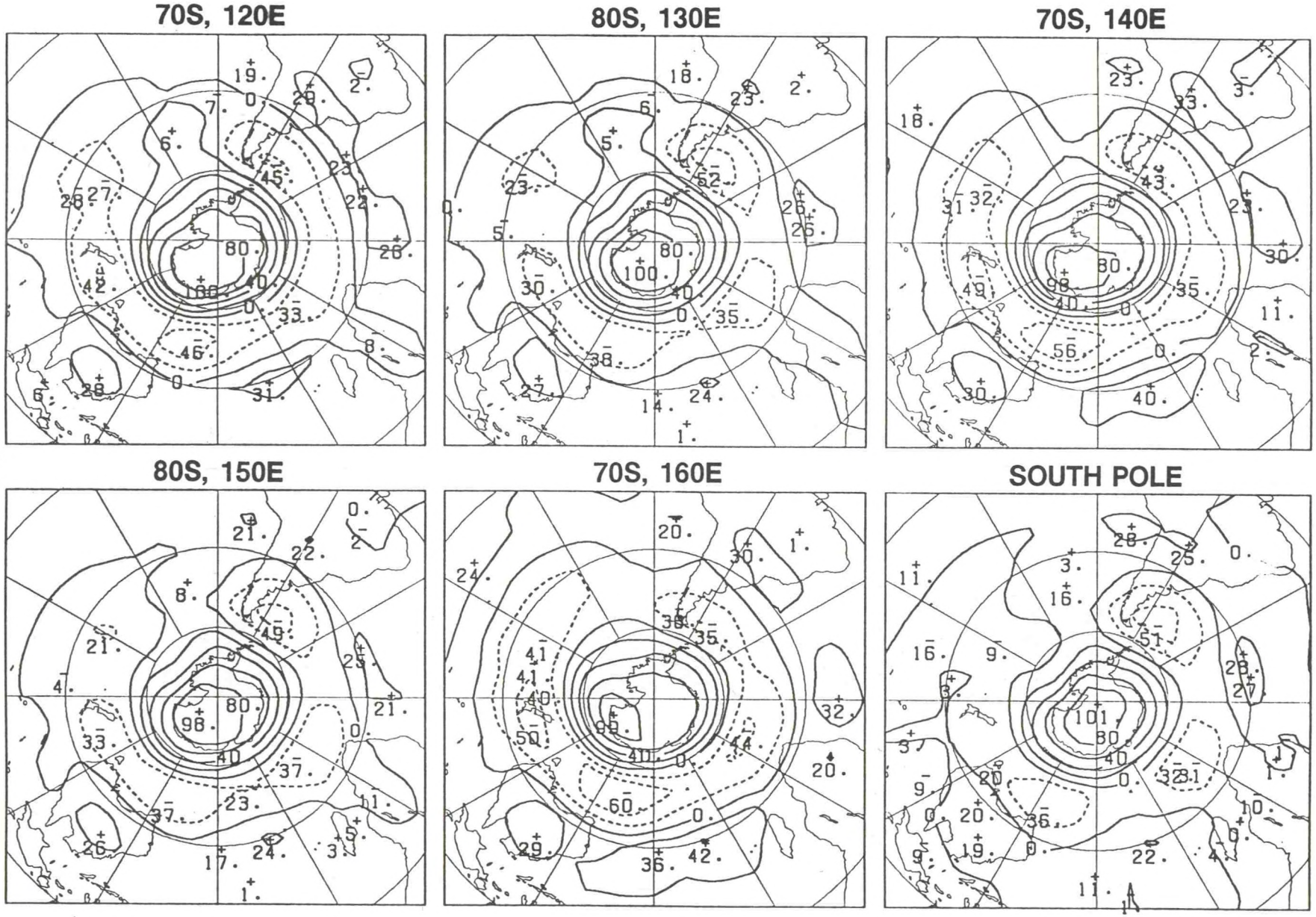
70S, 120E
80S, 130E
70S, 140E
80S, 150E
70S, 160E
SOUTH POLE

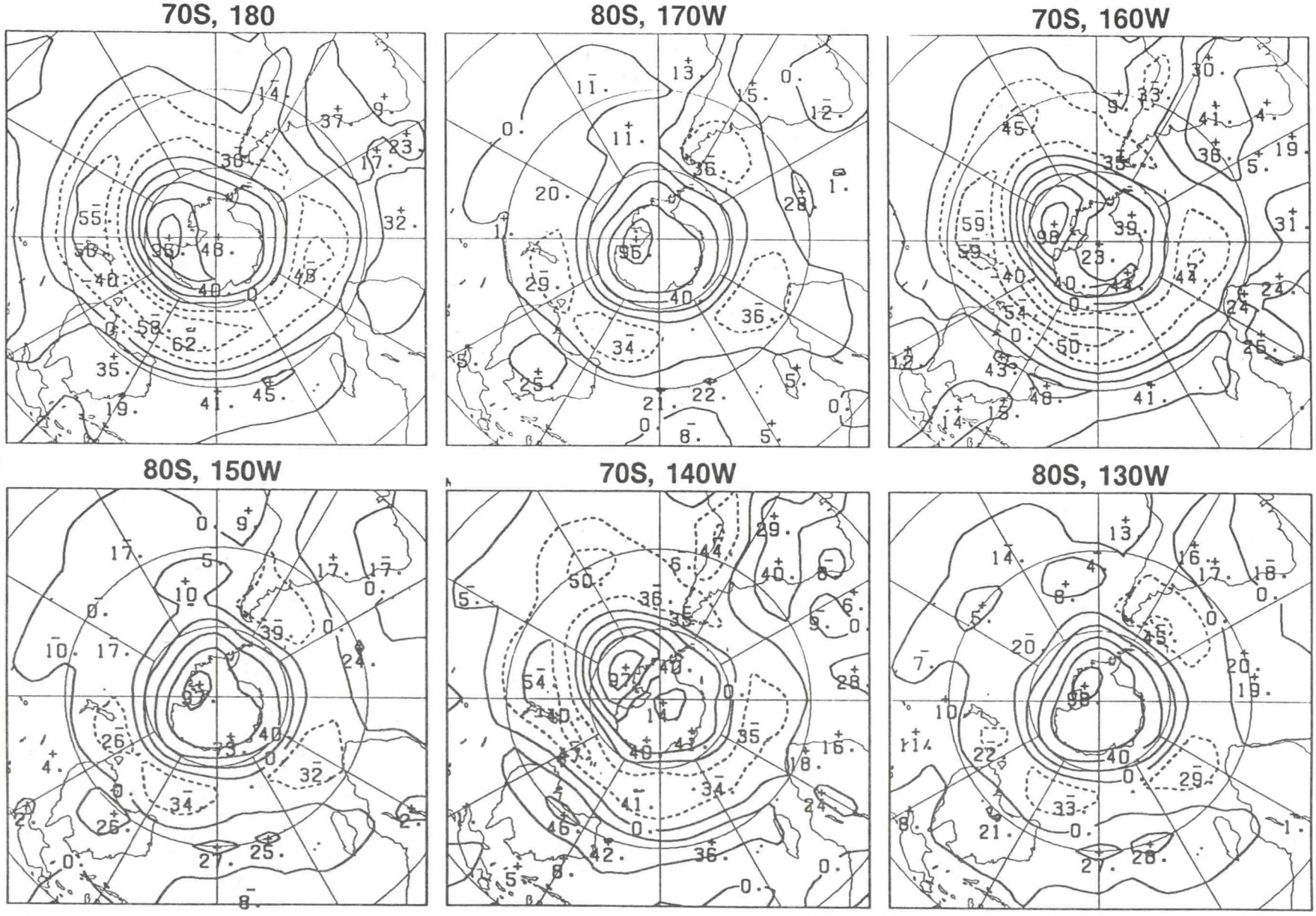
70S, 180
80S, 170W
70S, 160W
80S, 150W
70S, 140W
80S, 130W

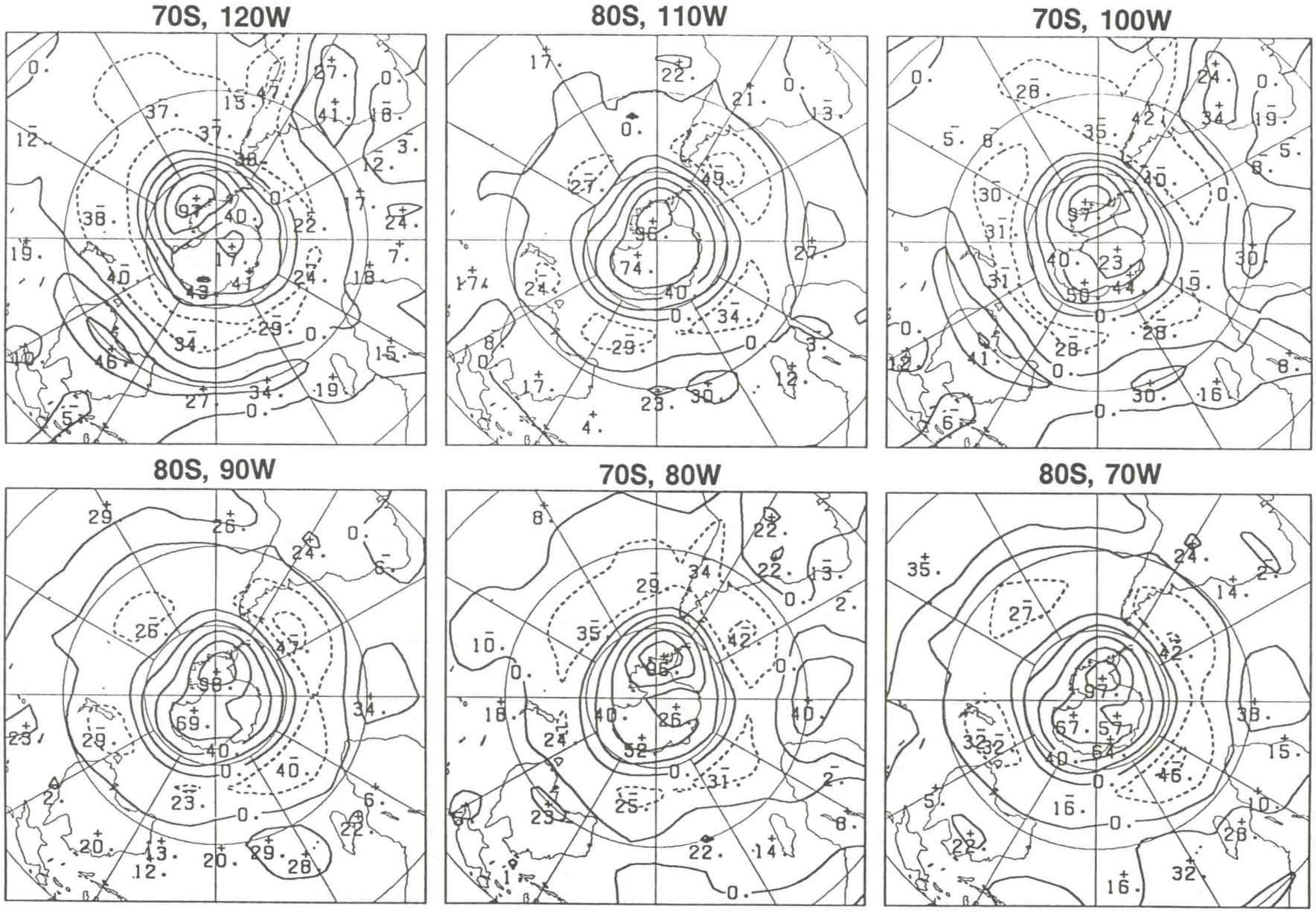
70S, 120W
80S, 110W
70S, 100W
80S, 90W
70S, 80W
80S, 70W

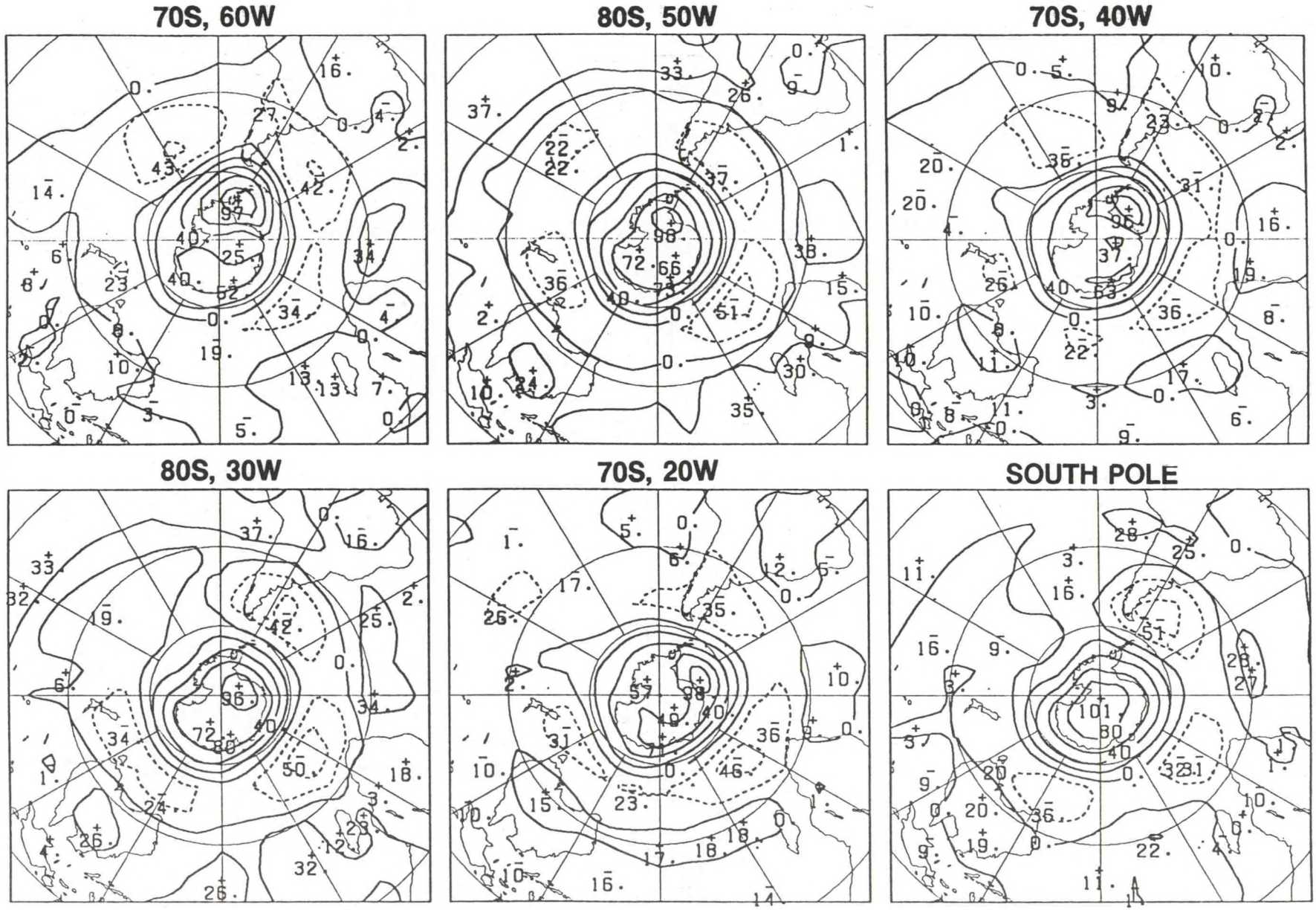
70S, 60W
80S, 50W
70S, 40W
80S, 30W
70S, 20W
SOUTH POLE